Westinghouse
Electric Company

Nuclear Systems

Box 355
Pittsburgh, Pennsylvania 15230-0355

DCP/NRC1480

Project 711

July 13, 2001

U. S. Nuclear Regulatory Commission
Attention: Document Control Desk
Washington, DC 20555

Attention: Mr. Alan C. Rae, AP1000 Project Manager
Future Licensing Organization
Office of Nuclear Reactor Regulation
One White Flint Pike - MS12E15
Rockville, MD 20852-2738

Dear Mr. Rae,

Subject: Transmittal of Non-Proprietary versions of AP1000 Reports

Attached please find the following non-proprietary versions of the AP1000 PIRT and Scaling Assessment Report and the AP1000 Code Applicability Report previously submitted under separate cover letters. The following reports are attached:

1. WCAP-15706 Revision 0, "AP1000 PIRT and Scaling Assessment Report (Non-Proprietary)
2. WCAP-15707 Revision 0, "AP1000 Code Applicability Report (Non-Proprietary)

Please contact me if you have further questions on this subject.

Very truly yours,

M. M. Corletti
Passive Plant Projects & Development

/Attachments

cc: H. A. Sepp, Westinghouse (w/o attachment)

D063

Westinghouse Non-Proprietary Class 3

WCAP - 15706

AP1000 PIRT and Scaling Assessment

Westinghouse Electric Company LLC

AP1000 DOCUMENT COVER SHEET

TDC: _____ Permanent File: _____ S _____

RFS#: _____ RFS ITEM #: _____

AP1000 DOCUMENT NO.	REVISION NO.		ASSIGNED TO
APP-GW-GL-503	0	Page 1 of	W-WINTERS

ALTERNATE DOCUMENT NUMBER: WCAP-15706 Rev. 0 WORK BREAKDOWN #:

DESIGN AGENT ORGANIZATION:

TITLE: **AP1000 PIRT AND SCALING ASSESSMENT REPORT**

ATTACHMENTS:	DCP #/REV. INCORPORATED IN THIS DOCUMENT REVISION:
CALCULATION/ANALYSIS REFERENCE: N/A	

ELECTRONIC FILENAME	ELECTRONIC FILE FORMAT	ELECTRONIC FILE DESCRIPTION

ORIGINATOR	SIGNATURE/DATE	
W. Brown	M M Corletti for W. Brown	
AP1000 RESPONSIBLE MANAGER	SIGNATURE*	APPROVAL DATE
J. W. Winters	M M Corletti for J. Winters	7-13-01

*Approval of the responsible manager signifies that document is complete, all required reviews are complete, electronic file is attached and document is released for use.

WCAP-15706

AP1000 PIRT and Scaling Assessment

July 2001

Westinghouse Electric Company LLC
P.O. Box 355
Pittsburgh, PA 15230-0355

TABLE OF CONTENTS

TABLE OF CONTENTS (cont.)

LIST OF TABLES

LIST OF TABLES (cont.)

LIST OF FIGURES

LIST OF FIGURES (cont.)

LIST OF ACRONYMS

ACRS	Advisory Committee on Reactor Standards
ADS	Automatic Depressurization System
ALWR	Advance Light Water Reactor
APEX	Advanced Plant Experiment
CCB	Configuration Control Board
CCFL	Counter Current Flow Limitation
CFD	Computational Fluid Dynamics
CHF	Critical Heat Flux
CL	Cold Leg
CMT	Core Makeup Tank
CNRC	Canadian National Research Council
CRDM	Control Rod Drive Mechanism
CSAU	Code Scaling, Applicability, and Uncertainty
CVS	Chemical and Volume Control System
CVTR	Carolina/Virginia Test Reactor
DAS	Data Acquisition System
DBA	Design Basis Accident
DCD	Design Control Document
DEG	Double-ended Guillotine
DNB	Departure from Nucleate Boiling
DOE	Department of Energy
DP	Differential Pressure
DVI	Direct Vessel Injection
EMI	Electro-Magnetic Interference
EPRI	Electric Power Research Institute
FID	Fixed In-Core Detector
FSER	Final Safety Evaluation Report
HDR	Heissdampfreaktor
HL	Hot Leg
H2TS	Hierarchical Two-Tiered Scaling
HX	Heat Exchanger
IET	Integrated Effects Test
IFM	Intermediate Flow Mixer
IRWST	In-containment Refueling Water Storage Tank

LIST OF ACRONYMS (cont.)

IST	In-Service Test
LBLOCA	Large Break LOCA
LOCA	Loss-of-Coolant Accident
LST	Large-Scale Test
LSTF	Large-Scale Test Facility
MSLB	Main Steam Line Break
NRC	Nuclear Regulatory Commission
NUPEC	Nuclear Power Engineering Corporation
NUREG	Nuclear Regulation
OSU	Oregon State University
PCS	Passive Containment Cooling System
PIRT	Phenomena Identification and Ranking Table
PRA	Probabilistic Risk Assessment
PRHR	Passive Residual Heat Removal
PXS	Passive Core Cooling System
RCCA	Rod Cluster Control Assembly
RCS	Reactor Coolant System
RNS	Normal Residual Heat Removal System
ROSA	Rig of Safety Assessment
RPC	Rate of Pressure Change
RTDP	Revised Thermal Design Procedure
SBLOCA	Small-break LOCA
SET	Separate Effects Test
SFWS	Startup Feedwater System
SG	Steam Generator
SGTR	Steam Generator Tube Rupture
SI	Safety Injection
SLB	Steam Line Break
SPES	Simulatore per Esperienze di Sicurezza
SPT	Static Pressure Taps
SSAR	Standard Safety Analysis Report
SSG	Simple Support Grids
WAESD	Westinghouse Advanced Energy Systems Division

LIST OF ACRONYMS (cont.)

WEMD	Westinghouse Electro-Mechanical Division
WSTC	Westinghouse Science and Technology Center

EXECUTIVE SUMMARY

In December 1999, The United States Nuclear Regulatory Commission (NRC) issued Design Certification of the AP600 standard nuclear reactor design. This culminated an eight-year review of the AP600 design, safety analysis and probabilistic risk assessment. The AP600 is a 600 MWe reactor that utilizes passive safety features that, once actuated, depend only on natural forces such as gravity and natural circulation to perform all required safety functions. Use of passive safety systems results in increased plant safety and has also significantly simplified plant systems and equipment, resulting in simplified plant operation and maintenance. The AP600 meets NRC deterministic safety criteria and probabilistic risk criteria with large margins.

The large safety margins of the AP600 can be attributed to the performance of the passive safety systems in response to accidents. To support the conservative safety analysis required by the NRC, an extensive test program was performed to provide confidence in Westinghouse's ability to adequately predict the performance characteristics of the passive safety systems. This test program consisted of separate effects and integral systems tests of the passive safety systems and is well documented in NUREG-1512, Final Safety Evaluation Report (FSER) Related to Certification of the AP600 Standard Design (Reference 1). Westinghouse used the test programs to validate analytical computer codes that can predict with adequate certainty, the performance of the passive safety systems in response to design basis and beyond design basis accidents. In addition to the extensive test program conducted by Westinghouse, the NRC also performed confirmatory tests and analyses at both the APEX test facility at Oregon State University and the ROSA test facility at the Japan Atomic Energy Research Institute. As a result, the Westinghouse computer codes were validated as sufficient for use in performing accident analyses in accordance with the applicable NRC regulations. In addition, the NRC performed independent analyses of the AP600 using different analysis codes to confirm the adequacy of the AP600 design as well as the AP600 safety analysis presented in the AP600 Standard Safety Analysis Report (Reference 2). These independent analyses also confirmed the large safety margins exhibited in the AP600.

Westinghouse has developed the AP1000, based on the AP600 design with a power output of approximately 1000 MWe. The AP1000 two-loop arrangement with passive safety and auxiliary systems are the same as the AP600, but the core, reactor coolant pumps, and steam generators have been increased in size. In order to maintain adequate safety margins, the capacity of the passive safety features have been selectively increased based on insights from the AP600 test and analysis results.

Westinghouse is designing the AP1000 to meet the NRC regulatory criteria of 10 CFR Part 52, including deterministic safety criteria and probabilistic risk criteria with large margins. The AP1000 design is intended to meet the NRC criteria in a manner similar to that found to be acceptable for the AP600. As discussed in NUREG-1512, 10 CFR 52.47(b)(2)(i)(A) states that "Certification of a standard design which differs significantly from the light water reactor designs described in paragraph (b)(1) of this section or utilizes simplified, inherent, passive, or other innovative means to accomplish its safety functions will be granted only if

1. The performance of each safety feature of the design has been demonstrated through either analysis, appropriate test programs, experience, or a combination thereof;

2. Interdependent effects among the safety features of the design have been found acceptable by analysis, appropriate test programs, experience, or a combination thereof;

3. Sufficient data exist on the safety features of the design to assess the analytical tools used for safety analyses over a sufficient range of normal operating conditions, transient conditions, and specified accident sequences, including equilibrium core conditions."

In December 2000, Westinghouse submitted "The AP1000 Plant Description and Analysis Report" (Reference 3) to the NRC. The report provides a description of the AP1000 plant design as well as accident analyses using the AP600 validated analysis codes and preliminary models of the AP1000 plant. These preliminary safety analyses were not a complete set of analyses as prescribed by 10 CFR Part 50, but rather, were provided to characterize the expected performance of the AP1000.

This report builds on the preliminary report and is intended to provide the information necessary for the NRC to decide whether the AP600 test programs are sufficient to meet the requirements of 10 CFR Part 52 for an application for Design Certification of an AP1000. This is accomplished by developing Phenomenon Identification and Ranking Tables (PIRT) for the AP1000 and then demonstrating through scaling that the AP600 test program applies to the AP1000, and therefore, that the AP600 analysis codes are applicable for the AP1000. This report provides the NRC with the information necessary to determine whether the AP1000 test data satisfies the requirements of items 1, 2, and 3 above for the AP1000.

A scaling review of the AP1000 to the AP600 tests using primarily top-down scaling techniques is provided in this report. This top-down scaling is supplemented with bottom-up scaling for important phenomenon. Phenomena Identification and Ranking Tables (PIRT) were developed based on a review of the AP600 by a wide range of thermal-hydraulic experts from within Westinghouse as well as outside of Westinghouse. In addition, the NRC independently developed PIRT for their review of the AP600 test and analysis program. These PIRT were then used to determine the important phenomenon that should be accounted for in the test and analysis program. For the AP1000, Westinghouse solicited independent review to develop AP1000 PIRT. Results of this independent review, as well as review by Westinghouse are presented. Although there was re-ranking of some phenomenon, it was determined that:

- the AP1000 PIRT is similar to that of the AP600, with high- and medium-ranked phenomena for both plants being the same,
- no new phenomena are identified as important for AP1000, and
- phenomena previously judged to be of low importance for AP600 are judged to be of low importance for AP1000.

Scaling studies are then performed for the AP1000 passive core cooling system and passive containment cooling system. Comparisons of the important non-dimensional scaling groups for the key AP600/AP1000 features are presented. Comparisons of these scaling groups for the AP600, AP1000, and applicable test facility are provided. The following table summarizes the results and conclusions from the various scaling studies presented in this report.

Table 1 Summary of AP1000 Scaling Studies	
Scaling Assessment	**Remarks**
Automatic Depressurization – Separate Effects	The ADS tests performed for the AP600 were full scale, full pressure tests of prototypical ADS stage 1-3 valves and sparger conducted under bounding conditions. Results of these tests are directly applicable to the AP1000. The conditions tested are within the range of conditions that will be experienced for the AP1000. The AP1000 employs the same ADS stage 1-3 valves and spargers as AP600.
Core Makeup Tank – Separate Effects	The core makeup tank test was a separate-effect, full pressure, scaled test used to assess CMT behavior under prototypical conditions. The AP1000 CMTs are located at the same elevation in relation to the RCS as in AP600, and are 25% larger by volume. The range of operating conditions for the AP600 and AP1000 are similar, and are within the same range of conditions in the CMT test program. Therefore it is judged that the CMT test results for the AP600 are directly applicable to the AP1000.
Passive Residual Heat Removal Heat Exchanger – Separate Effects	AP600 tests important for the PRHR include the separate effects PRHR heat exchanger tests and the ROSA confirmatory tests. The PRHR separate effects tests were heat transfer tests of 3 vertical heat exchanger tubes of prototypical dimension, operating pressures and flow rates. From these tests, a heat transfer correlation was developed for the AP600 PRHR. This correlation was then used to predict PRHR performance of selected ROSA tests and was found by the NRC to provide acceptable agreement with test results. Westinghouse also committed to pre-operational and startup tests to confirm the PRHR heat transfer performance. The AP1000 PRHR inlet and outlet lines have been increased in size to increase the flow rate through the heat exchanger. The AP1000 operating conditions are within the range tested for the AP600 and therefore it is concluded that the AP600 tests and heat transfer correlation are acceptable for the AP1000.
Integral System Performance – Automatic Depressurization	Scaling calculations of the dimensionless scaling groups were performed. Results show that the scaling ratios for the AP600 and AP1000 are within an acceptable range for key phenomena in the SPES facility.

Table 1 (cont.) Summary of AP1000 Scaling Studies

Scaling Assessment	Remarks
Integral System Performance -- Transition to IRWST Injection	Scaling calculations of the dimensionless scaling groups are performed. Results show that the scaling ratios for the AP600 and AP1000 are within an acceptable range for key phenomena in the OSU facility. CMT and IRWST gravity injection phenomenon in relation to reactor vessel inventory is well-represented in the OSU facility.
Integral System Performance -- Sump Injection	Scaling calculations of the dimensionless scaling groups are performed. Results show that the scaling ratios for the AP600 and AP1000 were within an acceptable range for key phenomena in the OSU facility.
Containment Performance Phenomena – Heat and Mass Transfer	The PCS separate effects test program covered the upper range of both the AP600 and AP1000 dimensionless parameters for the selected heat and mass transfer correlations for condensation on the inside of the shell and evaporation/ convection on the outside of the shell in the important riser region of the annulus. Therefore, the use of conservative heat and mass transfer correlations for condensation and evaporation is reasonable for both the AP600 and AP1000 evaluation models.
Containment Performance – Internal Circulation and Mixing	Following a design basis accident (DBA) and actuation of the PCS, both the AP600 and AP1000 containment buildings are heated by a rising plume of steam/air. Condensation on the containment shell cools the surrounding steam/air mixture. Conditions where the atmosphere is heated from below and cooled from above are inherently unstable resulting in turbulent mixing. Computational fluid dynamics (CFD) analysis results presented in this report show both the AP600 and AP1000 dome regions to be well mixed. The effects of internal circulation and mixing on the containment pressure calculation are bounded in the containment DBA evaluation model. The evaluation model ignores heat and mass transfer to conductors inside dead-ended compartments, ignores heat and mass transfer to floors (horizontal surfaces), and uses a bounded, free-convection correlation for calculating the heat and mass transfer to the internal surface of the containment shell.

Table 1 (cont.) Summary of AP1000 Scaling Studies	
Scaling Assessment	**Remarks**
Containment Performance – Liquid Film Coverage Fraction	The AP1000 containment dome is the same size and shape as the AP600. The AP1000 water distribution system is identical to the AP600 system, but the initial PCS water flow rate is slightly higher ([ ]^{a,b,c} gpm for AP600). Based on the water distribution system tests, this flow rate should yield an initial, steady state water coverage that is at least as good as AP600 and in less time.
Departure From Nucleate Boiling (DNB) Tests	The AP600 required additional DNB tests to be performed to extend the range of the applicable Westinghouse DNB correlation to a lower flow regime. The AP1000 flow rate and pump coastdown have been increased such that the AP1000 flow rate at the time of minimum DNB is above the AP600 low flow regime, and is within the range for existing operating reactors. Thus the margin to DNB on loss of flow is increased on the AP1000.

Conclusions from the AP1000 scaling assessments are as follows:

- The key separate effects tests conducted for the AP600 are applicable to the AP1000.
- The scaled integral systems tests conducted for the AP600 scale adequately to the AP1000 plant such that the data is sufficient for computer code validation.
- The range of conditions tested in the AP600 containment tests adequately cover the expected range of operating conditions for the AP1000.
- Computational fluid dynamics analyses of the AP1000 containment during design basis events conclude that mixing in the AP1000 containment atmosphere behaves similarly to the AP600.

Accident analyses were performed for the AP1000 using the AP600 validated analysis codes and preliminary models of the AP1000 plant. These scoping analyses are presented in WCAP-15612, "AP1000 Plant Description and Analysis Report," (Reference 3). These analyses were not a complete set of analyses as prescribed by 10 CFR 50. They were provided to characterize the expected performance of the AP1000. These analyses were performed using bounding assumptions and were performed in a consistent manner with the approach taken for the AP600, unless otherwise discussed in the report. In addition, the analysis results were compared to the AP600 analysis results for the same event to better demonstrate similarities to, or contrast differences with the performance of the AP600. The safety analysis results show that the timing and interactions predicted for the AP1000 are similar to the performance predicted for the AP600. Based on the results of these analysis assessments, it appears that the analysis results for the AP1000 will provide large safety margins for the range of postulated accidents and transient events. No new phenomenon or significant differences in performance characteristics were observed in the analysis results.

Based on these scaling studies, and based on the results of the analyses presented in WCAP-15612, Westinghouse concludes that the database of test data for the AP600 is sufficient to meet the requirements of 10 CFR Part 52.

References

1. NUREG-1512, "Final Safety Evaluation Report Related to Certification of the AP600 Standard Design," September 1998.

2. "AP600 Standard Safety Analysis Report," DE-AC03-90SF18495, June 26, 1992.

3. WCAP-15612, "AP1000 Plant Description and Analysis Report," M. M. Corletti et al., December 2000.

1.0 INTRODUCTION

Westinghouse Electric Company has designed an advanced 600 MWe nuclear power plant called the AP600. The AP600 uses passive safety systems to enhance plant safety and to satisfy U.S. licensing requirements. The use of passive safety systems provides significant and measurable improvements in plant simplification, safety, reliability, investment protection and plant costs. These systems use only natural forces such as gravity, natural circulation, and compressed gas to provide the driving forces for the systems to adequately cool the reactor core following an accident. The AP600 received Design Certification by the Nuclear Regulatory Commission in December 1999.

To further improve AP600 economics and in response to market demand for larger plants, Westinghouse initiated development of the AP1000 standard nuclear reactor design, with an output of approximately 1000 MWe, based on the AP600 design. The design features of the plant have been selected to preserve key features and performance characteristics embodied in the AP600. By preserving the design basis of the AP600 in the AP1000, Westinghouse seeks to preserve the licensing basis of the plant as well. A key factor in retention of the AP600 licensing basis for the AP1000 is the application of the AP600 test and analysis program.

The requirement for passive plant vendors to develop and perform sufficient design certification test programs was stated by the NRC in NUREG-1512, "Final Safety Evaluation Report Related to Certification of the AP600 Standard Design," (Reference 1). Separate effects and integral systems tests are required to provide data to assess the computer codes used to analyze plant behavior over the range of normal operating conditions, transient conditions, and accident sequences. Through scaling studies, Westinghouse proposes to use the AP600 test and analysis program as the basis for compliance with this requirement.

In December 2000, Westinghouse submitted "The AP1000 Plant Analysis and Description Report" (Reference 2) to the NRC. The report provides a description of the AP1000 plant design as well as accident analyses using the AP600 validated analysis codes and preliminary models of the AP1000 plant. These preliminary safety analyses were not a complete set of analyses as prescribed by 10 CFR Part 50, but rather, were provided to characterize the expected performance of the AP1000.

This report builds on the preliminary report and is intended to provide the information necessary for the NRC to decide whether the AP600 test programs are sufficient to meet the requirements of 10 CFR Part 52 for an application for Design Certification of an AP1000. This is accomplished by developing Phenomenon Identification and Ranking Tables (PIRT) for the AP1000 and then demonstrating through scaling that the AP600 test program applies to the AP1000, and therefore, that the AP600 analysis codes are applicable for the AP1000.

In the AP600, where scaling analyses of the tests identified that certain phenomenon were not well scaled for the AP600 plant, conservatisms were applied to the analysis codes such that their predictions of the plant response were conservative with respect to safety. It is proposed that such an approach also be used for the AP1000.

Section 2 of this report provides a discussion of the important thermal-hydraulic phenomenon for modeling AP1000 system performance based on AP1000 PIRT. As was done for the AP600 analysis, Westinghouse solicited independent reviewers to help in the development of the AP1000 PIRT. These PIRT were then used to determine the important phenomenon that should be accounted for in the test and analysis program.

Section 3 provides a summary of the AP600 test program and its applicability to the AP1000 program.

In Section 4, a scaling assessment of the AP600 tests to the AP1000 plant for key phenomenon is provided.

Section 5 provides conclusions and recommendations for additional scaling studies.

References

1. NUREG-1512, "Final Safety Evaluation Report Related to Certification of the AP600 Standard Design," December 1999.

2. WCAP-15612, "The AP1000 Plant Description and Analysis Report," December 2000.

2.0 IMPORTANT THERMAL-HYDRAULIC PHENOMENA FOR MODELING THE AP1000 SYSTEM PERFORMANCE

The AP1000 Plant Description and Analysis Report (Reference 1) provides a design description of the AP1000 with a comparison to the AP600. In that report, design margin assessments are provided which explain the design basis of the changes to the AP600 passive safety systems that are incorporated into AP1000. These design margin assessments are provided in Section 2.1, as a convenience to the reader when considering the possible changes to the AP600 Phenomenon Identification and Ranking Table (PIRT) that result in the AP1000 PIRT.

2.1 PASSIVE CORE COOLING SYSTEM (PXS) DESIGN MARGIN ASSESSMENT

The PXS features considered in this section are:

- Passive Residual Heat Removal Heat Exchanger (PRHR heat exchanger)
- Accumulator
- Core Makeup Tank (CMT)
- Incontainment Refueling Water Storage Tank (IRWST)
- Containment Recirculation
- Automatic Depressurization System (ADS)

The design approach for the AP1000 passive safety features is to selectively increase their capacity using insights from the AP600 design, testing, analysis and licensing activities. Two key factors in these insights are the uncertainty in the computer analysis tools and the margin between the calculated results and the licensing limits. These insights indicate that some features (like ADS stage 4 (ADS-4), IRWST injection and long-term recirculation from containment) should be increased at least as much as the change in core power, whereas other features (like CMT and Accumulators) may not need to be increased as much as the change in power.

This section provides an assessment of the margins provided in the AP1000 passive core cooling system as compared with the AP600 PXS. This margin assessment is intended to provide a simple quantitative comparison between the AP600 and the AP1000 PXS features and is intended to supplement other analysis/evaluation activities, such as preliminary safety analysis and scaling evaluations. Preliminary AP1000 safety evaluations are provided in Section 3.0 of Reference 1. Later, during the Design Certification licensing review of the AP1000, computer codes verified for use on AP1000 will be used to determine that the AP1000 passive safety features are capable of meeting the licensing requirements.

These PXS margin assessments are based on simple physical models that are independent of detailed safety and scaling analyses. The assessments compare AP1000 and AP600 safety system capacities under conditions where minimum margins occur. Consideration is also given to uncertainties due to the analysis models and the supporting tests. Appropriate plant conditions (RCS pressure/temperature, containment pressure, etc.) are applied to both the

AP600 and the AP1000 features. The performance of the feature is calculated by hand using simple equations, such as the Darcy formula for liquid flow:

Water Flow = (Pressure Drop/Resistance) ^ 0.5

Generally, conservative simplifying assumptions have been made as described. The resulting performance difference is compared to the difference in core power to determine margin.

The PXS assessments are based on simple, easily understood, physically based hand calculation methods and are not dependent upon test results, scaling, or safety analysis codes. They should provide useful input to the review of the AP1000 PXS design during this pre-application review.

2.1.1 Passive Residual Heat Removal Heat Exchanger

The primary parameter of interest for the PRHR heat exchanger is heat removal during natural circulation conditions. The PRHR heat exchanger operates in the natural circulation mode after a loss of offsite power or other events in which the reactor coolant pumps are not operating. The natural circulation heat removal capability is affected by the flow resistance of the PRHR heat exchanger flow path, the heat transfer surface area of the PRHR heat exchanger, and the elevation of the heat exchanger. For the AP1000, although the heat exchanger elevation is unchanged, the thermal center of the core has moved down one foot thus increasing the driving head during natural circulation conditions. This change was conservatively ignored in the assessment below. The AP1000 uses the same basic PRHR heat exchanger design, although the surface area has been increased to increase heat transfer. This increase has been accomplished by increasing the horizontal tube length and by adding additional tubes; the heat transfer area has been increased by 22 percent. In addition, the PRHR heat exchanger supply and return piping have been increased in size from 10-in. to 14-in. in order to reduce the flow resistance. This change results in the flow resistance being reduced by a factor of 3 of the AP600 flow resistance.

If the heat exchanger saw the same inlet temperature and was able to produce the same outlet temperature, the driving head would be the same and the reduced flow resistance would allow a 74 percent increase in flow and heat removal. This increase in flow is calculated by using the Darcy formula that in this case reduces to:

Flow ratio = (1/resistance ratio) ^ 0.5 = (1/33%) ^ 0.5 = 174%

Table 2.1-1 summarizes the results of a calculation of the PRHR heat exchanger heat transfer rate that accounts for both the change in flow resistance and the heat transfer area. In this calculation, the reactor coolant pumps are not assumed to operate, so the heat exchanger performance is based on natural circulation. The CMTs are also not assumed to operate to simplify the calculation and to separate the effects of the two features.

The PRHR inlet temperature [reactor coolant system (RCS) hot leg temperature] is assumed to be the saturated temperature at the steam generator safety valve setpoint. This temperature

was selected because without reactor coolant pump (RCP) and CMT operation the RCS tends to remain at this temperature for some time until the PRHR heat exchanger matches decay heat and then the PRHR heat exchanger starts to cool down the RCS. This steam generator (SG) safety valve pressure setpoint is 1100 psig for AP600 and 1200 psig for AP1000.

The time to match decay heat is calculated based on the above PRHR heat exchanger performance as discussed above, and assuming core operation at 102 percent power prior to trip and decay heat based on ANS 1979 plus 2 sigma.

The initial SG secondary side water mass is based on the SG narrow range low level reactor trip setpoint. The preliminary initial SG secondary side water mass at the reactor trip setpoint for the AP1000 [ ]^{a,b,c} is approximately 139 percent more than the water mass for the AP600 [ ]^{a,b,c}. The final SG water mass is calculated using the PRHR and plant operating conditions discussed above, and assuming that the decay heat in excess of the PRHR heat exchanger capacity is removed by boiling off some of the SG secondary side water. The SG water mass continues to decrease until the PRHR heat exchanger capacity matches decay heat.

As shown in Table 2.1-1, the AP1000 PRHR heat exchanger capacity has been increased substantially, almost as much as the increase in core power. In addition, the AP1000 SG secondary side inventory has been increased more than the ratio of core powers. The above table shows that the AP1000 initial SG water mass at the time of trip is 36 percent greater (per megawatt of core power) than the AP600. At the end of the transient, the AP1000 SG mass is more than twice as large as the AP600 SG mass, even though the AP1000 PRHR heat exchanger matches decay heat a few minutes later.

Based on this evaluation, the substantial increase in PRHR heat exchanger capacity resulting from the increase in PRHR heat exchanger heat transfer area and from the reduced flow resistance, together with the increased SG secondary side water mass should provide greater margin in non-LOCA (loss-of-coolant accident) decay heat removal transients than the AP600. Preliminary AP1000 non-LOCA safety analysis, in Section 3.0 of Reference 1, supports this conclusion.

2.1.2 Accumulator

The primary parameter of interest with the accumulator is the time it takes to refill the reactor vessel lower plenum in a large LOCA and the effect on the fuel peak clad temperature (PCT) occurring during reflood. The larger LOCA is limiting because it requires the highest injection rate.

For the AP1000, the accumulator tank, water level, gas pressure, discharge line resistance, and reactor vessel lower plenum volume are unchanged from the AP600.

In the AP600, the large LOCA PCT is much lower than it is in operating plants and occurs during blowdown. This blowdown PCT is [ ]^{a,b,c} with uncertainties, which is significantly less than the licensing limit of 2200°F. The reflood PCT is only [ ]^{a,b,c} with uncertainties. AP1000 has the same lower plenum volume such that with the same accumulator injection

capability, the time to refill the lower plenum will be about the same. However because of the higher core power density, higher PCTs are expected.

Simplified calculations have been performed to estimate the large LOCA PCT for the AP1000 (Table 2.1-2). The assumptions and results for the two cases calculated are given below.

Case 1 shows an approximation of the AP1000 reflood PCT made with the following assumptions:

- Same end of blowdown PCT
- Same time for core heatup, from the end of blowdown PCT to the reflood PCT
- Higher PCT heatup rate during this time based on the ratio of higher linear power

Case 2 shows the results using more conservative/bounding assumptions:

- 100°F higher end of blowdown PCT
- 7 second longer time for core heatup, from the end of blowdown PCT to the reflood PCT
- Higher PCT heatup rate during this time based on the ratio of higher linear power and the longer heatup time

Case 2 considers that the end of blowdown peak may be higher because of the higher linear power. It also considers that the time for core heatup, from end of blowdown PCT to the reflood PCT, may be longer because of the longer downcomer and fuel. Note that the lower plenum is not larger because the reactor vessel is the same diameter and the fuel is located at the same elevation relative to the bottom of the reactor vessel.

The Case 1 temperature rise is calculated:

= AP600 temp rise * AP1000 linear power/AP600 linear power

= [ ]a,b,c

The Case 2 temperature rise is calculated:

= AP600 temp rise * AP1000 linear power/AP600 linear power * AP1000 time/ AP600 time

= [ ]a,b,c

It is possible to increase the accumulator flow by changing the flow limiting orifice in the discharge line. However this would shorten the duration of the accumulator injection which can cause negative side effects.

Shortening the accumulator injection duration could impact multiple failure accident sequences considered in the Probabilistic Risk Assessment (PRA), including a DVI LOCA with failure of the intact CMT. During this accident the accumulator provides more than enough flow while it is injecting since the break flow with ADS operation is smaller than a large LOCA. The more limiting factor is its duration of injection. The challenge to core cooling comes after the accumulator empties and before IRWST injection starts. MAAP analysis was used to show that the AP600 provided adequate core cooling during this beyond design basis event. Preliminary AP1000 MAAP analysis shows that the AP1000 also provides adequate core cooling for this event with the proposed delivery rate.

Based on this evaluation, the AP1000 accumulators should refill the lower plenum and downcomer fast enough following a large LOCA to limit the reflood PCT to well below the licensing limit of 2200°F. The AP1000 PCTs are expected to be higher than the AP600 PCTs. In addition, maintaining the current AP600 accumulator delivery time helps during DVI LOCAs with multiple failures (PRA sequences). Large break LOCA analyses will be provided as part of the AP1000 Design Control Document (DCD).

2.1.3 Core Makeup Tank

The primary parameter of interest with the CMTs is its injection capability during a LOCA. The limiting design basis event is a direct vessel injection (DVI) LOCA because it causes the complete spill of one of the two CMTs and results in a quick actuation of ADS because of the rapid draining of the faulted CMT.

The AP1000 CMT volume and its injection capability have been increased by about 25 percent. The tank volume increase is accomplished by increasing the CMT diameter. The injection capability increase has been accomplished by changing the flow limiting orifice in the CMT discharge line. Increasing the CMT volume and its injection capability maintains the same injection duration which maintains the same (or similar) time when the ADS stages are actuated and the IRWST begins to provide safety injection.

Table 2.1-3 shows the flow capability margins available in the CMTs during a design basis DVI line break accident. Note that in such an accident the intact accumulator provides the RCS injection during the majority of the RCS depressurization activity which occurs during the first 500 seconds. When the accumulators empty at 600 seconds, the core is covered with water and the RCS pressure is already relatively low and the main function of the CMTs is to provide enough injection to remove core decay heat and sensible heat from the reactor vessel and its internals.

Note that the time when the accumulators empty in the AP1000 is expected to be later because the DVI lines are the same size for both plants and the AP1000 has a larger RCS volume and greater decay heat. As a result, the blowdown of the RCS is expected to be slower. Assuming the same time is conservative in the above evaluation because it requires more CMT flow due to the greater decay and sensible heat that occur at the earlier time.

The flow capability shown above is calculated in the same manner as for the PRHR heat exchanger using the Darcy formula assuming that the differential pressures are the same for the AP1000 and AP600. The differential pressures are expected to be the same since the DVI nozzle and the CMT top/bottom elevations are the same. Note that the line resistance of interest is between the CMT outlet and the DVI nozzle. The line resistance for the pressure balance line between the cold leg and the CMT top inlet is not important because of the low density of steam in the line when the accumulators empty at less than 100 psig.

Flow ratio = (1/resistance ratio) ^ 0.5 = (1/64%) ^ 0.5 = 125%

Note that the required CMT flow for the AP1000 is less than the ratio of core power because of differences in sensible heat in the reactor vessel. The AP1000 sensible heat per MW is lower than the AP600 because the reactor vessel diameter is the same diameter, although it is somewhat longer. Also note that the AP600 CMTs provide large margin to the required flow (61 percent). As a result, increasing the AP1000 CMT flow capability by 25 percent over that of the AP600 is sufficient to maintain a comfortable margin of 29 percent versus the AP1000 required flow.

Another potentially limiting event is a multiple failure accident sequence considered in the PRA, a DVI LOCA with failure of the intact accumulator. During this accident the CMT provides injection for a sufficient time because of its injection characteristics. The more limiting factor is the magnitude of the CMT injection since failure of the accumulator significantly reduces the peak injection available. MAAP analysis was used to show that the AP600 provided adequate core cooling during this beyond design basis event. Preliminary AP1000 MAAP analysis have been performed and results demonstrate that the AP1000 also provides adequate core cooling for this event.

Based on this evaluation, the AP1000 CMTs should provide sufficient injection to adequately cool the core during LOCAs. Preliminary AP1000 small LOCA safety analyses presented in Section 3.0 of Reference 1 supports this conclusion.

2.1.4 IRWST Injection

The primary parameter of interest with the IRWST is its gravity injection capability to the RCS. The limiting condition is the initiation of IRWST injection following a DVI LOCA. This event is limiting because the break location causes one IRWST line to spill and the rapid blowdown of one CMT results in an early actuation of ADS which requires earlier injection from the IRWST. The initiation of IRWST flow to the core in a DVI LOCA also has more uncertainty in the supporting test results and safety analysis computer code models than other phenomenon during the accident sequence.

The nominal size of the injection lines have been increased from [ ]^{a,b,c} in order to reduce the flow resistance. This change results in the flow resistance being reduced to about 32 percent of the AP600s. In addition, the initial water level in the IRWST has been increased from [ ]^{a,b,c} to increase the initial injection pressure. More accurate narrow range

IRWST level instruments have been added to decrease the instrument uncertainty and allow similar operating margins.

Table 2.1-4 shows the effect of these changes on the IRWST injection capability. The assumed RCS pressure (versus containment) is typical of the initial IRWST cut-in conditions.

The flow capability shown above has been is calculated using the Darcy formula. In this case, the differential pressure is not the same because of the difference in IRWST water levels.

Flow ratio = (DP ratio/resistance ratio) ^ 0.5 = (1.08%/32%) ^ 0.5 = 184%

Based on this evaluation, the AP1000 IRWST gravity injection capability has been increased by more than the AP1000/AP600 core power increase (3400/1933 or 176 percent). As a result, this feature should provide increased margins for the AP1000. Preliminary AP1000 small LOCA and long-term cooling safety analyses presented in Section 3.0 of Reference 1 support this conclusion.

2.1.5 Containment Recirculation

The primary feature of interest is the long-term recirculation flow capability from the flooded containment. The limiting condition is a DVI LOCA because it results in the lowest containment water level and an earlier time for the initiation of containment recirculation. The lower water level reduces the available driving head for containment recirculation. For the AP600, the worst DVI case was with Normal Residual Heat Removal System (RNS) injection because it increased the spill of IRWST water to the containment by pumping water from the IRWST to the break. This results in the earliest time for initiation of containment recirculation. However as discussed below, improvements have been made to the AP1000 such that operation of the RNS during a DVI LOCA is no longer the limiting case. For the AP1000, the limiting case is a DVI LOCA with gravity injection of the IRWST and no RNS pumped injection.

The nominal line size for the containment recirculation lines has been increased from 6-in. to 8-in. in order to reduce the flow resistance. This change results in the flow resistance being reduced to about 32 percent of the AP600s. In addition, several changes have been made to increase the containment water level at the time of recirculation as well as to delay the time when recirculation is initiated. All of these changes improve containment recirculation capability and are summarized below.

- The IRWST initial water level has been increased.

- The drain from the refueling cavity has been revised. The drain is now connected to the bottom of the pit. In addition, check valves have been added to prevent backflow from the loop compartments to the refueling cavity during the initial containment flooding. The revised refueling cavity drain arrangement makes the cavity similar to the design used in the two PXS valve rooms and in the CVS equipment room. It allows water that may initially overflow into this cavity from the IRWST due to ADS operation to drain out of the refueling cavity into the loop compartments. Later on as the IRWST injects

and the containment water level rises, check valves prevent water from flooding back into the refueling cavity. As a result, more water is available in the loop compartments which results in a higher containment recirculation water level.

- The normal RNS pump suction has been changed so that it will normally take suction from the spent fuel cask loading pit instead of the IRWST. In the longer term it will be re-aligned by the operators to the IRWST/containment so that it can provide a continuous water supply by recirculating water from the containment.

The limiting long term cooling event for the AP600 is a DVI line break where the RNS pumps are started by the operators in accordance with the emergency procedures. Their operation during IRWST injection results in a faster drain down of the IRWST and a quicker initiation of recirculation. In addition, it is assumed that the RNS pumps fail just as recirculation begins and gravity driven recirculation is required to provide injection flow. By changing the RNS water supply to outside containment, its potential adverse interaction can be prevented. In the AP1000, RNS operation will result in a less limiting condition than no RNS operation because the drain down of the IRWST will not be enhanced by the RNS pump and the recirculation water level will be higher because of the additional water injected from outside containment. The PXS/CVS room curbs have been increased to allow for the higher recirculation levels and to prevent flooding of the PXS valves before the recirculation valves actuate.

Table 2.1-5 compares the AP600 and the AP1000 containment recirculation conditions. The assumed RCS pressure (versus containment) is typical of the containment recirculation start conditions.

Note that the "desired" flow is adjusted from the AP600 DVI LOCA case with RNS operation. This flow is ratioed based on the difference in decay heat levels accounting for both rated core power and recirculation initiation times. As seen the AP1000 case without RNS operation has a longer time to recirculation than the AP600 (2.67 vs. 2.10 hr) which reduces the decay heat fraction so that the "desired" flow is shown as 159 percent, where-as the core power ratio is 176 percent.

The AP1000 case with RNS operation shown above is less limiting than the case without RNS operation. The reason is that the RNS takes water from outside containment instead of from the IRWST. As a result the IRWST drains about the same with or without RNS operation and RNS operation adds water to the containment which increases the recirculation level above the case without RNS operation.

The AP1000 case without RNS operation in the above table shows longer time until recirculation than the limiting AP600 case with RNS operation (2.67 hr without AP1000 RNS operation versus 2.10 hr with AP600 RNS operation), although this time is faster than the comparable AP600 case (without RNS operation). The reason for this is that the AP1000 has incorporated larger IRWST injection lines that result in greater spill of water to the containment during a DVI LOCA. Note that the AP1000 has incorporated features (discussed above) to raise the water level at the time of recirculation by [ ]^{a,b,c}. This results in an increase in net

recirculation driving pressure of 109 percent [ ]^{a,b,c}. The following shows the calculation of the increased recirculation flow capabilities:

With RNS operation:

Flow ratio = (DP ratio/resistance ratio) ^ 0.5

= (256%/39%) ^ 0.5 = 256%

Without RNS operation:

Flow ratio = (DP ratio/resistance ratio) ^ 0.5

= (209%/39%) ^ 0.5 = 231%

As shown in Table 2.1-5 the flow ratio with RNS operation is greater than the flow ratio without RNS operation. Since the desired flow ratio is about the same (159 percent), the case without RNS operation is the limiting case.

Based on this evaluation, the AP1000 containment recirculation capability should provide increased margin relative to the AP600 design. Preliminary AP1000 long term cooling safety analyses presented in Section 3.0 of Reference 1 support this conclusion.

2.1.6 Automatic Depressurization System

The primary parameter of interest in the ADS feature is the non-choked flow capability of the ADS-4 lines. The reason for this is that these lines provide essentially all of the ADS vent flow at the time of IRWST injection cut-in and afterwards during long term cooling (IRWST injection and containment recirculation). The reasons the ADS stages 1-3 (ADS-1/2/3) are ineffective at these low pressure conditions are:

- Their flow resistance is much greater.
- They discharge through the ADS spargers, which are located approximately 10 ft under water, increasing their backpressure.
- Venting through these ADS valves tends to drag water from the hot legs up into the pressurizer where it gets trapped, increasing their backpressure.

The nominal line size for the ADS-4 lines has been increased from 10 to 14 inches in order to reduce the flow resistance. In addition, the line size common to each pair of ADS-4 lines has been increased from [ ]^{a,b,c}. This change results in the flow resistance being reduced to about 28 percent of the AP600 system resistance. This change also increases the ADS-4 vent flow area 76 percent, which is the same increase as the core power increase.

Table 2.1-6 shows the effect of this reduction in flow resistance on the ADS-4 vent capacity.

The flow ratio shown in Table 2.1-6 was calculated in the same manor as previously using the Darcy formula. In this case it is assumed that the differential pressure between the core and the containment is the same. This is conservative because the elevation of the hot leg and ADS-4 discharge are the same, the IRWST injection/recirc capability are greater (tends to support a greater DP), and the ADS-4 vent flow ratio is greater than the core power ratio (tends to support a greater DP).

Flow ratio = (1/resistance ratio) ^ 0.5 = (1/28%) ^ 0.5 = 189%

Note that this calculation does not include velocity head, which is important in this line because of the large change in steam velocity from the hot leg to the discharge. Since the AP1000 valve vent area ratio is equal to the core power ratio, the velocity head loss will be the same if the vent flow is the same per megawatt. In the case shown above, the vent flow is calculated to be somewhat greater which would increase the velocity head and reduce the increase in flow ratio. The reduction in the flow ratio from this effect is not expected to be significant.

This evaluation shows that the ADS-4 low pressure, non-choked, vent flow capability has been increased greater than the core power increase of 176 percent. As a result, this feature should provide increased margins relative to the AP600 design. Preliminary AP1000 small LOCA safety analyses presented in Section 3.0 of Reference 1 support this conclusion.

2.1.7 Passive Core Cooling System Margin Assessment

Various changes have been made to the passive core cooling features in the AP1000 in order to increase the performance of the passive core cooling system to accommodate the increase in power from the AP600. These design changes have impacted the scaling of the AP1000 to the tests that were performed in support of the AP600 Design Certification. The effect of these changes on the scaling is presented in Section 4 of this report. In a broad sense the net result of all of the design changes is to make the AP1000 scaling results very similar to the AP600 scaling results. Phenomenon which were scaled well for the AP600 remain well scaled for the AP1000 and phenomenon which were not scaled well for the AP600 remain poorly scaled for the AP1000. While the design changes to the AP1000 passive core cooling systems were driven by the need to improve the safety system performance to handle the increase in core power, the changes had an additional effect of reducing the impact of the large core power increase on the scaling of the AP1000 plant to the tests run in support of the AP600 Design Certification.

Table 2.1-1 Comparison of AP600 and AP1000 – PRHR Parameters

a,b,c

Table 2.1-2 Comparison of AP600 and AP1000 – Large-Break LOCA PCT

a,b,c

[

Table 2.1-3 Comparison of AP600 and AP1000 – CMT Injection Capability		

] a,b,c

[

Table 2.1-4 Comparison of AP600 and AP1000 – IRWST Injection Capability		

] a,b,c

a,b,c

Table 2.1-5 Comparison of AP600 and AP1000 Containment Recirculation Conditions

Table 2.1-6 Comparison of AP600 and AP1000 – ADS-4 Vent Capacity a,b,c

2.2 AP600 PIRT BACKGROUND

The important thermal-hydraulic phenomena for modeling system performance during various design basis accidents are identified and ranked in Phenomena Identification and Ranking Tables (PIRT). The development of a PIRT is described in the Code Scaling, Applicability, and Uncertainty (CSAU) methodology (Reference 2). The PIRT is useful for developing road maps to computer code models and correlations for a conservative design basis accident (DBA) calculation and to document the methodology in accordance with Title 10 of the Code of Federal Regulations Part 52.47(b)(2)(i)(A), subparagraphs (1) and (3).

Five separate PIRT were developed as part of the AP600 licensing effort as follows:

- Large-break LOCA (WCAP-14171, Rev. 2) (Reference 3)
- Small-break LOCA (WCAP-14807, Rev. 5) (Reference 4)
- Long-term cooling (WCAP-14727, Rev. 1) (Reference 5)
- Non-LOCA transient (WCAP-14234, Rev. 1) (Reference 6)
- Containment (WCAP-14845, Rev. 3) (Reference 7)

Design changes were made to the AP1000 as discussed in Reference 1 and Section 2.1 of this report. Although the capacities of systems and components have been adjusted to accommodate the higher core power of the AP1000, the basic configuration of the passive safety systems have been maintained. Analyses presented in Reference 1 generally show similar performance of the AP1000 and AP600 passive safety systems. Due to the similarities of the two designs, it is expected that the AP600 PIRT will be similar to the AP1000.

The AP600 PIRT were developed by a cross-section of nuclear industry experts and Westinghouse thermal-hydraulic experts. They were reviewed and approved during the AP600 Design Certification by the USNRC and members of the ACRS. For this report, the AP600 PIRT were re-evaluated by Westinghouse thermal-hydraulic experts, and by six of the nuclear industry experts that participated in the AP600 Design Certification program.

The industry experts are:

- Dr. S. M. Bajorek, Department of Nuclear and Mechanical Engineering, Kansas State University
- Dr. S. G. Bankoff, Department of Chemical Engineering, Northwestern University
- Dr. L. E. Hochreiter, Department of Mechanical and Nuclear Engineering, Penn State University
- Dr. T. K. Larson, Engineering Fellow, Bechtel BWXT Idaho, LLC, Idaho National Engineering & Environmental Laboratory
- Dr. P. F. Peterson, Department of Nuclear Engineering, University of California

- Mr. G. E. Wilson, Consulting Engineer, Bechtel BWXT Idaho, LLC, Idaho National Engineering & Environmental Laboratory

In the following sections, the AP1000 PIRT are presented and compared to the AP600 PIRT. Westinghouse system engineers and thermal-hydraulic analysts familiar with the AP600 developed the PIRT for AP1000. Significant comments from the outside experts are discussed and reconciliation of these comments is presented. In some cases, the AP1000 PIRT was adjusted. In other cases, design features and AP1000 operating characteristics were evaluated and changes to the plant design were incorporated. These changes have been incorporated in the design described in Reference 1 and the design margin assessment presented in Section 2.1 of this report.

2.3 AP1000 LARGE-BREAK LOCA PIRT

The AP600 large-break LOCA PIRT is shown in Table 2.3-1. The AP600 large-break LOCA PIRT is divided into three transient phases: blowdown, refill and reflood. The long term cooling phases (IRWST injection and sump recirculation) are considered in a separate PIRT.

The AP600 plant large-break LOCA process rankings are compared with the CSAU expert rankings (developed for a Westinghouse four-loop plant) and the Westinghouse rankings for three-and four-loop operating PWRs. Only the high (7-9) and medium (4-6) rankings are shown.

The AP1000 plant design is described and compared with the AP600 in Reference 1. A number of the AP1000 design changes would affect the large-break LOCA transient response. The increase in the vessel, pressurizer and SG tube volumes increases the RCS initial mass and results in a longer blowdown period.

The increase in core power level would increase the post-blowdown steaming rate. This would increase the pressure drop and could potentially decrease the reflood rate and make the transition to IRWST injection more difficult. The increase in core height (from 12 to 14 feet) could result in a longer time to quench the core during reflood. The increase in the fourth stage ADS line size permits an increase in the post-blowdown steam release rate to offset the higher core steam generation rate. This, in combination with increases in the injection piping sizes should help maintain core cooling during the IRWST injection and sump recirculation phases.

The accumulator discharge is ranked 9 for AP600 and Dr. Hochreiter thought it should remain high for the AP1000 as well. The large-break LOCA CMT phenomena are not currently modeled in the AP600 PIRT. Dr. Hochreiter thought Westinghouse should add the CMT phenomena to the AP1000 large-break LOCA PIRT.

Dr. Bajorek commented that "with the higher core power in AP1000, it is likely that the second reflood PCT will be higher than the AP600." Therefore, for the reflood period, Dr. Bajorek suggested the reflood heat transfer process ranking, which was assigned a '7' in AP600, be increased to an '8' for AP1000. Dr. Bajorek also suggested the core entrainment/de-entrainment process ranking be increased from a '6' to a '7' to account for the power increase. He noted that with these changes, the AP1000 large-break LOCA rankings would still remain below those for conventional plants.

The AP1000 large-break LOCA PIRT is shown in Table 2.3-2. The expert review comments were incorporated in the PIRT. In Reference 5, conclusions regarding the AP600 LBLOCA PIRT were that "the new and additional passive systems, which have been added to the AP600 (CMTs, IRWST, ADS), do no contribute to the core cooling in the short term, nor do they influence the calculated PCT for the large-break transient. The PRHR can condense steam, which will enhance the AP600 reflood for some time period; however, it is not essential to an acceptable calculation of the PCT. The effect of the downcomer injection location for the AP600 has been addressed with specific additional code validation, which is contained in the WCOBRA/TRAC code applicability document." Based on the review of the AP1000 PIRT, these conclusions remain valid for the AP1000 LBLOCA PIRT.

Table 2.3-1 PIRT for Large-Break Processes Current Plants Versus AP600

Process	Blowdown			Refill			Reflood		
	EXPERT	AP600	W3&4 LOOP	EXPERT	AP600	W3&4 LOOP	EXPERT	AP600	W3&4 LOOP
Fuel Rod									
Stored energy	9	9	9		5	5			
Oxidation							8	5	7
Decay heat					5	5	8	8	8
Reactivity - Void		6	6						
Reactivity - Boron								5	5
Gap conductance		8	8				8		
Core[1]									
DNB		8	8						
Post-CHF	7	8	8	8	8	8			
Rewet	8	7	6	7	5	5			
Reflood heat transfer							9	7	9
Nucleate boiling									
1-phase vapor natural circulation									
3-D flow		7	7				9	5	5
Void generation/ distribution		7	7				9		
Entrainment/ de-entrainment								6	8
Flow reversal/ stagnation		8	8						
Radiation heat transfer									
Level								8	8
Upper Head									
Initial water temperature		8	5						
Flow path area		8	5						
Blowdown flow		8	5						
Upper Plenum									
Hot assembly location	–	7	7						
Entrainment/ de-entrainment							9	6	6
Phase separation								6	6
Counter current flooding (CCF) drain/fallback									
2-phase convection									

Table 2.3-1 PIRT for Large-Break Processes Current Plants Versus AP600 (cont.)

Process	Blowdown			Refill			Reflood		
	EXPERT	AP600	W3&4 LOOP	EXPERT	AP600	W3&4 LOOP	EXPERT	AP600	W3&4 LOOP
Hot Leg									
Entrainment/ de-entrainment							9		
Flow reversal		5	5						
Void distribution									
2-phase convection									
Pressurizer									
Early quench/flow	7	5	5						
Critical flow in surge line									
Flashing									
ADS interaction		N/A			N/A			N/A	
Steam Generator									
Steam binding							9	7	7
Delta P, form losses									
PRHR		–			–			–	
Pump									
2-phase performance	9	5	5						
Delta P, form losses		8	8		5	5	8	7	7
Cold Leg/Accumulator									
Condensation				9	N/A	8		–	5
Noncondensible gases							9	5	5
Discharge					8	8		9	6
Flow asymmetries		6	5						
High pressure injection (HPI) mixing									
CMT mixing/ interaction		–			N/A			N/A	
Downcomer									
Entrainment/ de-entrainment				8	8	8		6	7
Condensation				9	8	8			
Countercurrent, slug, nonequilibrium					8	8			
Hot wall (vessel/barrel)				5			7	7	7
Hot wall (radial reflector)								5	

Table 2.3-1 PIRT for Large-Break Processes Current Plants Versus AP600 (cont.)

Process	Blowdown			Refill			Reflood		
	EXPERT	AP600	W3&4 LOOP	EXPERT	AP600	W3&4 LOOP	EXPERT	AP600	W3&4 LOOP
2-phase convection									
Saturated nucleate boiling									
3-D effects		5	5	9	8	8			
Flashing									
Liquid level oscillations								7	7
Direct vessel injection - Accumulator	–				8			7	–
IRWST mixing	–	N/A			N/A			N/A	–
CMT mixing/ interaction	–	–			N/A			N/A	–
Lower Plenum									
Sweep-out				7	6	6			
Hot wall								7	7
Multidimensional effects									
Break									
Critical flow	9	9	9	7	6	6			
Flashing									
Containment pressure								6	8
ADS flow	–	N/A	–	–	N/A			N/A	–
Loop									
2-phase delta-P	7								
Oscillations				7					
Flow split		8	8	7	5	5	–		

Note:

1. Core heat transfer includes the effects of spacer grids.

Table 2.3-2 PIRT for Large-Break Processes for AP1000			
Process	**Blowdown**	**Refill**	**Reflood**
Fuel Rod			
Stored energy	9	5	
Oxidation			5
Decay heat		5	8
Reactivity - Void	6		
Reactivity - Boron			5
Gap conductance	8		
Core[1]			
DNB	8		
Post-CHF	8	8	
Rewet	7	5	
Reflood heat transfer			8
Nucleate boiling			
1-phase vapor natural circulation			
3-D flow	7		5
Void generation/distribution	7		
Entrainment/de-entrainment			7
Flow reversal/stagnation	8		
Radiation heat transfer			
Level			8
Upper Head			
Initial water temperature	8		
Flow path area	8		
Blowdown flow	8		
Upper Plenum			
Hot assembly location	7		
Entrainment/de-entrainment			6
Phase separation			6
Counter current flooding (CCF) drain/fallback			
2-phase convection			

Table 2.3-2 PIRT for Large-Break Processes for AP1000 (cont.)			
Process	**Blowdown**	**Refill**	**Reflood**
Hot Leg			
Entrainment/de-entrainment			
Flow reversal	5		
Void distribution			
2-phase convection			
Pressurizer			
Early quench/flow	5		
Critical flow in surge line			
Flashing			
ADS interaction	N/A	N/A	N/A
Steam Generator			
Steam binding			7
Delta P, form losses			
PRHR	–	–	–
Pump			
2-phase performance	5		
Delta P, form losses	8	5	7
Cold Leg/ Accumulator			
Condensation		N/A	–
Noncondensible gases			5
Discharge		8	9
Flow asymmetries	6		
High pressure injection (HPI) mixing			
CMT mixing/interaction	–	N/A	N/A
Downcomer			
Entrainment/de-entrainment		8	6
Condensation		8	
Countercurrent, slug, nonequilibrium		8	
Hot wall (vessel/barrel)			7

Table 2.3-2 PIRT for Large-Break Processes for AP1000 (cont.)

Process	Blowdown	Refill	Reflood
Hot wall (radial reflector)			5
2-phase convection			
Saturated nucleate boiling			
3-D effects	5	8	
Flashing			
Liquid level oscillations			7
Direct vessel injection - Accumulator		8	7
IRWST mixing	N/A	N/A	N/A
CMT mixing/interaction	–	N/A	N/A
Lower Plenum			
Sweep-out		6	
Hot wall			7
Multidimensional effects			
Break			
Critical flow	9	6	
Flashing			
Containment pressure			6
ADS flow	N/A	N/A	N/A
Loop			
2-phase delta-P			
Oscillations			
Flow split	8	5	

Note:

1. Core heat transfer includes the effects of spacer grids.

Bold - Ranking increased for AP1000

2.4 AP1000 SMALL-BREAK LOCA PIRT

The AP600 small-break LOCA PIRT was merged with the AP600 long term cooling PIRT to create the combined PIRT shown in Table 2.4-1. Similar phenomena that were ranked higher in the long-term cooling PIRT than the small-break LOCA PIRT were left higher in the combined PIRT. The combined PIRT is warranted since sump injection is the final phase of the small-break LOCA recovery transient. The combined PIRT is divided into five transient phases: blowdown, natural circulation, ADS blowdown, IRWST injection cooling, and sump injection.

The AP1000 plant design is described and compared with the AP600 in Reference 1. A number of the AP1000 design changes affect the small-break LOCA and long-term cooling transient response. The increase in core power level increases the post-blowdown steaming rate. This increases the pressure drop and could potentially make the transition to IRWST injection more difficult. The increase in the fourth stage ADS line size allows for an increase in the post-blowdown steam release rate. This, in combination with increases in the injection piping sizes helps during the IRWST injection and sump recirculation phases.

Dr. Hochreiter suggested that the ranking for the ADS-1/2/3 two-phase pressure drop and valve loss coefficient phenomena be increased to 'M' for both the IRWST injection cooling and sump injection phases due to the higher core steam generation rate for AP1000. Dr. Hochreiter also suggested that during the IRWST injection cooling phase, the ADS-4 subsonic and two-phase flow phenomena should be increased in rank from 'M' to 'H'. Even though the ADS-4 flow area is larger, IRWST injection could be lost if the RCS begins to pressurize, so the pressure drop of this system is most important. Based on what was observed in the OSU experiments, Dr. Hochreiter suggested an additional phenomenon be added to the ADS-4 list, chugging/intermittent flow. He recommended that this should be ranked 'H' during both the IRWST injection cooling and sump injection phases, at least until Westinghouse has had a chance to examine the NRC sponsored ROSA test data to determine a more appropriate value.

A higher two-phase pressure drop within the Vessel/Core region (due to the increased core steam generation) will extend the AP1000 ADS blowdown phase longer than the AP600. Therefore, Dr. Hochreiter suggested that the Vessel/Core Resistance phenomena ranking should be increased from 'L' to either 'M' or 'H' during the ADS blowdown and IRWST injection cooling phases and 'M' during the sump injection phase.

Dr. Hochreiter suggested that the CMT draining effects condensation, circulation wall heat transfer, and balance line pressure drop phenomena be revised from 'N/A' to 'L' for both the AP600 and AP1000 during the IRWST injection cooling and sump injection phases since continued condensation due to heat losses occurred in both the OSU and ROSA experiments.

The Hot Leg Entrainment phenomena ranking may be more important for AP1000 during the ADS blowdown period due to the higher core steam generation rate. Likewise, entrainment and de-entrainment in the upper plenum and countercurrent flow in the hot legs during the IRWST and sump injection periods may also be more important in the AP1000 design. This may delay the pressurizer draining and increase the two-phase pressure drop through the ADS-4 valves. This could limit the IRWST injection flow rate. Dr. Hochreiter suggested that the

ranking for the hot leg countercurrent flow phenomena during the IRWST injection period be changed from 'N/A' to 'L' or 'M' and both Dr. Hochreiter and Dr. Bajorek suggested the ranking for entrainment in the upper plenum be changed from 'M' to 'H'. Similarly, Dr. Bajorek suggested that the ranking for hot leg entrainment phenomena during the ADS blowdown period be increased from 'M' to 'H'.

The DVI line pressure drop phenomena is ranked 'M' during all phases. Dr. Hochreiter suggested that this might be more important with the higher core steam generation rate for AP1000.

Both Dr. Hochreiter and Dr. Bajorek suggested that the pressurizer surge line flooding and pressure drop phenomena could be more important during the IRWST injection phase with the higher core steam generation rate for AP1000. Even though the pressurizer volume is larger, the surge line diameter was not increased. The surge line could remain flooded for a longer period and delay draining of the pressurizer. Water that does not drain from the pressurizer could be swept through the ADS-4 lines resulting in a larger pressure drop that could subsequently impact the IRWST injection flow rate into the vessel. Dr. Hochreiter suggested that the ranking should be increased from 'N/A' to either 'L' or 'M' during the IRWST injection phase. Dr. Bajorek suggested that if pressurizer inventory was important in preventing core uncovery in AP600 during the ADS blowdown and IRWST injection phases, then this ranking should be 'H' for the AP1000. Dr. Hochreiter agreed, but suggested the pressurizer level should be ranked 'M'.

The AP1000 small-break LOCA PIRT is shown in Table 2.4-2. The expert review comments were incorporated in the PIRT with the exception of Dr. Hochreiter's suggestion to add an additional ADS-4 phenomenon for chugging/intermittent flow. This phenomenon is already addressed via other processes such as entrainment two-phase pressure drop and flow pattern transition in the hot leg and ADS-4. These processes are already ranked 'H'.

In conclusion, no new phenomena were identified for AP1000. The Blowdown, Natural Circulation, and ADS Blowdown phases were unchanged from AP1000. A few unranked or low-ranked phenomena were re-ranked as 'low' or 'medium' importance for the IRWST Injection Cooling phase and Sump Injection phase. Hot leg entrainment was re-ranked from 'medium' to 'high' for these phases. These phenomena were considered in AP600 scaling and code applicability. See Section 2.7 for a discussion regarding the application of the AP1000 PIRT in the scaling studies presented in this report.

Scaling of these phenomena for AP600 and AP1000 is presented in Section 4 of this report. These scaling studies show that the test facilities are adequately scaled to simulate entrainment in the hot legs that may be experienced in the AP1000.

Table 2.4-1 PIRT for AP600 Small-Break Loss-of-Coolant Accident

Component Phenomenon	Blowdown	Natural Circulation	ADS Blowdown	IRWST Injection Cooling	Sump Injection
ADS Stages 1-3					
Critical Flow	H (inadvertent ADS)	H (inadvertent ADS)	H	M	N/A
Subsonic Flow				M	L
Two-Phase Pressure Drop	N/A	N/A	H	L	L
Valve Loss Coefficients	N/A	N/A	H	M	L
Single-Phase Pressure Drop	N/A	N/A	N/A	M	L
ADS-4					
Critical Flow	N/A	N/A	N/A	H	N/A
Subsonic Flow	N/A	N/A	N/A	H	H
Two-Phase Pressure Drop	N/A	N/A	N/A	M	H
Break					
Line Resistance	N/A	N/A	L	L	N/A
Critical Flow (in complex geometries)	H	H	H	M	N/A
Subsonic Flow	N/A	N/A	L	M	L
Discharge Coefficient	M	M	L	L	L
Accumulators					
Injection Flow Rate	N/A	M	H	N/A	N/A
Noncondensible Gas Entrainment	N/A	N/A	L	L	N/A
Cold Legs					
Flashing or Condensation	N/A	N/A	L	L	L
Cold Leg Balance Line-to-Cold Leg Tee	N/A	H	H	L	N/A
Phase Separation	N/A	H	H	L	L
Stored Energy Release	N/A	L	N/A	L	L
Vessel/Core					
Decay Heat	H	H	H	H	H
Forced Convection	M	N/A	N/A	N/A	N/A
Flashing	M	N/A	M	L	N/A
Wall Stored Energy	M	N/A	M	M	M
Natural Circulation Flow and Heat Transfer	M	M	M	M	M
Mixture Level Mass Inventory	H	H	H	H	H
Mass Flow	M	M	L	L	L
Flow Resistance	L	L	L	L	L

Table 2.4-1 PIRT for AP600 Small-Break Loss-of-Coolant Accident (cont.)

Component Phenomenon	Blowdown	Natural Circulation	ADS Blowdown	IRWST Injection Cooling	Sump Injection
CMT Draining Effects					
Condensation on Cold Thick Steel Surfaces	N/A	N/A	M	N/A	N/A
Transient Conduction in CMT Walls	L	L	M	N/A	N/A
Interfacial Condensation on CMT Water Surface (break-size dependent)	N/A	N/A	H	N/A	N/A
Dynamic Effects of Steam Injection and Mixing with CMT Liquid and Condensate	N/A	N/A	H	N/A	N/A
Thermal Stratification and Mixing of Warmer Condensate with Colder CMT Water	L	H	H	N/A	N/A
CMT Circulation					
Natural Circulation of CMT and Cold Leg Balance Line	H	H	N/A	N/A	N/A
Liquid Mixing of Cold Leg Balance Line, Condensate, and CMT Liquid	H	H	N/A	N/A	N/A
Flashing Effects of Hot CMT Liquid Layer	N/A	L	M	N/A	N/A
CMT Wall Heat Transfer	L	M	M	N/A	N/A
CMT Balance Lines					
Pressure Drop	M	H	H	N/A	N/A
Flow Composition	M	H	H	L	L
Downcomer/Lower Plenum					
Flashing or Condensation	N/A	N/A	L	M	M
Level	M	M	H	H	H
Loop Asymmetry Effects	M	M	L	L	L
Stored Energy Release	L	L	L	L	L
Hot Legs					
Countercurrent Flow	N/A	L	L	N/A	L
Entrainment	L	L	M	M	M
Flashing	L	L	L	N/A	N/A
Horizontal Fluid Stratification	N/A	M	M	M	M
Flow Pattern Transition				H	H
Phase Separation in Tees	N/A	M	M	H	H
IRWST					
Discharge Line Flashing	N/A	N/A	N/A	N/A	N/A
Temperature Distribution	L	M	L	M	M
Pool Level	N/A	M	L	H	H
Gravity Draining	N/A	N/A	N/A	H	M
Vapor Condensation	N/A	M	M	L	L
DVI Line Pressure Drop (flow resistance)	M	M	M	M	M

Table 2.4-1 PIRT for AP600 Small-Break Loss-of-Coolant Accident (cont.)

Component Phenomenon	Blowdown	Natural Circulation	ADS Blowdown	IRWST Injection Cooling	Sump Injection
Pressurizer					
CCFL	N/A	N/A	M	N/A	N/A
Entrainment/De-entrainment	N/A	N/A	M	N/A	N/A
Flashing	H	N/A	M	N/A	N/A
Level (inventory)	M	M	M	L	N/A
Level Swell	M	L	M	N/A	N/A
Stored Energy Release	L	L	L	L	N/A
Vapor Space Behavior	N/A	N/A	L	N/A	N/A
Pressurizer Surge Line					
Pressure Drop	L	L	M	L	L
Flooding	L	L	M	N/A	N/A
Steam Generator					
Two-Phase Natural Circulation	M	M	N/A	N/A	N/A
Steam Generator Heat Transfer	M	M	L	N/A	N/A
Secondary Conditions	L	M	L	N/A	N/A
U-Tube Condensation	L	L	N/A	N/A	N/A
Secondary Level	L	M	N/A	N/A	N/A
Secondary Pressure	M	M	N/A	N/A	N/A
Steam Generator Tube Draining	L	M	N/A	N/A	N/A
PRHR					
Single-Phase Heat Transfer	M	M	N/A	N/A	N/A
Two-Phase Heat Transfer Condensation	N/A	M	L	N/A	N/A
Noncondensible Gas Effects	N/A	N/A	L	N/A	N/A
Recirculation Flow	M	M	L	N/A	N/A
Upper Head/Upper Plenum					
Draining Effects	L	M	M	N/A	M
Flashing	L	N/A	M	N/A	N/A
Mixture Level	H	H	H	H	H
Entrainment/De-entrainment	N/A	L	M	M	M
RCP					
Coast Down	L	N/A	N/A	N/A	N/A
Flow Resistance	L	L	N/A	N/A	N/A
Sump					
Gravity Drain	N/A	N/A	N/A	N/A	H
Level	N/A	N/A	N/A	N/A	H
Temperature	N/A	N/A	N/A	N/A	H

Table 2.4-2 PIRT for AP1000 Small-Break Loss-of-Coolant Accident

Component Phenomenon	Blowdown	Natural Circulation	ADS Blowdown	IRWST Injection Cooling	Sump Injection
ADS-1/2/3					
Critical Flow	H (inadvertent ADS)	H (inadvertent ADS)	H	M	N/A
Subsonic Flow				M	L
Two-Phase Pressure Drop	N/A	N/A	H	M	M
Valve Loss Coefficients	N/A	N/A	H	M	L
Single-Phase Pressure Drop	N/A	N/A	N/A	M	L
ADS-4					
Critical Flow	N/A	N/A	N/A	H	N/A
Subsonic Flow	N/A	N/A	N/A	H	H
Two-Phase Pressure Drop	N/A	N/A	N/A	H	H
Break					
Line Resistance	N/A	N/A	L	L	N/A
Critical Flow (in complex geometries)	H	H	H	M	N/A
Subsonic Flow	N/A	N/A	L	M	L
Discharge Coefficient	M	M	L	L	L
Accumulators					
Injection Flow Rate	N/A	M	H	N/A	N/A
Noncondensible Gas Entrainment	N/A	N/A	L	L	N/A
Cold Legs					
Flashing or Condensation	N/A	N/A	L	L	L
Cold Leg Balance Line-to-Cold Leg Tee	N/A	H	H	L	N/A
Phase Separation	N/A	H	H	L	L
Stored Energy Release	N/A	L	N/A	L	L
Vessel/Core					
Decay Heat	H	H	H	H	H
Forced Convection	M	N/A	N/A	N/A	N/A
Flashing	M	N/A	M	L	N/A
Wall Stored Energy	M	N/A	M	M	M
Natural Circulation Flow and Heat Transfer	M	M	M	M	M
Mixture Level Mass Inventory	H	H	H	H	H
Mass Flow	M	M	L	L	L
Flow Resistance	L	L	L	M	M

Table 2.4-2 PIRT for AP1000 Small-Break Loss-of-Coolant Accident (cont.)

Component Phenomenon	Blowdown	Natural Circulation	ADS Blowdown	IRWST Injection Cooling	Sump Injection
CMT Draining Effects					
Condensation on Cold Thick Steel Surfaces	N/A	N/A	M	L	L
Transient Conduction in CMT Walls	L	L	M	N/A	N/A
Interfacial Condensation on CMT Water Surface (break-size dependent)	N/A	N/A	H	N/A	N/A
Dynamic Effects of Steam Injection and Mixing with CMT Liquid and Condensate	N/A	N/A	H	N/A	N/A
Thermal Stratification and Mixing of Warmer Condensate with Colder CMT Water	L	H	H	N/A	N/A
CMT Circulation					
Natural Circulation of CMT and Cold Leg Balance Line	H	H	N/A	N/A	N/A
Liquid Mixing of Cold Leg Balance Line, Condensate, and CMT Liquid	H	H	N/A	N/A	N/A
Flashing Effects of Hot CMT Liquid Layer	N/A	L	M	N/A	N/A
CMT Wall Heat Transfer	L	M	M	L	L
CMT Balance Lines					
Pressure Drop	M	H	H	L	L
Flow Composition	M	H	H	L	L
Downcomer/Lower Plenum					
Flashing or Condensation	N/A	N/A	L	M	M
Level	M	M	H	H	H
Loop Asymmetry Effects	M	M	L	L	L
Stored Energy Release	L	L	L	L	L
Hot Legs					
Countercurrent Flow	N/A	L	L	L	L
Entrainment	L	L	H	H	H
Flashing	L	L	L	N/A	N/A
Horizontal Fluid Stratification	N/A	M	M	M	M
Flow Pattern Transition				H	H
Phase Separation in Tees	N/A	M	M	H	H
IRWST					
Discharge Line Flashing	N/A	N/A	N/A	N/A	N/A
Temperature Distribution	L	M	L	M	M
Pool Level	N/A	M	L	H	H
Gravity Draining	N/A	N/A	N/A	H	M
Vapor Condensation	N/A	M	M	L	L
DVI Line Pressure Drop (flow resistance)	M	M	M	M	M

Table 2.4-2 PIRT for AP1000 Small-Break Loss-of-Coolant Accident (cont.)

Component Phenomenon	Blowdown	Natural Circulation	ADS Blowdown	IRWST Injection Cooling	Sump Injection
Pressurizer					
CCFL	N/A	N/A	M	N/A	N/A
Entrainment/De-entrainment	N/A	N/A	M	N/A	N/A
Flashing	H	N/A	M	N/A	N/A
Level (inventory)	M	M	M	**M**	N/A
Level Swell	M	L	M	N/A	N/A
Stored Energy Release	L	L	L	L	N/A
Vapor Space Behavior	N/A	N/A	L	N/A	N/A
Pressurizer Surge Line					
Pressure Drop	L	L	M	L	L
Flooding	L	L	M	M	N/A
Steam Generator					
Two-Phase Natural Circulation	M	M	N/A	N/A	N/A
Steam Generator Heat Transfer	M	M	L	N/A	N/A
Secondary Conditions	L	M	L	N/A	N/A
U-Tube Condensation	L	L	N/A	N/A	N/A
Secondary Level	L	M	N/A	N/A	N/A
Secondary Pressure	M	M	N/A	N/A	N/A
Steam Generator Tube Draining	L	M	N/A	N/A	N/A
PRHR					
Single-Phase Heat Transfer	M	M	N/A	N/A	N/A
Two-Phase Heat Transfer Condensation	N/A	M	L	N/A	N/A
Noncondensible Gas Effects	N/A	N/A	L	N/A	N/A
Recirculation Flow	M	M	L	N/A	N/A
Upper Head/Upper Plenum					
Draining Effects	L	M	M	N/A	M
Flashing	L	N/A	M	N/A	N/A
Mixture Level	H	H	H	H	H
Entrainment/De-entrainment	N/A	L	M	**H**	M
RCP					
Coast Down	L	N/A	N/A	N/A	N/A
Flow Resistance	L	L	N/A	N/A	N/A
Sump					
Gravity Drain	N/A	N/A	N/A	N/A	H
Level	N/A	N/A	N/A	N/A	H
Temperature	N/A	N/A	N/A	N/A	H

Note:

Bold - Ranking increased for AP1000

2.5 AP1000 NON-LOCA TRANSIENT PIRT

The AP600 non-LOCA transient PIRT is shown in Table 2.5-1. The AP600 non-LOCA transient PIRT is divided into 14 events. With the exception of the SGTR event, the other events are analyzed to show the system dynamic response to various heatup and cooldown transients. The criteria of interest for these events are the core integrity (margin to DNB), RCS integrity (pressurizer level and pressure) and offsite doses.

The AP1000 plant design is described and compared with the AP600 in Reference 1. A number of the AP1000 design changes affect the various non-LOCA transients. The increase in core power level relative to the flow coastdown rate following RCP trip could have reduced the margin to DNB. To address this, the AP1000 reactor coolant pump flow coastdown characteristics have been enhanced by the pump rotating inertia by a factor of 3. The analyses presented in Reference 1 demonstrate that the AP1000 flow at the time of minimum DNBR is higher than AP600.

The decrease in the pressurizer volume-to-power ratio and increase in SG secondary volume could make the RCS more sensitive to shrink and swell events. During an AP1000 cooldown event associated with either a steamline or feedwater line break, if the RCS pressure were to decrease enough to cause the CMTs to begin to inject, then the gravity drain injection and vapor condensation rate phenomena may become important. Dr. Hochreiter suggested that these phenomena should be ranked 'H' instead of 'N/A' for these events in the AP1000.

Westinghouse agrees that if the CMTs were to begin to inject (rather than recirculate) during the cooldown portion of the steam line or feed line break, then these phenomena would become important. Since it is not yet known if this will occur in the AP1000, Westinghouse recommends that the ranking for these phenomena be increased from 'N/A' to 'M' instead of 'H'. Note that for the AP600, this phenomenon was not predicted to occur during a steamline break or feedwater line break.

The revised AP1000 non-LOCA transient PIRT is shown in Table 2.5-2. The expert review comments have been incorporated into the PIRT. Section 2.7 provides a discussion of the application of the AP1000 PIRT in this report.

Table 2.5-1 PIRT for AP600 Non-LOCA and Steam Generator Tube Rupture Design Basis Analyses

Component & System Phenomena	(1) FW Malf	(2) ELI	(3) SLB	(4) Inad-vertent PRHR	(5) LOL	(6) Loss ac & LONF	(7) FLB	(8) Loss of RCS Flow	(9) LR & BS	(10) SUIL	(11) RWAP	(12) Inad-vertent CMT or CVS	(13) RCS Dep.	(14) SGTR
Critical Flow	N/A	N/A	H	N/A	N/A	N/A	H	N/A	N/A	N/A	N/A	N/A	H	H
Vessel														
Mixing	H	L	H	H	L	M	M	L	L	H	L	M	L	M
Flashing in Upper Head	N/A	N/A	M	N/A	N/A	L	L	N/A	N/A	N/A	N/A	L	L	L
Core														
Reactivity Feedback	H	M	H	H	M	L	M	M	M	H	M	L	L	L
Reactor Trip	H	L	H	L	H	H	H	H	H	H	H	H	H	H
Decay Heat	L	L	L	L	L	H	H	L	L	L	L	H	L	H
Forced Convection	H	H	H	H	H	H	H	H	H	H	H	M	H	L
Natural Circulation Flow and Heat Transfer	N/A	L	H	N/A	L	H	H	L	L	L	L	H	L	M
RCP Coastdown Performance	L	N/A	L	N/A	N/A	L	L	H	H	N/A	N/A	L	L	L
Pressurizer														
Pressurizer Fluid Level	L	L	M	L	L	H	L	L	L	L	L	H	L	M
Surge Line Pressure Drop	L	L	L	L	H	L	L	M	H	L	L	L	L	L
Steam Generator Heat Transfer	H	H	H	L	H	H	H	L	L	L	M	L	L	M
Secondary Conditions	M	L	H	L	L	M	M	L	L	L	L	L	L	H
RCS Wall Stored Heat	L	L	L	L	N/A	L	L	N/A	N/A	L	N/A	L	L	M
CMT														
Recirculation Injection	N/A	N/A	H	N/A	N/A	H	M	N/A	N/A	N/A	N/A	H	N/A	L
Gravity Draining Injection	N/A	N/A	N/A	N/A	N/A	N/A	N/A	N/A	N/A	N/A	N/A	N/A	N/A	N/A
Vapor Condensation Rate	N/A	N/A	N/A	N/A	N/A	N/A	N/A	N/A	N/A	N/A	N/A	N/A	N/A	N/A
Balance Line Pressure Drop	N/A	N/A	H	N/A	N/A	H	M	N/A	N/A	N/A	N/A	H	N/A	L
Balance Line Initial Temperature Distribution	N/A	N/A	H	N/A	N/A	H	M	N/A	N/A	N/A	N/A	H	N/A	L

Table 2.5-1 PIRT for AP600 Non-LOCA and Steam Generator Tube Rupture Design Basis Analyses (cont.)

Component & System Phenomena	(1) FW Malf	(2) ELI	(3) SLB	(4) Inad-vertent PRHR	(5) LOL	(6) Loss ac & LONF	(7) FLB	(8) Loss of RCS Flow	(9) LR & BS	(10) SUIL	(11) RWAP	(12) Inad-vertent CMT or CVS	(13) RCS Dep.	(14) SGTR
Accumulators														
Injection Flow Rate	N/A	N/A	M	N/A	N/A	N/A	N/A	N/A	N/A	N/A	N/A	N/A	N/A	N/A
PRHR														
Flow Rate and Heat Transfer	N/A	N/A	M	H	N/A	H	H	N/A	N/A	N/A	N/A	H	N/A	H
IRWST Initial Temperature	N/A	N/A	M	H	N/A	M	M	N/A	N/A	N/A	N/A	M	N/A	H
ADS	N/A	N/A	N/A	N/A	N/A	N/A	N/A	N/A	N/A	N/A	N/A	N/A	H	N/A

(1) FW Malf - Feedwater Malfunction that Results in a Decrease in Feedwater Temperature or an Increase in Feedwater Flow
(2) ELI - Excessive Increase in Secondary Steam Flow
(3) SLB - Steamline Break
(4) Inadvertent PRHR - Inadvertent Operation of the PRHR
(5) LOL - Loss of Secondary Side Load Events
(6) Loss ac & LONF - Loss of ac Power and Loss of Normal Feedwater
(7) FLB - Feedline Break
(8) Loss of RCS Flow - Loss of Forced RCS Flow
(9) LR & BS - Locked RCP Rotor and Broken RCP Shaft
(10) SUIL - Startup of an Inactive Reactor Coolant Pump at an Incorrect Temperature
(11) RWAP - RCCA Withdrawal at Power
(12) Inadvertent CMT or CVS - Inadvertent Operation of the CMT or Chemical and Volume Control System
(13) RCS Dep. - Inadvertent RCS Depressurization
(14) SGTR - Steam Generator Tube Rupture

H - High Importance M - Moderate Importance L - Low Importance N/A - Not Applicable

Table 2.5-2 PIRT for AP1000 Non-LOCA and Steam Generator Tube Rupture Design Basis Analyses

Component & System Phenomena	(1) FW Malf	(2) ELI	(3) SLB	(4) Inad-vertent PRHR	(5) LOL	(6) Loss ac & LONF	(7) FLB	(8) Loss of RCS Flow	(9) LR & BS	(10) SUIL	(11) RWAP	(12) Inad-vertent CMT or CVS	(13) RCS Dep.	(14) SGTR
Critical Flow	N/A	N/A	H	N/A	N/A	N/A	H	N/A	N/A	N/A	N/A	N/A	H	H
Vessel														
Mixing	H	L	H	H	L	M	M	L	L	H	L	M	L	M
Flashing in Upper Head	N/A	N/A	M	N/A	N/A	L	L	N/A	N/A	N/A	N/A	L	L	L
Core														
Reactivity Feedback	H	M	H	H	M	L	M	M	M	H	M	L	L	L
Reactor Trip	H	L	H	L	H	H	H	H	H	H	H	H	H	H
Decay Heat	L	L	L	L	L	H	H	L	L	L	L	H	L	H
Forced Convection	H	H	H	H	H	H	H	H	H	H	H	M	H	L
Natural Circulation Flow and Heat Transfer	N/A	L	H	N/A	L	H	H	L	L	L	L	H	L	M
RCP Coastdown Performance	L	N/A	L	N/A	N/A	L	L	H	H	N/A	N/A	L	L	L
Pressurizer														
Pressurizer Fluid Level	L	L	M	L	L	H	L	L	L	L	L	H	L	M
Surge Line Pressure Drop	L	L	L	L	H	L	L	M	H	L	L	L	L	L
Steam Generator Heat Transfer	H	H	H	L	H	H	H	L	L	L	M	L	L	M
Secondary Conditions	M	L	H	L	L	M	M	L	L	L	L	L	L	H
RCS Wall Stored Heat	L	L	L	L	N/A	L	L	N/A	N/A	L	N/A	L	L	M
CMT														
Recirculation Injection	N/A	N/A	H	N/A	N/A	H	M	N/A	N/A	N/A	N/A	H	N/A	L
Gravity Draining Injection	N/A	N/A	M	N/A	N/A	N/A	M	N/A	N/A	N/A	N/A	N/A	N/A	N/A
Vapor Condensation Rate	N/A	N/A	M	N/A	N/A	N/A	M	N/A	N/A	N/A	N/A	N/A	N/A	N/A
Balance Line Pressure Drop	N/A	N/A	H	N/A	N/A	H	M	N/A	N/A	N/A	N/A	H	N/A	L
Balance Line Initial Temperature Distribution	N/A	N/A	H	N/A	N/A	H	M	N/A	N/A	N/A	N/A	H	N/A	L

Table 2.5-2 PIRT for AP1000 Non-LOCA and Steam Generator Tube Rupture Design Basis Analyses (cont.)

Component & System Phenomena	(1) FW Malf	(2) ELI	(3) SLB	(4) Inad-vertent PRHR	(5) LOL	(6) Loss ac & LONF	(7) FLB	(8) Loss of RCS Flow	(9) LR & BS	(10) SUIL	(11) RWAP	(12) Inad-vertent CMT or CVS	(13) RCS Dep.	(14) SGTR
Accumulators														
Injection Flow Rate	N/A	N/A	M	N/A	N/A	N/A	N/A	N/A	N/A	N/A	N/A	N/A	N/A	N/A
PRHR														
Flow Rate and Heat Transfer	N/A	N/A	M	H	N/A	H	H	N/A	N/A	N/A	N/A	H	N/A	H
IRWST Initial Temperature	N/A	N/A	M	H	N/A	M	M	N/A	N/A	N/A	N/A	M	N/A	H
ADS	N/A	N/A	N/A	N/A	N/A	N/A	N/A	N/A	N/A	N/A	N/A	N/A	H	N/A

(1) FW Malf - Feedwater Malfunction that Results in a Decrease in Feedwater Temperature or an Increase in Feedwater Flow
(2) ELI - Excessive Increase in Secondary Steam Flow
(3) SLB - Steamline Break
(4) Inadvertent PRHR - Inadvertent Operation of the PRHR
(5) LOL - Loss of Secondary Side Load Events
(6) Loss ac & LONF - Loss of ac Power and Loss of Normal Feedwater
(7) FLB - Feedline Break
(8) Loss of RCS Flow - Loss of Forced RCS Flow
(9) LR & BS - Locked RCP Rotor and Broken RCP Shaft
(10) SUIL - Startup of an Inactive Reactor Coolant Pump at an Incorrect Temperature
(11) RWAP - RCCA Withdrawal at Power
(12) Inadvertent CMT or CVS - Inadvertent Operation of the CMT or Chemical and Volume Control System
(13) RCS Dep. - Inadvertent RCS Depressurization
(14) SGTR - Steam Generator Tube Rupture

H - High Importance M - Moderate Importance L - Low Importance N/A - Not Applicable

Bold – Ranking increased for AP1000

2.6 AP1000 CONTAINMENT PIRT

The AP600 containment PIRT for LOCA and main steam line break (MSLB) was documented in Reference 8. The high ranked phenomena in the AP600 PIRT were: the break source, condensation on the inside surfaces of the containment, evaporation from the outside surface of the containment shell, natural circulation flow through the PCS annulus, circulation and stratification, inter-compartment flow, source fog, and liquid film stability. The AP600 containment PIRT is shown in Table 2.6-1.

A comparison of the AP600 and AP1000 containment designs is documented in Reference 1. The main differences between the AP600 and AP1000 containment designs are the height (AP1000 is [ ]^{a,b,c} taller), the shell thickness (AP1000 is [ ]^{a,b,c}), and the shell material (AP1000 is using SA738, Grade B). The change in height affects the shell surface area and containment free volume and the changes in shell material and thickness allow an increase in the design pressure.

A comparison of the AP600 and AP1000 reactor designs is also documented in Reference 1. The main differences between the AP600 and AP1000 reactor designs that would affect a containment DBA mass and energy release are: the RCS volume, the SG volume, the initial conditions, and the power level. The pressurizer and SG primary side volume are both larger in AP1000; the RCS volume is about 1.35 times larger than AP600. The SG secondary side volume for AP1000 is about 1.7 times larger than AP600. The AP1000 reactor vessel inlet temperature is about [ ]^{a,b,c} higher and the outlet temperature is about [ ]^{a,b,c} higher. The AP1000 core power is about 1.75 times greater than the AP600.

The experts found that none of the geometrical or power density changes in the AP1000 design would alter the relative ranking of phenomena from the original AP600 containment PIRT. The basis for this conclusion was that none of the AP1000 design changes alters the method by which the passive containment cooling system operates. Therefore, they concluded that the AP600 containment PIRT could be applied to the AP1000.

An analytical confirmation of the high ranked phenomena identified in the AP600 containment PIRT was one of the objectives of the AP600 component level containment pressure scaling analysis that was documented in WCAP-14845, Rev. 3 (Reference 7). The containment and reactor coolant system design changes made to create the AP1000 primarily affect the component π group normalization parameters used in the component level containment pressure scaling analysis. The π group normalization parameters are: break mass, break energy, shell conductance, and buoyancy. The basis for selecting these normalization parameters for the scaling analysis is discussed in WCAP-14845, Rev. 3 (Reference 7).

The AP1000 DBA break mass and energy releases are expected to be higher, based on the differences in the reactor designs. The initial LOCA mass and energy inventory is larger than AP600 due to the larger RCS volume and higher temperatures of AP1000. The RCS piping sizes are the same, so the LOCA blowdown release rate should be about the same as AP600, however, it should take longer to complete blowdown due to the higher RCS volume. The higher decay heat will result in higher post-blowdown steam releases. With regard to MSLB,

the initial SG mass and energy inventory is larger than AP600 due to the larger SG volume and higher temperatures of AP1000. However, the steam line flow restricting orifice size has been maintained to reduce the impact on the mass and energy release for an MSLB accident.

The AP1000 containment shell resistance for conduction heat transfer will be higher than AP600 due to the increased thickness of the AP1000 containment shell. The AP1000 buoyancy normalization parameters (inside and outside containment) are higher than AP600 due to the increased height of the AP1000 containment shell.

Although the changes in the normalization parameters affect the calculated values of the various π groups in the scaling analysis, they do not affect the relative ranking of those π groups. Condensation on the inside and evaporation from the outside of the shell into the natural circulation driven PCS air flow is still the most highly ranked phenomena for removal of the break energy. Therefore, the AP1000 design changes do not affect the results of the AP600 PIRT confirmation that was documented in the scaling analysis. The highly ranked phenomena for AP600 remain highly ranked for AP1000 and no lower ranked phenomena increase in importance. See Section 2.7 for a discussion of the application of the AP1000 PIRT in this report.

Table 2.6-1 PIRT According to Effect on Containment Pressure

Component or Volume	Phenomenon or Parameter	LOCA				MSLB
		Blowdown (0-30 sec)	Refill (30-90 sec)	Peak Pressure (90-1200 sec)	Long Term (>1200 sec)	Blowdown (0-400 sec)
Inside Containment:						
1. Break Source	A. Mass and Energy	H	N/A	H	H	H
	B. Direction and Elevation	H	N/A	H	L	H
	C. Momentum	H	N/A	H	L	H
	D. Density	H	N/A	H	L	H
	E. Droplet/liquid flashing (thermal)	L	L	L	L	N/A
2. Containment Volume	A. Circulation/ Stratification	H	H	H	H	H
	B. Intercompartment Flow	L	H	H	H	H
	C. Gas Compliance	H	H	H	H	H
	D. Fog (circulation)	L	H	H	H	N/A
	E. Hydrogen Release	L	L	L	L	N/A
3. Containment Solid Heat Sinks (Steel and Concrete)	A. Liquid Film Energy Transport	L	L	L	L	L
	B. Vertical Film Conduction	L	L	L	L	L
	C. Horizontal Film Conduction	L	H	H	H	H
	D. Internal Heat Sink Conduction	M	H	H	M	H
	E. Heat Capacity	M	H	H	M	H
	F. Condensation	M	H	H	M	H
	G. Convection from containment	L	M	L	L	L
	H. Radiation from containment	L	M	L	L	L
4. Initial Conditions	A. Initial temperature	M	M	M	M	M
	B. Initial humidity	M	M	M	M	M
	C. Initial pressure	M	M	M	M	M

Table 2.6-1 PIRT According to Effect on Containment Pressure (cont.)

Component or Volume	Phenomenon or Parameter	LOCA				MSLB
		Blowdown (0-30 sec)	Refill (30-90 sec)	Peak Pressure (90-1200 sec)	Long Term (>1200 sec)	Blowdown (0-400 sec)
5. Break Pool	A. Circulation/ Stratification in the pool	L	L	L	M	L
	B. Condensation/ evaporation	L	L	L	M	L
	C. Convection within containment volume	L	L	L	L	L
	D. Radiation within containment volume	L	L	L	L	L
	E. Conduction in pool	L	L	L	M	L
	F. Compartment filling	L	L	L	L	L
Inside Containment:						
6. IRWST	A. Mixing/ Stratification (gas & water)	L	L	L	L	L
	B. Condensation	L	L	L	L	L
	C. Convection	L	L	L	L	L
	D. Radiation	L	L	L	L	L
	E. Conduction in liquid	L	L	L	L	L
	F. Liquid level changes	L	L	L	L	L
Containment Shell:						
7. Steel Shell	A. Convection from containment	L	L	L	L	L
	B. Radiation from containment	L	L	L	L	L
	C. Condensation	H	H	H	H	H
	D. Inside film conduction	L	L	L	L	L
	E. Inside film energy transport	L	L	L	M	L
	F. Conduction through shell	H	H	H	H	H

Table 2.6-1 PIRT According to Effect on Containment Pressure (cont.)

Component or Volume	Phenomenon or Parameter	LOCA				MSLB
		Blowdown (0-30 sec)	Refill (30-90 sec)	Peak Pressure (90-1200 sec)	Long Term (>1200 sec)	Blowdown (0-400 sec)
	G. Heat capacity of shell	H	H	H	L	H
	H. Convection to riser annulus	L	L	L	M	L
	I. Radiation to baffle	L	L	L	M	L
	J. Radiation to chimney	L	L	L	L	L
	K. Radiation to fog/air mixture	L	L	L	L	L
	L. Outside film conduction	N/A	N/A	L	L	L
	M. Outside film energy transport	N/A	N/A	M	M	L
	N. Evaporation to riser annulus	N/A	N/A	H	H	M
8. PCS Cooling Water	A. PCCWST flow rate	N/A	N/A	H	H	L
	B. PCCWST water temperature	N/A	N/A	M	M	L
	C. Water film stability and coverage	N/A	N/A	H	H	L
	D. Film stripping	N/A	N/A	L	L	L
	E. Film drag	N/A	N/A	L	L	L
Outside Containment:						
9. Riser Annulus & Chimney Volume	A. PCS Natural Circulation	L	L	M	M	M
	B. Vapor acceleration	N/A	N/A	L	L	L
	C. Fog	N/A	N/A	L	L	N/A
	D. Flow stability	L	L	L	L	L
10. Baffle	A. Convection to riser annulus	N/A	N/A	L	M	N/A
	B. Convection to downcomer	N/A	N/A	L	M	N/A
	C. Radiation to shield building	N/A	N/A	L	L	N/A
	D. Conduction through baffle	N/A	N/A	L	M	N/A

Table 2.6-1 PIRT According to Effect on Containment Pressure (cont.)

Component or Volume	Phenomenon or Parameter	LOCA				MSLB
		Blowdown (0-30 sec)	Refill (30-90 sec)	Peak Pressure (90-1200 sec)	Long Term (>1200 sec)	Blowdown (0-400 sec)
	E. Condensation	N/A	N/A	L	L	N/A
	F. Heat capacity	N/A	N/A	L	L	N/A
	G. Leaks through baffle	N/A	N/A	M	M	N/A
11. Baffle Supports	A. Convection to riser air	L	L	L	L	L
	B. Radiation from shell	L	L	L	L	L
	C. Conduction from shell	L	L	L	L	L
	D. Heat capacity	L	L	L	L	L
12. Chimney Structure	A. Conduction through chimney	L	L	L	L	L
	B. Convection from chimney air	L	L	L	L	L
	C. Heat capacity of structure	L	L	L	L	L
	D. Condensation on chimney	L	L	L	L	L
13. Downcomer Annulus	A. PCS Natural Circulation	L	L	M	M	M
	B. Air flow stability	L	L	L	L	L
14. Shield Building	A. Convection to downcomer	N/A	N/A	L	L	L
	B. Conduction through shield building	N/A	N/A	L	L	N/A
	C. Convection to environment	N/A	N/A	L	L	N/A
	D. Radiation to environment	N/A	N/A	L	L	N/A
15. External Atmosphere	A. Temperature	N/A	N/A	L	L	L
	B. Humidity	N/A	N/A	L	L	L
	C. Recirculation	N/A	N/A	L	L	L
	D. Pressure Fluctuations	N/A	N/A	L	L	L

2.7 APPLICATION OF AP1000 PIRT IN AP1000 SCALING

In the previous section, the AP1000 PIRT have been identified and compared to the AP600 PIRT. In this section, the application of these PIRT in the scaling studies presented in Section 4 is discussed. This summary is presented here to provide a comprehensive description of how the high-ranked phenomena identified for AP1000 are addressed through either scaling or analysis or both.

2.7.1 Large-Break LOCA

For LBLOCA, the major conclusions presented in Section 2.3 are as follows:

- The AP600 and AP1000 PIRT are very similar.
- There is no new high-ranked phenomenon identified for AP1000.
- There are minor changes in the ranking of low and medium phenomena from the AP600 PIRT.
- The conclusions from the AP600 PIRT that the passive systems do not contribute to the short-term core cooling nor do they influence the calculated PCT for the large-break transient is also valid for AP1000.

Therefore, for the AP1000, the LBLOCA phenomena are similar to conventional PWRs, and therefore, scaling studies for LBLOCA were not performed for AP1000. This is consistent with the approach licensed for AP600.

2.7.2 Small-Break LOCA

For SBLOCA, the most important phase of the transient is the ADS-IRWST transition. In this phase, the minimum vessel/core inventory typically occurs, which poses the greatest challenge to core cooling. This was demonstrated in the AP600 tests, and was shown in the AP600 SSAR (Reference 9) analysis. This was also shown in the AP1000 analysis results presented in Reference 1. Therefore, the scaling studies presented in this report will focus on this phase.

ADS-IRWST Transition

As reactor vessel inventory is of greatest importance, the processes that have the most influence on reactor vessel inventory will be scaled from a top-down perspective. In view of the AP1000 PIRT and insight gained from the AP600 testing, scaling, and analysis, the processes of greatest influence include:

- liquid inventory depletion due to decay heat steaming in the core, and
- liquid inventory replenishment due to CMT gravity injection and IRWST gravity injection.

Steaming in the core depends largely upon the core decay power, and the gravity injection processes are strongly dependent upon the gravity head in the CMT or IRWST and the flow resistance in the injection paths. CMT injection depends upon density difference between the CMT and CMT balance line while IRWST injection depends upon the pressure in the vessel which acts as a backpressure to gravity injection.

Reactor vessel pressure depends upon the pressure of the steam volume in the vessel. The processes that have the greatest impact on reactor vessel pressure are:

- decay heat steaming in the core, and
- venting of steam via the ADS paths, primarily the ADS-4 vent path, as its flow area is large.

As these processes are important in influencing the pressure in the reactor vessel, they will also be scaled from the top-down [via the rate of pressure change (RPC) equation].

The steam venting process via the ADS-4 paths can be influenced by:

- entrainment of liquid from the hot leg at the ADS-4 tee, and
- flow pattern and flow pattern transition in the hot leg.

As these are very complex physical processes, they are difficult to address at a top-down, system level perspective. Therefore, they will be scaled at a bottom-up level.

The steam venting process via the ADS-1/2/3 path can be influenced by:

- countercurrent flow limitation (CCFL) in the surge line, and
- draining of the pressurizer.

The CCFL in the surge line will be scaled from the bottom-up using the Kutateladze number and the flooding correlation for vertical tubes. Draining of the pressurizer has been previously assessed for the AP600 in Reference 10, and the conclusions from this report are judged to be applicable to the AP1000.

ADS

The ADS is important as it depressurizes the RCS to allow gravity injection core cooling via the IRWST. The RCS depressurization is largely characterized as a rapid venting of steam from the upper volume of the RCS via the pressurizer. The processes of greatest influence on RCS pressure during this phase include:

- decay heat steaming in the core, and
- venting of steam via the ADS-1/2/3 paths.

These processes will therefore be scaled from a top-down level (via the RPC equation).

The venting processed via the ADS-1/2/3 can be influenced by the pressure drop and flow regime in the surge line leading to the pressurizer. Scaling analyses of flow regime transitions were performed for the test facilities relative to AP600, and it was found that some distortion is inevitable in the integral effects test facilities. This distortion did not preclude the use of data from these test facilities for AP600 code validation. Therefore, no scaling analysis will be performed for AP1000 as it is expected that similar distortion will exist. However, data from these test facilities may be used for AP1000 code validation.

Natural Circulation (PRHR), IRWST Injection, and Sump Injection

These phases are all characterized as a two-phase natural circulation through the reactor core. They do not experience any challenges to reactor vessel inventory, and system pressure is quasi-steady. Therefore, the main interest is in scaling the state of the two-phase system during these phases. As the RCS pressure is nearly constant and known, quality or void fraction is needed to establish the similarity of the state of the two-phase systems in the test facilities and the plants. Therefore, core exit quality and void fraction will be scaled.

Core exit quality in two-phase natural circulation is dependent upon:

- core decay steaming/removal, and
- two-phase natural circulation through the core, which is influenced by gravity head and resistance in the flow path.

Core exit quality will be scaled from a top-down perspective. As void fraction can be related to quality, it does not need to be scaled top-down. It will be scaled bottom-up using the Yeh correlation.

Blowdown

The blowdown phase for SBLOCAs does not typically pose a challenge to reactor vessel inventory. There is a rapid depressurization, after which the RCS pressure quickly equilibrates with the secondary side pressure and is maintained during the natural circulation phase until the ADS is actuated. The processes involved in blowdown are similar to conventional PWRs (i.e., break and core power dominated) for which an ample test database exists. Therefore, the blowdown phase did not receive much attention for AP600 and will not be scaled for AP1000.

2.7.3 Non-LOCA

The non-LOCA transient analyses cover a wide range of initiating events and phenomena. These transients include increases in heat removal from the primary system, decreases in heat removal by the secondary system, decreases in reactor coolant flow rate, reactivity and power distribution anomalies, increases in reactor coolant inventory, RCS depressurization, and steam generator tube ruptures.

A review of the AP1000 components, systems and phenomena important to the analysis of non-LOCA events indicates that many are the same as those of conventional licensed operating PWRs. The architecture and size of the AP1000 reactor coolant system is similar to that of operating plants. The AP1000 fuel assembly uses a 17x17 rod arrangement similar to that of operating plants. Conventional recirculating U-tube steam generators are used on the AP1000 like those of operating plants. While the steam generator size is larger for the AP1000, the flow restrictors in the steam exit nozzles will limit flow during postulated high energy line breaks to that observed in operating plants. The AP1000 uses hermetically sealed canned reactor coolant pumps in comparison to the shaft seal pumps of licensed operating plants. The flow characteristics and inertia of the AP1000 sealed canned reactor coolant pumps are such that existing DNB correlations and methodology can be adapted for use in the AP1000 analyses of events where a decrease in RCS flow occurs.

With respect to non-LOCA analyses, the principle difference between the AP1000 and operating plants lies in the passive safety systems of the AP1000. However, the passive safety systems are not required for mitigation of many non-LOCA events. Many non-LOCA events are mitigated by the same systems and features found in licensed operating plants such as reactor trip, turbine trip, feedwater line isolation, steam line isolation, or opening of safety relief valves. For many non-LOCA events, the initiating fault may be quickly terminated by automatic protection system actuation.

For example, a fault that causes an inadvertent rod cluster control assembly (RCCA) withdrawal at power event will cause reactor power to increase until an overpower type reactor trip occurs. The reactor trip causes an immediate reduction in power and also terminates the inadvertent RCCA withdrawal. Immediately following reactor trip, the plant will be in a safe state and the plant may be maintained in a safe, stable state or cooled down further using normal plant shutdown procedures. The behavior during this event on the AP1000 will be identical to that observed on operating plants.

With respect to non-LOCA analyses, the principle differences between the AP1000 and conventional operating plants are the AP1000 CMTs and the heat removal through the PRHR heat exchanger to the IRWST. The AP1000 ADS and IRWST injection are not used for mitigation of non-LOCA transients.

Of all the non-LOCA events for AP600, only the following events involve passive safety systems:

- Steam Line Break
- Inadvertent CMT and Inadvertent PRHR Activation
- Feedwater Line Break
- Loss of Normal Feedwater
- Loss of ac Power
- Steam Generator Tube Rupture

For these seven events, only two passive safety system components are involved in mitigating the events: CMTs and PRHR heat exchangers.

CMT circulation is an important process for the non-LOCA transients. Therefore, scaling of CMT circulation will be addressed for the CMT separate effects test facility.

PRHR circulation and the associated core decay heat removal are also important processes. Therefore, scaling of PRHR circulation will be addressed from a top-down perspective for the integral effects test facilities. PRHR heat removal will be addressed from a bottom-up perspective for the PRHR separate effects facility.

2.7.4 Containment

For containment, the major conclusions presented in Section 2.6 are as follows:

- No new containment phenomena were identified for AP1000.
- No changes to the ranking of the phenomena were identified for AP1000 compared to AP600.

In the AP600, it was shown through scaling that the transient containment performance was not scaled well in the AP600 test facilities. Therefore, the containment tests were not used to model transient containment response. Rather, the tests were used to develop heat transfer correlations over the range of expected operating conditions for the AP600 passive containment cooling system. This data was then used to develop the condensation, convection, and evaporation heat transfer correlations used in the WGOTHIC (Reference 11) containment analysis models. The heat transfer models used in conjunction with conservative analysis assumptions and techniques was acceptable for analysis of containment performance of design basis accidents.

Since there are no new phenomena identified for the AP1000, if the data from AP600 containment tests is shown to bound the AP1000 operating conditions, then it can be concluded that the AP600 containment tests are sufficient for the AP1000. To demonstrate this, studies are performed in Section 4 to show that the AP1000 operating conditions are reasonably characterized by the AP600 tests. The studies show that the correlation ranges developed for AP600 are applicable to the AP1000. In addition, results of computational fluid dynamics analysis are presented that demonstrate that mixing inside containment for the AP1000 is similar to the AP600.

2.8 REFERENCES

1. WCAP-15612, "AP1000 Plant Description and Analysis Report," M. M. Corletti et al., December 2000.

2. "Topical Issue on Quantifying Reactor Safety Margins, Part 2: Characterization of Important Contributors to Uncertainty," G. E. Wilson et al., 1990, Nuclear Engineering and Design, Vol. 119, No. 1, pp. 17-31.

3. WCAP-14171, Rev. 2, "WCOBRA-TRAC Applicability to AP600 Large-Break Loss-of-Coolant Accident," L. E. Hochreiter et al., March 1998.

4. WCAP-14807, Rev. 5, "NOTRUMP Final Validation Report for AP600," R. L. Fittante et al., 1998.

5. WCAP-14727, Rev. 2, "AP600 Scaling and PIRT Closure Report," W. L. Brown et al., February 1998.

6. WCAP-14234, Revision 1, "LOFTRAN & LOFTTR2 AP600 Code Applicability Document," U. Bachrach, E. L. Carlin, August 1997.

7. WCAP-14845, Rev. 3, "Scaling Analysis for AP600 Containment Pressure During Design Basis Accidents," D. R. Spencer et al., March 1998.

8. WCAP-14812, Rev. 1, "AP600 PIRT Closure Report," June 1997.

9. "AP600 Standard Safety Analysis Report," DE-AC03-90SF18495, June 26, 1992.

10. "Transition from Depressurization to Long-Term Cooling in AP600 Scaled Integral Test Facilities," D. Bessette and M. di Marzo, Nuclear Engineering and Design, Vol. 188, 1999, pp. 331-344.

11. WCAP-14382, "WGOTHIC Code Description and Validation," M. Kennedy et al., May 1995.

3.0 APPLICABILITY OF AP600 TEST PROGRAM TO AP1000

This section provides a summary description of the important AP600 test programs that were conducted to support AP600 design certification. In addition, it summarizes how the test data obtained from these tests will be used in support of design certification for the AP1000. Additional test description information is provided in Appendix A.

3.1 AP600 TEST PROGRAM OVERVIEW

From the start of the AP600 program, Westinghouse recognized the importance of verifying the innovative system features of the AP600 by dedicated testing. In the beginning, key concepts and principles were researched and, where data was lacking, small basic research tests were conducted to demonstrate fundamental principles and feasibility of concepts. Based on these tests, larger and more sophisticated tests were designed to evaluate further the engineering and safety concepts of the AP600. Finally, tests were conducted to provide data for computer code validation of the components and systems being used in the AP600.

The purpose of the AP600 test program was to validate the safety analysis computer codes used to verify the performance of key systems, structures, and components used in the AP600. In addition, design information needed to verify performance of key components used in the AP600 was provided. The AP600 test program was organized to provide both design information and data for computer code validation. Testing began in 1988, beginning with the earliest basic research testing under the Advanced Light Water Reactor (ALWR) Technology Programs sponsored by the DOE and the EPRI. The AP600 test program evolved into a larger program, with emphasis on performing tests to obtain data to support design certification for the AP600 plant from the NRC.

Since the primary mission of the AP600 test program was to obtain data to support design certification from the NRC, the tests were organized into three major areas:

- Passive Core Cooling System (PXS) tests
- Passive Containment Cooling System (PCS) tests
- Equipment and component design verification tests

These test areas were chosen to facilitate NRC review of the individual tests being conducted in the AP600 test program. Primarily, the NRC focused on those tests that support the PXS and PCS, although the design verification tests of equipment used to support the safety systems are also of interest to the NRC.

Types of Tests Performed

Several different types of tests were performed in each of these areas based on the scope and primary purpose of the individual test. The different types of tests included are:

- Basic research tests
- Engineering tests

- Component separate effects tests
- Integral systems tests

Basic research tests were experimental in nature and were used to provide engineering guidance or detailed information on specific phenomena to be studied. These tests were also used to determine the feasibility of an engineering concept before proceeding to a larger-scale test or development program. While these tests were not required by the NRC for design certification, they did support design certification test and analysis activities.

Engineering tests were primarily performed to obtain specific design information or to verify the design of a particular component. They were also used to provide boundary conditions for analysis of other components or systems, or to determine initial conditions for other separate effect or integral systems tests. Generally, these tests were mechanical in nature.

Separate effects tests were performed to obtain data for computer code model development of specific thermal-hydraulic phenomena anticipated to occur as result of the use of an individual component. In these tests, the boundary conditions for the individual component were controlled to provide the range of conditions expected to be experienced by that component. In addition, tests were performed to separate the phenomena of interest in order to investigate the effect of those phenomena.

Integral systems tests examined the performance of the reactor through simulation of all interconnecting systems, subsystems, components, and piping to provide thermal-hydraulic data for computer code validation. These data verified that the interaction of the individual components produced the desired effect on the plant and that the computer code models predicted the appropriate system and plant response.

PXS System Tests

The relevant new features of the AP600 PXS were included in the tests performed in this area. These tests were designed to obtain the thermal-hydraulic data over and beyond the range of operating conditions anticipated to occur in the AP600. Since these tests were not to demonstrate the performance of the AP600, but to obtain thermal-hydraulic data for computer code validation, success of these tests was measured by their ability to provide high-fidelity data. As a result, confidence in the computer codes to predict overall plant performance was enhanced.

Table 3.1-1 provides a summary listing of the PXS tests. This table indicates the objective/ conclusion and the primary purpose of the tests for both the AP600 and the AP1000.

PCS Tests

The PCS tests were designed to characterize the heat removal capabilities of the AP600 containment design. Tests and analysis show that the PCS performs its intended function reliably and efficiently. Heat transfer data and other physical properties are measured and compare favorably with respect to predictions. The ability of the PCS to distribute water over

containment is proven, and the ability of the coating to promote wetting of the surface was not adversely affected by exposure to weather. Due to the extensive testing and favorable comparisons of results with computer analysis, a high degree of confidence in the performance of the PCS was established.

Table 3.1-2 provides a summary listing of the PCS tests. This table indicates the objective/ conclusion and the primary purpose of the tests for both the AP600 and the AP1000.

Equipment Design Verification Tests

Equipment tests were performed to confirm the design of individual components that cannot be validated by the use of analytical tools or manufacturing experience. Tests were required to verify the performance of complex designs that cannot be easily addressed or predicted by analytical models. Phenomena that occur in components that are difficult to predict, such as fluid dynamics and impact wear, are areas that require such testing. Equipment tests were also required to demonstrate manufacturability when using new construction techniques or new materials.

Table 3.1-3 provides a summary listing of the equipment design verification tests. This table indicates the objective/conclusion and the primary purpose of the test for both the AP600 and the AP1000.

Table 3.1-1 AP600 Passive Core Cooling System Tests

PXS Tests	Test Objective/Conclusion	Completion Date	AP600 Use		AP1000 Use	
			NRC Licensing	Design	NRC Licensing	Design
DNB (Columbia University)	Extended the existing critical heat flux correlation for W fuel assemblies at lower flow conditions	2/94	X		(1)	
PRHR HX (W STC) Phase 1 Phase 2	Determined heat transfer characteristics of the PRHR HX and mixing characteristics in the IRWST	12/89 10/90	X X		X X	
ADS (Cassacia, Italy) Phase A - sparger performance and tank loads	Confirmed the capacity of the sparger and determined the dynamic effects on the IRWST structure	11/92	X	X	X	X
Phase B - ADS	Simulated the operation of the ADS and its valves	12/94	X	X	X	X
CMT (Westinghouse AESD)	Verified gravity-drain behavior of the CMT over a full range of flow rates and pressures and verified operation of the tank level instrumentation	9/94	X	X	X	X
Long-term cooling (1/4-scale) (OSU)	Provided data to evaluate the operation of the PXS at low pressure	10/94	X		X	
	NRC conducted additional confirmatory tests at this facility		(2)		(3)	

Table 3.1-1 AP600 Passive Core Cooling System Tests (cont.)

PXS Tests	Test Objective/Conclusion	Completion Date	AP600 Use		AP1000 Use	
			NRC Licensing	Design	NRC Licensing	Design
Full-height, full-pressure integral systems test (SPES facility in Italy)	Provided data to evaluate the operation of the PXS at high pressure, including response to SBLOCA, SGTR, and SLB transients	11/94	X		X	
Full-height, full-pressure integral systems test (ROSA facility in Japan)	NRC conducted confirmatory tests at this facility	6/95	(2)		(3)	

Note:
1. AP1000 provides higher RCS flows during normal operation and during reactor coolant pump coast down. As a result, the AP1000 will not have to utilize the low flow DNB correlation developed from this test. Refer to subsection 3.2.1.1 for additional discussion.
2. NRC conducted confirmatory tests at these facilities that were used by the NRC during the licensing of the AP600.
3. Westinghouse may utilize results from these tests in the licensing of the AP1000.

Table 3.1-2 AP600 Passive Containment Cooling System Tests

PCS Tests	Test Objective/Conclusion	Completion Date	AP600 Use		AP1000 Use	
			NRC Licensing	Design	NRC Licensing	Design
Air flow path pressure drop test (W STC)	Measured air annulus loss coefficients are predictable; form losses minimized	1/88	X	X	X	X
Water film formation test (W STC)	Plate wetting characteristics with and without coating are excellent	2/88		X		X
Wind tunnel bench experiment (W STC)	Wind from any direction always enhances air flow with high air inlet	8/88	X	X	X	X
Condensation tests (U. of Wisconsin)						
Surface tests	Heat transfer coefficients measured for various surfaces and orientations	11/90	X		X	
Noncondensable tests	Assessed effect of helium on heat transfer coefficient	7/93	X		X	
Two-dimensional test models	Obtain data on heat and mass transfer phenomena using a small 2-D test model of the AP600 large-scale test	9/94	X		X	
PCS water distribution (W AESD)						
Phase 1 - center of dome, 20-in. dia.	Demonstrated the effectiveness of water distribution on the center of the containment dome	6/91	X	X	X	X
Phase 2 - full-scale, 1/8-section	Demonstrated the effectiveness of water distribution on the containment dome and upper sidewall	1/92	X	X	X	X
Phase 3 - full-scale, 1/8-section	Verified design of water distribution system	9/93	X	X	X	X

Table 3.1-2 AP600 Passive Containment Cooling System Tests (cont.)

PCS Tests	Test Objective/Conclusion	Completion Date	AP600 Use		AP1000 Use	
			NRC Licensing	Design	NRC Licensing	Design
PCS Wind Tunnel (U. of Western Ontario)						
Phase 1 - overall building effects (1/100-scale)	Measured the wind-induced pressure on the containment shield building due to air inlet/outlet configurations and site structures.	7/91	X	X	X	X
Phase 2 - detailed model, final verification (1/100-scale)	Measured baffle loading and the effect of wind on containment annulus air flow.	2/92	X	X	X	X
Phase 4A/4B (1/30-scale and 1/800-scale)	Performed tests at higher Reynolds numbers and determined effects on site geography.	11/93	X		X	
Heated plate test (W STC)	Water film behavior is stable under all conditions; heat transfer rates are predictable.	5/88	X		X	
Integral PCS test (W STC)						
Phase 1	Established the capability of the PCS to provide adequate heat removal using an integrated test facility.	10/89	X		X	
Phase 2	Obtained data during PCS operation over the full range of design basis operating conditions.	7/92	X		X	
Large-scale integral PCS test (W STC)	Obtained data during PCS operation on larger containment dome and sidewall heat transfer areas. Included inside containment structures.	Phase 1 - 5/92	X		X	
		Phase 2 - 9/93	X		X	

Table 3.1-3 AP600 Equipment Design Verification Tests

Component Design Tests	Test Objective/Conclusion	Completion Date	AP600 Use		AP1000 Use	
			NRC Licensing	Design	NRC Licensing	Design
RNS suction nozzle test (East Pittsburgh)	Eliminated suction vortex	9/88		X		X
RCP/SG channelhead air flow (W EMD)	No SG to pump flow anomalies	3/91		X		X
RCP journal bearing (W STC) Phase 1 Phase 2	Demonstrated manufacturability of depleted uranium rotor sections and large radial bearings and determined rotor drag losses	 12/89 2/91		 X X		 X X
RCP high-inertia rotor (W STC)	Minimized rotor drag losses	8/92	X	X	X	X
In-core instrumentation tests EMI (W EMD)	Demonstrated that system is not susceptible to electromagnetic interference from the CRDMs	9/90		X		X
Reactor vessel internals test Flow visualization (U. of Tennessee)	Demonstrated that no abnormal flow distribution occurs in the reactor vessel downcomer and lower plenum	2/92		X		X
Boron transport test (U. of Tennessee)	Determined transport of boron from DVI/SI injection point to core.		X		X	
Check valve Preliminary hydraulic (W AESD) In situ (operating nuclear plants)	 Determined flow vs. differential pressure for prototypic check valves Assessed operation of check valves following prolonged exposure to plant conditions	 6/91 9/94	 X X	 X	 X X	 X

3.2 TEST SUMMARIES

The following provides a brief summary of each AP600 test and its utilization in the AP1000 program. Additional information can be found on each test in Appendix A.

3.2.1 PXS Test Summaries

The following tests were performed for the PXS.

- Departure from Nucleate Boiling (DNB) test (subsection 3.2.1.1)
- Passive Residual Heat Removal Heat Exchanger (PRHR HX) test (subsection 3.2.1.2)
- Automatic Depressurization System (ADS) test , phase A (subsection 3.2.1.3)
- ADS test , phase B (subsection 3.2.1.4)
- Core Makeup Tank (CMT) test (subsection 3.2.1.5)
- Low-pressure, integral systems test, OSU (subsection 3.2.1.6)
- Low-pressure, integral systems test, OSU – NRC (subsection 3.2.1.7)
- High-pressure, integral systems test, SPES-2 (subsection 3.2.1.8)
- High-pressure, integral systems test, ROSA – NRC (subsection 3.2.1.9)

3.2.1.1 DNB Tests

Test data accumulated over years of testing on the current Westinghouse fuel designs have concentrated on the higher flow range associated with operating conditions of conventional, higher-power density cores. The purpose of the AP600 DNB tests were to determine the critical heat flux (CHF) performance of the AP600 fuel assembly design, at low-flow conditions. The results of the DNB tests were used to extend the existing Westinghouse DNB correlation to lower flow rates than previously tested. Other correlations, however, did extend to lower flow rates, and the DNB margin has been shown to exist using these correlations over the lower range of flow rates. Since the AP600 has ample DNB margin, this test did not impact the core or fuel design.

AP1000 Applicability

This test is not needed for the AP1000 because the normal reactor/core flow rates are higher and the reactor coolant pump inertia is greater such that the low flow DNB correlation developed from this test data will not be required.

3.2.1.2 PRHR HX Test

The purpose of the AP6000 PRHR HX tests was to characterize the thermal performance of the PRHR HX and the mixing behavior of the in-containment refueling water storage tank (IRWST). The experiment used full size tubes, tube diameter, pitch and height. The tubes were oriented vertically inside a full height IRWST that had a scaled volume. Since the vertical length was preserved, the buoyant-induced flow patterns inside the tank simulated the AP600. The main scaling parameter for the experiment was the pool volume per HX tube so that the heat load characteristics, resulting tank fluid conditions, and induced flow pattern would be similar to

those in the AP600. The test conditions covered the full range of AP600 flow rates (forced to natural circulation), RCS hot leg temperatures and IRWST temperatures.

A boiling heat flux correlation similar to recognized correlations was developed from the PRHR data. These correlations were used to size the PRHR HX and to evaluate the PRHR performance during postulated accidents. Mixing of the water in the simulated IRWST was very good. Localized boiling did not occur until the entire IRWST water volume was significantly heated. The test demonstrated that the IRWST water would not steam into the AP600 containment for about 2 hours.

AP1000 Applicability

The AP1000 has a PRHR HX that is similar to the AP600 PRHR HX. The AP1000 HX has a few more tubes and the length of the horizontal section has been increased. In addition, the diameter of the pipes connecting the HX to the RCS have been increased. It is estimated that the AP1000 HX will be able to remove about the same amount of heat per MW of core power as the AP600 HX. The scaling evaluation performed in subsection 4.1.1.3 concludes that the heat transfer correlations that were developed from the AP600 test data would be valid for the AP1000 HX. In addition, the expected operating conditions for the AP1000 PRHR HX result in external tube heat flux values that are far below critical heat flux limits and are bounded by forced flow test data from the AP600 integral tests.

3.2.1.3 ADS Test - Phase A

The purpose of the ADS phase A tests were to confirm the design of the ADS sparger and to determine the dynamic effects on the IRWST structure. The ADS phase A test was a full-sized, full-pressure simulation of one of the two AP600 depressurization system flow paths from the pressurizer to the IRWST. Phase A testing was performed at ENEA's VAPORE test facility in Casaccia, Italy. The test conditions bounded the volumetric flow through the AP600 ADS valves to the sparger and IRWST. The dynamic effects of the steam condensation and air clearing generated by sparger operation were measured, as were loadings on the sparger and its support and temperatures and pressures throughout the test arrangement. Sparger steam quenching was demonstrated from ambient to fully saturated IRWST water temperatures.

Phase A testing covered both the maximum volumetric blowdown rate when all three stages of the AP600 ADS were open, and the minimum blowdown rate (end of blowdown) when the pressurizer was essentially depressurized. Results of the phase A tests were used to verify the design of the ADS sparger and obtain sufficient information to perform preliminary design of the IRWST. These tests were also used to select the sparger submergence below the IRWST water level.

AP1000 Applicability

The AP1000 has ADS-1/2/3 that are the same as the AP600. This includes the size of the pipes, valves, spargers, and sparger placement in the IRWST. The scaling evaluation performed in subsection 4.1.1.1 concludes that the test data obtained for the AP600 is applicable to the

AP1000. This is due to the use of the same ADS-1/2/3 arrangement, sparger design and location, size of pipes, and types of valves.

3.2.1.4 ADS Test - Phase B

The ADS phase B test used the same test facility at ENEA's VAPORE test facility in Casaccia, Italy, that was used for the phase A tests except that prototypical ADS-1/2/3 valves were used to initiate ADS flow. In addition, the facility was modified to provide adjustable mixtures of saturated steam/water into the ADS valves. The loadings on the sparger and its support were measured, as were temperatures and pressures throughout the test arrangement. The test collected sufficient thermal-hydraulic performance data to support the development and verification of analytical models of the ADS used in safety analyses during critical and subsonic flow conditions with two-phase flow. In addition, it provided design requirements for the ADS components including specification of the ADS valves.

The key results and observations for ADS phase B were:

- The sparger operated properly over the full range of ADS flow rates, fluid qualities, and IRWST temperatures.
- IRWST loads resulting from sparger-induced pressure pulses during phase A are conservative.
- Blowdowns into a hot (212°F) quench tank produced small loads.

AP1000 Applicability

The AP1000 has ADS-1/2/3 that are the same as the AP600. This includes the size of the pipes, valves and spargers. The scaling evaluation performed in subsection 4.1.1.1 concludes that the test data obtained for the AP600 is applicable to the AP1000. This is due to the use of the same ADS-1/2/3 arrangement, sparger design, size of pipes, and types of valves.

3.2.1.5 CMT Test

The purpose of the AP600 CMT test was to simulate the operation of the CMT and its level instrumentation over a wide range of prototypic pressures and temperatures and to obtain data to support the development and verification of computer models to be used in safety analyses and licensing of the AP600 design. The CMT test facility is a full pressure/temperature scaled facility that simulates the flow path from an RCS cold leg to a CMT and back to the reactor vessel. The test matrix covered hot water circulation and steam displacement drain down operation. Steam condensation in the top of the CMT was investigated.

The key results and observations were:

- The test operated over the full range of pressures, temperatures, and flow rates.
- Sufficient data were obtained for model development and code validation for recirculation and draindown.
- The steam diffuser reduced condensation and limited mixing to the top of the CMT, without waterhammer.
- Hydraulics of the test were well predicted by using simple mass and energy equations.

AP1000 Applicability

The AP1000 has CMTs that are very similar to the AP600. The AP1000 uses the same arrangement including pipe/valve sizes and elevations. The AP1000 CMTs have been increased in volume by about 25 percent by increasing their diameter. In addition, the flow tuning orifice in the CMT injection lines has been changed to reduce its resistance, such that the CMT flow will increase by about 25 percent. The scaling evaluation performed in subsection 4.1.1.2 concluded that the test data obtained for the AP600 should be applicable to the AP1000.

3.2.1.6 Low-Pressure Integral Systems Test (OSU)

The low-pressure, 1/4-height integral systems test was conducted at the Corvalis campus of OSU. Scaling studies indicated that a scaled low-pressure test facility could capture the thermal-hydraulic phenomena of interest for the lower pressure behavior of the AP600. The test design accurately modeled the detail of the AP600 geometry including the primary system, pipe routings, and layout for the passive safety systems. The core was simulated with electrical heater rods. The primary system consisted of two loops, each with one hot leg and two cold legs with two pumps and an SG. The passive safety systems included the PRHR HX, CMTs, accumulators, IRWST injection, containment recirculation, and ADS flow paths.

The time period for the simulation included not only IRWST injection, but also long-term containment recirculation. A range of small-break loss-of-coolant accidents (SBLOCAs) was simulated at different locations and orientations on the primary system were tested.

The key results and observations for the OSU test were:

- The core remained covered for all design basis transients although there were oscillations during long-term recirculation operation.
- All passive systems functioned as expected, with no adverse consequences.
- Minor steam condensation events occurred in the upper downcomer region.
- Thermal stratification occurred in both the hot and cold legs.

AP1000 Applicability

The AP1000 has the same configuration of the passive safety features and the active nonsafety features as the AP600. The important passive features with respect to long term cooling have been increased in capacity more than the increase in power. These passive features include ADS stage 4, IRWST injection and containment recirculation. The scaling evaluation performed in subsection 4.1.2 concludes that OSU is adequately scaled to AP1000 during the low-pressure phases of the small break LOCA transient when pressure similitude exists. This includes blowdown to ADS phases. At least one integral test facility (OSU or SPES-2) is acceptably scaled to AP600 to cover all important phenomena. This includes the phases of operation from ADS initiation to containment recirculation.

3.2.1.7 Low-Pressure Integral Systems Test – NRC (OSU)

The NRC conducted confirmatory testing at the OSU test facility. Some small changes were made to the facility with respect to the ADS-1/2/3 flow capacity to improve scaling at low pressure and some instrumentation was improved. The objective of the tests were to provide the NRC confirmatory data in support of licensing the AP600. Tests performed included multiple failure scenarios that would severely challenge the passive safety systems capabilities and demonstrated the robustness in the AP600 design. Westinghouse did not use this test data in its AP600 design or licensing activities.

AP1000 Applicability

The scaling studies performed in Section 4 show that the OSU test facility scales similarly to the AP1000 as to the AP600. Therefore, the test data obtained from these tests can be used by the NRC as confirmatory test data in a similar fashion as was used for the AP600.

3.2.1.8 Full-Pressure, Full-Height Integral Systems Test (SPES-2)

A full-pressure, full-height integral systems test was performed to provide a simulation of the PXS system integrated performance. The existing SPES test facility was modified to simulate an AP600, including two loops with one hot leg and two cold legs per loop, CMTs, accumulators, a PRHR HX, an IRWST, and an ADS. Nonsafety systems providing makeup to the reactor and SGs were simulated. Core power was simulated with electric heater rods. The test facility was designed to be capable of performing tests representative of a SBLOCA, steam generator tube rupture (SGTR), and steam line break (SLB) transients. The objective of the tests were to obtain detailed experimental results for verification of safety analysis computer codes.

Key results and observations for the SPES-2 test were:

- The core remained covered following all simulated events, including a double-ended guillotine (DEG) direct vessel injection (DVI) line break with only passive safety systems operating.

- There was no CMT draindown; therefore, no ADS actuation occurred following the single SGTR with no operator action or nonsafety systems operating.

- Nonsafety system operation had no adverse interaction with passive system operation, and actually added margin to the plant safety response.

- All passive safety systems functioned as expected with no adverse occurrences including CMT recirculation and draindown, PRHR HX heat removal, ADS depressurization, and IRWST gravity draining.

- Timely Normal Residual Heat Removal System (RNS) operation following a LOCA can limit CMT draindown and prevent ADS fourth-stage actuation.

AP1000 Applicability

The AP1000 has the same configuration of the passive safety features and the active nonsafety features as the AP600. The scaling evaluation performed in subsection 4.1.2 concludes that SPES-2 is adequately scaled to AP1000 during the high-pressure phases of small LOCAs. This includes the accident phases of blowdown to ADS stage 4 actuation. The oversized ADS-4 in SPES-2 distorts the facilities use for the later low pressure portions of the accident.

3.2.1.9 Full-Pressure, Full-Height Integral Systems Test (ROSA-AP600)

A full-pressure, full-height integral systems test was performed to provide a simulation of the PXS system integrated performance. The existing ROSA test facility was modified to simulate an AP600, including two loops with one hot leg and one cold leg per loop, CMTs, accumulators, a PRHR HX, an IRWST, and an ADS. Nonsafety systems providing makeup to the reactor and SGs were simulated. Core power was simulated with electric heater rods. The test facility was designed to be capable of performing tests representative of a SBLOCA, SGTR, SLB and station blackout transients. The objective of the tests were to provide the NRC confirmatory data in support of licensing the AP600. Westinghouse did not use this test data in its AP600 design or licensing activities.

AP1000 Applicability

Although Westinghouse has not done formal scaling of the ROSA test facility, based on the scaling studies performed in Section 4, and the similarity of the AP600 and AP1000 plants, it is expected that scaling will demonstrate the applicability of this test facility to AP1000.

3.2.2 PCS Test Summaries

The following tests were performed for the PCS.

- Air flow path pressure drop test (subsection 3.2.2.1)
- Water film formation test (subsection 3.2.2.2)
- Wind tunnel bench experiment (subsection 3.2.2.3)

- Condensation test (subsection 3.2.2.4)
- PCS water distribution test (subsection 3.2.2.5)
- PCS wind tunnel test (subsection 3.2.2.6)
- Heated plate test (subsection 3.2.2.7)
- Integral PCS test (subsection 3.2.2.8)
- Large-scale integral PCS test (subsection 3.2.2.9)

3.2.2.1 Air-Flow Path Pressure Drop Test

A one-sixth scale replica of a 14-degree section of the entire PCS air-flow path was constructed to quantify the air-flow path resistance, determine if aerodynamic improvements were needed, and demonstrate the effectiveness of these improvements. Delta-P measurements were made for each section of the flow path so that the resistance of each section was characterized. As a result of the initial tests, changes were made to the air flow path to reduce pressure losses. The resulting design was adopted for the AP600 and used in subsequent analysis of the PCS performance. This test for the AP600 demonstrated that the pressure coefficients in the air flow path could be estimated, verified, and improved with simple design changes.

AP1000 Applicability

The AP1000 air flow path is very similar to that of the AP600; the main difference being that the length is increased due to the increase in containment height. The increase in the straight downcomer and riser portions of the air flow path will have a very small impact on the overall flow resistance and can be straight forwardly calculated. Note that this impact is small, since most of the pressure losses were in other portions of the flow path.

3.2.2.2 Water Film Formation Test

A simple qualitative test was performed to demonstrate the wetability of the prototypic paint selected for use on the containment outer surface, and to characterize general requirements for forming a water film over a large surface area. The test apparatus consisted of a flat steel plate, 8 ft. long in the flow direction and 4 ft. wide. The plate was pivoted so that it could simulate nearly horizontal sections of the dome as well as the vertical containment sidewalls.

Summarized results of the test are:

- The selected paint readily wetted and rewetted after being dried.
- With a point source of water, without additional distribution, most of the flow was in a 12-in. wide path down the 8-ft. length.
- Several methods were able to create a water film across the entire width of the plate at various flow rates. Once formed, this water film was stable, did not form into rivulets, and wetted the entire length of the plate surface.

AP1000 Applicability

The containment dome of the AP1000 is the same size/shape as the AP600 and will use the same coating and water spreading devices. The maximum water flow rate will be only slightly larger and the minimum flow rate will be about 70 percent larger. As a result, water spreading/coverage is expected to be as good or better than for the AP600.

3.2.2.3 Wind Tunnel Bench Experiment

Bench wind tunnel tests of the PCS were conducted at the Westinghouse Science and Technology Center using 1/100-scale models of the AP600 shield building, air inlets and outlets, annulus baffle, and containment. These tests were performed to establish the proper location of the air inlets and to confirm that wind will always aid containment cooling air flow. Two models were used: one consisted of only the shield building and diffuser discharge without inlets and internal flow; the second included the air inlets, air baffle, containment, tank support structure, and a fan to simulate convective air flow.

The results from this test were used to select the current AP600 air inlet location at the top of the shield building sidewalls. With this inlet location wind always provided an increase in PCS air cooling flow.

Other significant conclusions from this test were:

- Deep beams behind the air inlets (as provided in the PCS water storage tank structure in the original shield building design) increased wind-induced containment air cooling flow.

- Containment air cooling flow was insensitive to wind direction and to a 15-degree downward wind inclination. Cooling flow was increased by a 15-degree upward wind inclination.

AP1000 Applicability

The AP1000 air inlets are located in the same place as the AP600. The diameter of the containment shield building is the same. The height of the containment/shield building is greater which if anything should have a beneficial effect by moving the inlets further above surrounding buildings.

3.2.2.4 Condensation Test

A series of condensation experiments to examine, in detail, condensation of air/steam mixtures flowing over cold surfaces were performed under Westinghouse funding to the University of Wisconsin. These experiments were used to develop improved models for the containment interior heat transfer. These small-scale, well-instrumented tests provided the basis for computer code model improvements, so that the AP600 containment interior heat transfer performance could be accurately predicted.

AP1000 Applicability

Results of this test contributed to the composite heat transfer data used to develop the evaporation, conduction and convection heat transfer correlations used in WGOTHIC. As shown in Section 4, the AP1000 is bounded by the composite heat-transfer data, and therefore this test is applicable and sufficient for AP1000.

3.2.2.5 PCS Water Distribution Tests

The PCS water distribution test was conducted to provide a large-scale demonstration of the capability to distribute water on the steel containment dome outer surface and top of the containment sidewall. The overall objectives of the PCS water distribution test were to quantify the effectiveness of the water distribution over the containment dome and top of the containment sidewall, and to provide data to finalize the design of the AP600 containment water distribution.

The test was conducted in several phases. Phase 1 utilized a full-scale simulation of the center of the containment dome out to the 10-ft. radius. The test was used to evaluate water delivery to the dome. Phase 2 was conducted on a full-scale 1/8 sector of the containment dome at the Westinghouse Waltz Mill facility located in Madison, Pennsylvania. The phase 2 test modeled both the AP600 water supply and a distribution system arrangement. The surface of the test model incorporated the maximum allowable weld tolerances between the steel plates and other maximum allowable deviations and was coated with the prototypic AP600 containment coating to provide similarity to the AP600 plant design. Phase 3 was used to confirm the final design of the water distribution system and to verify its performance to be used in subsequent safety analysis.

AP1000 Applicability

The containment dome of the AP1000 is the same size/shape as the AP600 and will use the same coating and water spreading devices. The maximum water flow rate will be only slightly larger and the minimum flow rate will be about 70 percent larger. As a result, water spreading/coverage is expected to be as good or better than for the AP600.

3.2.2.6 PCS Wind Tunnel Tests

The PCS wind tunnel test was conducted primarily in a boundary layer wind tunnel at the University of Western Ontario. The overall objectives of the PCS wind tunnel test were to demonstrate that wind does not adversely affect natural circulation air cooling through the shield building and around the containment shell and to determine the loads on the air baffle. The test was conducted in four phases (1, 2, 4A, and 4B).

Phases 1 and 2 were conducted with a 1/100-scale model of the AP600 shield building and surrounding site structures, including the cooling tower. Phase 2 used the model from phase 1 testing, modified to include a representation of the shield building air-flow path. The purpose of phase 2 was to explore the effects of the flow path on the developed pressure coefficients and

to determine wind loads on the air baffle. Phase 3 was cancelled. Phase 4A was conducted at both the University of Western Ontario and the Canadian National Research Council's (CNRC's) wind tunnel in Ottawa, Ontario, on both the 1/100-scale model and a 1/30-scale model. The primary objectives of the test were to confirm that the detailed phase 2 results at the University of Western Ontario conservatively represented those expected at full-scale Reynolds numbers and to obtain better estimates of baffle loads in the presence of a cooling tower. The first portion of phase 4A was conducted at the University of Western Ontario using the existing 1/100-scale model of the shield building and site-surrounding structures. The phase 4A tests at CNRC were conducted on a 1/30-scale model of the shield building. The objectives of the phase 4B tests were to explore variations in site layout and topography to determine whether or when such variations significantly affect the net pressure difference between the inlet and chimney of the AP600 and, by implication, the convected flow and net baffle loads. A small-scale model of the site buildings and local topography was built at a scale of about 1/800.

The data from the phase 1 base case design indicated a significant positive pressure difference between the inlets and the chimney. The phase 2 data indicated that the distributions were fairly uniform, even at the top of the annulus. The presence of the cooling tower increased the pressure fluctuations, but the mean remained about the same. The phase 4A tests at CNRC verified that the tests at the University of Western Ontario were conducted at a sufficiently high Reynolds number so that the results were directly applicable to the full-sized plant. Phase 4B site geography testing conducted at the University of Western Ontario consisted simulated several different sites. The test verified that the AP600 could be located on sites with extreme topographies with no adverse PCS impact.

AP1000 Applicability

The containment shield building of the AP1000 is the same size/shape as the AP600 although the PCS water storage tank is somewhat larger in diameter. The shield building is taller which is expected to reduce the effects of surrounding buildings on the air flow over the containment shell from the air inlet vents.

3.2.2.7 PCS Heated Plate Test

Th PCS heated plate test was performed in order to obtain data for the heat and mass transfer processes, and to observe film hydrodynamics including possible formation of dry patches due to surface tension instabilities. The test was performed on a thick steel plate heated on one side and with an evaporating water film and ducted air flow on the other side. The plate could be placed in a vertical position to simulate the containment side wall or inclined somewhat from horizontal to simulate the different slopes on the elliptic containment dome.

Experiments were performed with no water on the plate and for a range of water film flow rates simulating the high water flow on the upper part of containment down to the lower part of containment where the water was nearly completely evaporated at the high heat flux.

The evaporation rate of water from the heated plate was shown to agree with or exceed those expected and confirmed the overall heat transfer capability of the PCS concept. The following conclusions were drawn from the test results:

- Heat transfer from the containment, including water film evaporation and radiation to the air baffle, agreed with or exceeded expected values.

- A water film was easily formed on the coated steel surface even in the vertical orientation. Once formed, the film showed no instability or tendency to form rivulets or dry patches. This was true at all tested water flow rates.

- The water film was not adversely affected by the countercurrent cooling air flow up to the maximum air velocity of the test (e.g., no water-film stripping occurred).

AP1000 Applicability

Results of this test contributed to the composite heat transfer data used to develop the evaporation, conduction and convection heat transfer correlations used in WGOTHIC. As shown in Section 4, the AP1000 is bounded by the composite heat-transfer data, and therefore this test is applicable and sufficient for AP1000.

3.2.2.8 Small-Scale Integral PCS Test

This test simulated PCS heat transfer processes occurring on both the inside and outside containment surfaces. The test apparatus included a 3-ft. diameter, 24-ft. high steel pressure vessel internally heated by steam supplied at various pressures. A transparent wall around the pressure vessel was used to create an annulus for fan-driven or natural circulation air flow. The test simulated the full range of internal pressures/temperatures and external water/air flow rates, pressures/temperatures/humidities.

The following conclusions and observations were drawn from this test:

- The heat removal capability from the external surface of the test vessel for both wetted and dry conditions agreed well with previous heated plate experiments and analytic predictions and supported the AP600 containment analysis.

- The local heat removal rate at the top of the vessel where "cool" water was first applied was significantly higher than the vessel average heat removal rate.

- The water film behavior was stable and predictable even at evaporating heat fluxes three times higher than is likely to be encountered in actual application.

- A uniform water film was easily formed on the coated steel containment surface using simple weirs.

- The water film on the vertical side walls of the coated steel surface of the vessel had no tendency to become less uniform or form rivulets, so that no water film redistribution was required on the vertical walls.

AP1000 Applicability

The AP1000 containment diameter and dome size/shape are the same as the AP600 and will use the same coating and water spreading devices. Results of this test contributed to the composite heat transfer data used to develop the evaporation, conduction and convection heat transfer correlations used in WGOTHIC. As shown in Section 4, the AP1000 is bounded by the composite heat-transfer data, and therefore this test is applicable and sufficient for AP1000.

3.2.2.9 Large-Scale Integral PCS Test

The large-scale PCS test consisted of a 1/8-scale model of the AP600 containment in which both internal steam/air noncondensable gas conditions and external PCS operation were simulated in order to demonstrate the AP600 PCS heat transfer capability. The purpose of this test was to examine, on a large scale, the natural convection and steam condensation on the interior of the AP600 containment combined with exterior water film evaporation, air cooling heat removal, and water film behavior. The PCS heat transfer test results provided data for the verification of the computer model used to predict the containment response.

The test facility was located at the Westinghouse Science and Technology Center in Churchill, Pennsylvania. Key results and observations for the PCS large-scale heat transfer test were:

- The presence of helium had a negligible effect on heat transfer removal rates. Helium mixed well inside the test vessel; no helium stratification was observed.

- Additional condensation and evaporation heat/mass transfer were obtained with a thick walled vessel.

- Noncondensable distribution and internal velocity were important to the condensation rate.

- Tests simulating LOCAs show that internal velocities are sufficiently low, free convection dominates, and momentum does not carry from above to below the deck.

- Tests simulating Main Steam Line Break (MSLB) events show that internal velocities are significant, mixed convection exists, and momentum is transported from above to below deck (which induces uniform concentrations).

- The wetting and water coverage characteristics of the coated steel shell during heat transfer operation were characterized and combined with the water coverage test data to establish a water coverage model.

AP1000 Applicability

The AP1000 containment diameter and dome size/shape are the same as the AP600 and will use the same coating and water spreading devices. The internal structures are the same except for the larger SG and pressurizer and the taller containment shell. Results of this test contributed to the composite heat transfer data used to develop the evaporation, conduction and convection heat transfer correlations used in WGOTHIC. As shown in Section 4, the AP1000 is bounded by the composite heat-transfer data, and therefore this test is applicable and sufficient for AP1000.

3.2.3 Equipment Design Verification Tests

The following tests were performed for equipment design verification.

- Normal Residual Heat Removal System (RNS) suction nozzle test (subsection 3.2.3.1)
- Reactor Coolant Pump (RCP)/SG channelhead air flow test (subsection 3.2.3.2)
- RCP high-inertia rotor/journal and bearing test (subsection 3.2.3.3)
- In-core instrumentation Electro-Magnetic Interference (EMI) test (subsection 3.2.3.4)
- Reactor Vessel air-flow visualization test (subsection 3.2.3.5)
- Boron transportation simulation test (subsection 3.2.3.6)
- PXS check valve hydraulic test (subsection 3.2.3.7)
- Operating plant check valve test (subsection 3.2.3.8)

3.2.3.1 RNS Suction Nozzle Test

In order to ensure that the AP600 hot-leg RNS suction nozzle configuration was optimized and that loss of the RNS function during mid-loop operation will not be a concern in the AP600, a series of tests were performed using an existing test facility.

Among the different nozzle arrangements tested, the optimum arrangement was a step nozzle at the bottom of the hot leg. As the hot-leg level was reduced, vortex formation in the hot leg was prevented, as water just spilled into and filled the large nozzle. Air entrainment during the "spill" mode was small and would not result in unstable pump/system operation.

AP1000 Applicability

AP1000 utilization of this data will be primarily for design of the AP1000. The AP1000 uses the same size hot leg stepped nozzle in the RNS pump suction line as the AP600.

3.2.3.2 RCP SG Channel Head Air-Flow Test

The air-flow test was performed to identify effects on pump performance due to non-uniform channel head flow distribution, pressure losses of the channel head nozzle dam supports and pump suction nozzle, and possible vortices in the channel head induced by the pump impeller rotation. The air test facility was constructed as an approximate 1/2-scale mockup of the outlet half of the channel head, two pump suction nozzles, and two pump impellers and diffusers.

The channel head tubesheet was constructed from clear plastic to allow smoke flow stream patterns to be seen.

The results of the test confirmed that no adverse flow condition, anomalies, or vortices in the channel head were induced by the dual impellers.

AP1000 Applicability

AP1000 utilization of this data is primarily for design of the AP1000. The AP1000 utilizes the same SG/RCP suction arrangement as the AP600. Although the AP1000 has larger RCS flow rates, the number of SG tubes and the size of the RCP suction have been increased. Therefore, the velocity in the channel head region is not impacted significantly.

3.2.3.3 RCP High-Inertia Rotor/Journal and Bearing Tests

In order to provide sufficient flow during coastdown of a RCP pump during a loss-of-power transient rotational inertia is added to the pump shaft.

The AP600 canned motor RCP provides enhanced rotating inertia by housing a high-density (depleted uranium alloy) insert on the shaft. The insert is enclosed in stainless steel for corrosion protection.

An engineering test program was conducted to experimentally confirm theoretical predictions of the parasitic and bearing losses arising from the "high-inertia" rotor concept applied to canned motor pumps. The test program also verified manufacturability and confirmed the adequacy of the design of both the thrust and journal bearings. Additional objectives were to confirm the satisfactory performance of the radial and thrust bearings, and to demonstrate the manufacturability and integrity of a full-scale encapsulated depleted-uranium journal.

Testing successfully demonstrated the design and construction of a full-scale encapsulated high-inertia rotor. It also demonstrated proper operation of the journal bearing and the effectiveness of changes to reduce parasitic drag losses.

AP1000 Applicability

AP1000 utilization of this data will be primarily for design of the AP1000. The AP1000 uses a canned motor RCP similar to the AP600 except that it has a larger rotating inertia.

3.2.3.4 In-Core Instrumentation Electro-Magnetic Interference (EMI) Tests

A test was performed to demonstrate that the system would not be susceptible to EMI from the nearby control rod drive mechanisms (CRDMs). The test was performed by mocking up instrument cables, bringing them into close proximity with an operating CRDM, and measuring the resulting noise induced on simulated flux signals.

The tests demonstrated that induced currents in the fixed in-core detector (FID) cables were acceptably small compared to the FID signals.

AP1000 Applicability

AP1000 utilization of this data will be primarily for design of the AP1000. The design of the incore instrumentation and CRDMs will be the same as for the AP600.

3.2.3.5 Reactor Vessel Air-Flow Visualization Tests

A 1/9-scale model of the AP600 reactor vessel and the four cold legs was constructed at the University of Tennessee. This model was used to visualize the vessel lower plenum to determine if vortices were present and, if so, the effect on them from surrounding features. The model was designed for flow visualization in the lower plenum, so the flow region from the SG outlet through the core support plate was accurately scaled. This included representations of the cold legs, downcomer, lower plenum, and support plate, including the hot-leg segments and the radial support keys in the downcomer and the vortex suppression ring in the lower plenum.

These tests confirmed that vortices were effectively eliminated by the design. The absence of adverse effects was confirmed.

AP1000 Applicability

AP1000 utilization of this data will be primarily in the design of the AP1000.

3.2.3.6 Boron Transport Simulation Test

The principal objective of this test program was to simulate the transport of borated water from the safety injection (SI) nozzles to the core inlet region in support of the AP600 reactor design. This information is important when predicting the consequences of reactivity transients that are terminated by boron injection.

To determine the characteristics of fluid transport in the reactor, a 1/9 scaled experiment was performed at the University of Tennessee. The model included accurate reproductions of the cold legs, downcomer, SI nozzles, vortex suppression ring and secondary core support, lower plenum, and core support plate. Air was used as the working fluid, with a denser gas serving as the injected fluid. A detailed scaling analysis of the AP600 reactor was performed to determine model flow velocities necessary to accurately model the effects of convection, diffusion, turbulence, and gravity as they apply to fluid transport in the reactor system.

The resulting mixing characteristics have been incorporated into the transient accident analysis models for the AP600.

AP1000 Applicability

The portion of the RCS/reactor vessel modeled in this experiment is the same for the AP1000 except for the height of the downcomer.

3.2.3.7 PXS Check Valve Hydraulic Test

The AP600 PXS uses check valves that operate at low differential pressure during gravity-drain injection from the IRWST and from the containment recirculation lines to the reactor vessel.

The PXS check valve test conducted at the Westinghouse Waltz Mill site used an hydraulic test facility configured to model the AP600 PXS line from the containment sump to the reactor vessel injection connection.

The test facility contained 3 series check valves of the types expected to be used in the flow path from the containment to the reactor vessel. During the testing, the flow rate of water was varied to bound the minimum and maximum flow rates expected in the AP600. The check valves performed properly throughout these tests and no disc fluctuation was observed that would be expected to result in valve damage.

AP1000 Applicability

The AP1000 will use simple check valve designs like those tested in this experiment, except that they will be of a larger size to accommodate the larger flow rates required by the AP1000.

3.2.3.8 Operating Nuclear Plant Check Valve Tests

The original AP600 design utilized check valves in series in the IRWST injection lines. These check valves were normally held closed by the RCS pressure, and during a LOCA they would be required to open with a low differential pressure.

Tests were conducted at two domestic nuclear power plants to assess the opening performance of check valves after prolonged exposure to reactor coolant system temperature, pressure, and chemistry conditions.

These tests were conducted on check valves of a similar size and type as would be used in these AP600 lines. The check valves opened as expected with no discernible increase in differential pressure required. Note that the AP600 valve arrangement was changed during the licensing process to replace one of the series check valves with a squib valve. As a result, these check valves no longer see high seating differential pressures and this testing was not used to support licensing of the AP600.

AP1000 Applicability

This test is not needed for the AP1000 because the AP1000 uses squib valves in these lines like the AP600.

4.0 SCALING ASSESSMENT OF THE AP600 TEST PROGRAM

Licensing an uprated version of AP600 requires demonstration that sufficiently scaled test data covering all important (high-ranked) phenomena (see PIRT Section 2.0) exists for safety analysis code validation. A very extensive test database already exists for the AP600 passive plant design. In order to utilize this extensive AP600 database for the AP1000 passive plant design, a scaling evaluation is performed to assess the applicability of the AP600 test database to AP1000. This scaling evaluation provides a quantitative means for showing how well important phenomena are preserved in test facilities originally scaled for AP600 relative to the AP1000 plant. Establishing a test database for AP1000 lays the foundation for code validation that allows simulation of the AP1000 safety system performance.

This AP1000 scaling evaluation addresses the important phenomena associated with the two key passive plant safety systems; the passive core cooling system (PXS) and the passive containment cooling system (PCS). This scaling evaluation assesses the applicability of AP600 data from both separate effects tests and integral effects tests.

The basis for the AP1000 scaling assessment is the AP600 scaling analysis. The AP1000 scaling assessment presented herein uses the methodology and data developed for the various scaling analyses for AP600 (References 1 – 6). Results, insights, and lessons learned from the AP600 scaling effort are incorporated in the AP1000 scaling assessment as much as possible.

Processes, phenomena, components, and interactions found to be less important for AP600 as a result of testing, scaling, and analysis are not scaled for AP1000 so as to focus attention on the those phenomena found to be dominant. Instead, attention will be focused on the influence of important scaled parameters such as core power, volume, hydraulic resistance and gravity head.

4.1 PASSIVE CORE COOLING SYSTEM

The AP600 tests included in this scaling assessment are as follows:

- Separate Effects Tests (SETs)
  - The Automatic Depressurization System (ADS) Test – Full geometric scale; prototypic range of pressures and fluid properties.
  - The Core Makeup Tank (CMT) Test – Full height; prototypic range of pressures and fluid properties.
  - The Passive Residual Heat Removal (PRHR) Test – Full Height; one to three tube geometry; prototypic range of in-tube pressures and fluid properties.

- Integral Effects Tests (IETs)

  - The Oregon State University (OSU) APEX Test – Scaled height (1/4); scaled initial pressure (1/3) ⇒ Scaled time; scaled fluid properties until after ADS is actuated, then pressure similitude exists.

  - The SPES-2 (Simulatore Per Esperienze di Sicurezza) Test – Full height; full pressure ⇒ Time preserved; fluid properties preserved.

  - Rig of Safety Assessment (ROSA) AP600 Test – Full height; full pressure ⇒ Time preserved; fluid properties preserved.

Large-Break LOCA (LBLOCA) Scaling

LBLOCA scaling was not performed for AP600 as the passive plant design mitigates this event just as a conventional plant. Following the LBLOCA blowdown, the core is reflooded and the fuel temperature rise is terminated by accumulator injection only. Thus, the LBLOCA safety analysis did not rely upon passive core cooling systems. Since the AP1000 LBLOCA recovery is similar to the AP600, there is no need for new test data or scaling for AP1000. The continued core cooling at low pressure, following peak clad temperature turn-around, is similar to the IRWST injection phase discussed below for small-break LOCA but with the break flow area added.

Small-Break LOCA (SBLOCA) Scaling

The key SBLOCA accident scenarios addressed in AP600 PXS scaling were the:

- 2-inch cold leg break
- Double-ended Direct Vessel Injection (DVI) break

The 2-inch cold leg break is considered the base case for SBLOCAs, since the behavior of the other small breaks as seen from the AP600 integral effects test results include the same processes and behave similarly to this break. Also, since the 2-inch break is relatively small, it challenges the ADS to adequately depressurize the reactor coolant system (RCS) to allow long term gravity injection from the IRWST and finally from the flooded containment.

The double-ended DVI break is the most limiting SBLOCA, since it results in spilling of half of the passive core cooling system injection and results in the lowest reactor vessel inventory. Also, the double-ended DVI break is the lowest elevation break that can occur in both the AP600 and AP1000.

Therefore, the scaling assessment for AP1000 focuses on the SBLOCA scenarios for the 2-inch cold leg break and the double-ended DVI break, just as in the AP600.

Non-LOCA Scaling

Components important for non-LOCA events for AP600 such as the PRHR and CMTs were scaled in separate effects tests. This scaling is reviewed for applicability to the AP1000. It should be pointed out that the passive safety component scaling in the integral effects tests is also performed to provide additional verification of component scaling for the non-LOCA component performance. The performance of passive safety features, such as the CMT and the PRHR heat exchanger, is similar for non-LOCA transients as they are for small-break LOCAs.

Dominant Phenomena Scaling

The high ranked or dominant phenomena of a SBLOCA transient that are scaled for the AP1000 assessment are shown in Table 4.1-1. The table also indicates the portion of the transient over which the phenomena are most important. The scaling of these phenomena are assessed for AP1000 because they are ranked highly in the PIRT and they were found to be important in the AP600 test and analysis program.

Applicability of Integral Systems Test Matrices

The AP600 IET matrices for the PXS are applicable to AP1000 as the designs, PIRTs and simulated behavior are very similar. The differences in the physical scale and power do not affect the applicability of the test matrices. They affect the scaling which is addressed herein.

4.1.1 Separate Effects Phenomena

The AP600 plant design incorporated several new passive safety components or systems for core cooling that are unique and not found in conventional plants. These included the ADS, CMTs, and PRHR heat exchanger (HX).

Since key phenomena identified in the AP600 PIRTs occurred within or resulted from these components or systems, test data from scaled test facilities was obtained. The basis for scaling of the ADS, CMT, and PRHR HX test facilities can be found in AP600 reports [WCAP-14324 (Reference 7), WCAP-13963 (Reference 8), WCAP-12980 (Reference 9)]. Note that the ADS test covers ADS Stages 1, 2, and 3 (ADS-1/2/3) operation only and that ADS Stage 4 (ADS-4) separate effects testing was not performed as it was treated/sized conservatively and tested as part of the integral effects tests. The same approach will be taken for AP1000.

The separate effects tests for ADS, CMT, and PRHR HX are assessed for applicability to AP1000 in the following sections. The approach to separate effects test assessment is to examine the range of test conditions, and the thermal-hydraulic and geometric similarity with the AP1000. The AP600 ADS-1/2/3 was tested at full scale. Since the AP1000 ADS-1/2/3 is the same size and operates over the same range of conditions as AP600, there are no separate effects test scaling issues. The AP600 CMT and PRHR HX were rigorously scaled for the integral effects tests. Therefore, these components or systems will be addressed from a scaling perspective in subsection 4.1.2, Integral System Phenomena, for AP1000.

4.1.1.1 AP600 SET ADS Test Data

Applicability for AP1000 Safety Analysis Code Validation

The automatic depressurization system consists of two sets of valves connected to the top of the pressurizer, which are used to depressurize the RCS in the event of a design basis LOCA event. Each set of ADS valves consists of Stage 1, 2, and 3 valves. The first stage ADS valves are opened when the water level in the core makeup tank reaches 55 percent. At the same time, a timer is started that automatically opens the second stage valves 120 seconds after the first stage valves open, and the third stage valves 300 seconds after that. RCS inventory that is released through these valves is sparged into the in-containment refueling water storage tank (IRWST) where the steam portion is condensed. The final fourth stage of ADS, which is provided off each of the two hot legs and which reduces RCS pressure to near the containment pressure, was not studied in these tests. Figure 4.1-1 depicts the functioning of the ADS-1/2/3.

A series of separate effects tests were performed on the valves, sparger and associated piping (Reference 10). These tests were conducted over a range of supply pressures and two-phase mixture qualities, which represent expected RCS conditions following ADS valve opening. The ADS valves were also opened in various combinations to provide a range of expected flow rates. In addition, several tests were performed to provide data for a range of design basis events (References 11 and 12). It was confirmed in Reference 13 that these test results bracketed all expected RCS conditions for design basis events.

The purpose of this study is to show that these test data effectively bracket expected ADS conditions in the AP1000, and that the computer code validation that was performed for AP600 is valid for AP1000.

Comparison of Expected ADS Operating Conditions for AP600 and AP1000

In Reference 13, the data overlap between the ADS separate effects tests and the two integral effects tests was established. In all, six integral tests and 25 separate effects tests were reviewed. By comparing key data from the integral tests from SPES and OSU scaled up to AP600, with the ADS SET test conditions, it was determined that the ADS tests effectively represent the range of operating conditions expected in AP600.

For the AP1000, the operating pressure is the same as AP600 (2250 psia). The pressure transient for a typical SBLOCA is shown in Figure 4.1-2. Thus, a design basis accident is initiated from the same pressure. For a LOCA event, the core makeup tanks are expected to drain at a similar rate (level vs. time) for both plants. Thus, the actuation of the ADS is expected to occur at approximately the same pressure for AP1000. As discussed in Reference 14, the valve size and configuration for ADS-1/2/3 are the same as AP600. Since the AP1000 valves are identical to the AP600, the valve pressure drop characteristics are expected to be the same. Also, the mass flow rate, which for choked flow is a function of the upstream pressure and enthalpy, is expected to be in the same range. It is possible that the inlet quality might be higher for the higher power plant, but the test range covers the entire range of quality.

One difference in the ADS behavior for the two plants is that the larger RCS mass and energy inventory for AP1000 may lengthen the depressurization time relative to AP600. However, the code models are valid since the physical characteristics of the valves are identical, and the mass flows and fluid properties are within the test ranges. Therefore, the analysis codes can accurately predict the RCS performance during ADS.

The key parameters governing ADS performance and results are summarized for the tests and the plant in Table 4.1-2.

Conclusion

The results of this evaluation show that the ADS test data that was developed for AP600 is applicable to AP1000. This is due to the similar operating conditions for both plants, and the use of the same valves for the first 3 stages of ADS. Computer codes that have been validated with this test data can therefore be used with confidence to perform safety analysis for AP1000.

4.1.1.2 Core Makeup Tank Test

The Westinghouse Core Makeup Tank test facility is a full-pressure (20 to 2250 psia) separate effects test facility that simulates the CMT circulation path including balance and discharge lines. The test facility has a steam/water reservoir that can simulate single-phase recirculation or two-phase draining modes of operation. The CMT test vessel, which is about 1/8th the diameter of an AP600 CMT, is elevated above the steam/water reservoir to fully simulate the gravity draining mode of operation.

Scaling of the Westinghouse CMT test facility relative to AP600 can be found in References 4 and 8. These scaling reports derived and evaluated several key groups to scale CMT circulation and heat transfer including Richardson number (Π_{Ri}), Friction number (Π_F) Biot number (Π_{Bi}), Stanton number (Π_{St}), Grashoff (Π_{Gr}) and Prandtl (Π_{Pr}) numbers. Since the CMT design, material, and wall thickness are the same for AP1000 and similar fluid conditions exist, the key scaling groups for AP1000 should not be much different than AP600 with the exception of the Richardson (Π_{Ri}) and Friction (Π_F) numbers, as discussed below.

The AP1000 CMT piping resistance has been reduced from that in AP600 and is reflected in both the Richardson and Friction numbers. The AP1000 Richardson and Friction numbers are about 25-percent smaller than AP600. However, as with AP600 the ratio of Richardson number to Friction is preserved between AP1000 and the Westinghouse CMT test facility and thus preserves the natural circulation flow (Reference 8). As such the Westinghouse CMT test data obtained for AP600 is applicable to the AP1000. Table 4.1-3 shows the CMT scaling groups.

4.1.1.3 Passive Residual Heat Removal System Test

4.1.1.3.1 AP600 PRHR Test Results

One of the components that was tested in a separate effects test is the passive residual heat removal (PRHR) heat exchanger. The objective of the PRHR separate effects test program was

to generate data on heat transfer to be used in the design and characterization of the prototype heat exchanger in the AP600. The test article consisted of three vertical (straight) type 304 stainless steel tubes, approximately 18 feet in length, with an outer diameter of 0.75 inches and wall thickness of 0.067 inches. The tubes were placed in a water tank approximately 4 feet in diameter and 32 feet tall, with a nominal water depth inside the tank of 24 feet. The tubes were placed in a radial straight line near a wall of the tank, with a center-to-center spacing of 1.5 inches. A baffle was placed near the tubes, almost at the same height as the tank water level to limit natural convection flow around the tubes.

The tube dimensions and spacing were characteristic of the original AP600 PRHR system design. Subsequent design changes resulted in a vertical C-shaped tube heat exchanger. Thermal-hydraulic correlations that were developed from the vertical straight tube test data were applied to the new design. Subsequent tests in the ROSA large scale facility were performed using a scaled C-tube heat exchanger. The NRC found that the correlations that were developed for the vertical straight tube heat exchanger adequately predicted the performance of the C-tube heat exchanger (Reference 15).

An additional issue that was addressed during AP600 design certification was the sizing of the PRHR heat exchanger with respect to the heat rejection requirements. Specifically, it was determined that the heat flux from the outside of the tubes to the water in the IRWST did not exceed the critical heat flux, and that the spacing between the tubes was sufficient to assure that tubes would not be steam-blanketed. Sensitivity studies were performed with the top of the tubes uncovered to demonstrate that the heat exchanger could remove adequate heat from the RCS with a portion of the tubes unavailable for effective heat transfer (Reference 9). These tests showed that the AP600 PRHR heat exchanger is oversized with margin available for all anticipated operating conditions.

4.1.1.3.2 AP1000 PRHR Design

The AP1000 PRHR is designed to operate in the same manner and for the same events as AP600. The operating conditions are also expected to be the same. The design has been slightly modified to accommodate the increased reactor power by increasing the heat transfer area. Eighteen tubes have been added to the 671 tubes for the AP600 design. These tubes have been added at the top and bottom of the tube sheet and the original tube diameter, spacing and pitch have been preserved. In addition, the tube horizontal inlet and outlet portions have been lengthened a total of 8 feet resulting in an increase in the total heat transfer area of approximately 22 percent relative to AP600. The line resistances for the PRHR inlet have also been reduced to increase the natural circulation flow, which results in increased heat transfer.

Calculations were performed to determine the heat flux on the outside of the tubes and the margin to the core critical heat flux (CHF) limit. RCS conditions representing PRHR cooldown to steam generator (SG) secondary side temperature are simulated. For this case, the hot leg temperature that serves as the PRHR inlet boundary condition is assumed to be [ ]^{a,b,c} (temperature established by the setting of the main steam safety relief valves). The PRHR outlet temperature is calculated by performing a series of heat transfer calculations on sections of the PRHR tubes. Various heat transfer correlations are used on the inside and outside of the PRHR

tubes depending on the flow regime, tube orientation, and the heat transfer regime on the outside of the tubes. Nominal line resistances are assumed for these calculations. The resulting outlet temperature is used to determine the thermal driving head and the subsequent flow rate through the heat exchanger. A separate calculation is performed to determine the heat transfer with forced flow through the PRHR heat exchanger during operation with the reactor coolant pumps operating.

Figure 4.1-3 shows the estimated heat flux for AP600 and AP1000 PRHR for both forced and natural circulation flow. AP600 testing included forced flow conditions to determine the maximum heat transfer rates although this is not a normal operating condition for the PRHR. As expected, the heat flux is maximum at the tube inlet. These results show that the heat flux for the AP1000 is marginally higher than AP600, but still far below the critical heat flux limit. In addition, the expected operating conditions for the AP1000 PRHR are bracketed by the forced flow AP600 results, which were conducted in the integral test facilities (References 9, 11, and 12).

In addition, a comparison of the PRHR performance for various non-LOCA events was completed in Reference 14. Figures 4.1-4, 4.1-5, and 4.1-6 show the comparison for AP600 and AP1000 developed using LOFTRAN for Loss of Power, Loss of Normal Feedwater, and Main Feedline Break events, respectively. The results are normalized to the reactor power under operating conditions. These results show that the PRHR will remove the same fraction of reactor power for the AP1000. Since the tube surface area is increased 22 percent, but the reactor power is increased 73 percent; the average heat flux for the AP1000 is about 42 percent higher than AP600. This is the same order of magnitude as the results in Figure 4.1-3, and is well within the CHF limits.

Based on these observations, the following conclusions can be reached:

- The AP1000 PRHR functional requirements are the same as AP600, and the expected operating conditions are the same.

- The AP1000 PRHR design is basically the same as AP600 since it has the same configuration, tube diameter, spacing and pitch. Increased heat exchanger capacity is achieved by increasing the tube length by a total of [ ]^{a,b,c}, by adding [ ]^{a,b,c} additional tubes, and by increasing the natural circulation flow rate.

- The expected operating conditions for the AP1000 PRHR result in external tube heat flux values that are far below the critical heat flux limits, and are bracketed by forced flow test data from the AP600 integral tests.

- Heat transfer correlations that were developed from the AP600 test data are valid for the AP1000 PRHR.

- Calculated performance comparisons of the AP1000 and AP600 PRHR heat exchangers indicate that the AP1000 PRHR removes the same proportion of full power decay heat as the AP600 PRHR heat exchanger.

4.1.2 Integral System Phenomena

Integral system phenomena in AP1000 and AP600 were tested for small-break LOCA transients. All of the core cooling passive safety features are employed to mitigate the transient and the transient includes broad ranges of thermal-hydraulic behavior. Therefore, three scaled integral effects test facilities were employed in the AP600 test program to provide data for computer code validation. Detailed scaling studies of two integral effect tests (SPES-2 and OSU) are presented in this report.

The SBLOCA transient will be divided into six major phases similar to the Reyes and Hochreiter approach, (Reference 3) with a transition phase added between ADS and IRWST injection phases. The ADS to IRWST transition phase is added, as it is the critical period for maintaining core cooling during a small-break LOCA. (See subsection 4.1.2.4 below for further discussion.) These phases of the SBLOCA are listed below:

- Blowdown (subsection 4.1.2.1)
- Natural Circulation (subsection 4.1.2.2)
- ADS (subsection 4.1.2.3)
- ADS to IRWST Transition (subsection 4.1.2.4)
  - CMT injection dominant
  - IRWST injection dominant
- IRWST Injection (subsection 4.1.2.5)
- Sump Injection (subsection 4.1.2.6)

Of the SBLOCA transient phases listed above, the most important phase is the period from ADS to IRWST injection. This is supported in subsection 21.5.10 of the AP600 FSER, Volume 2, which states that the:

> "...end of the ADS blowdown period to the inception of IRWST injection..." is referred as the "...critical period...during which the minimum mixture level in the reactor vessel is expected to occur."

This is verified in the AP600 test program, where this transition period is shown to be where the minimum reactor vessel inventory occurs and consequently, the scaling assessment focuses on the processes during this transition as they influence reactor vessel inventory.

Scaling Approach

The approach taken in this scaling analysis is derived from the hierarchical two-tiered scaling (H2TS) methodology of Zuber (Reference 16) as applied by Reyes (Reference 1) and Brown, Hochreiter, and Loftus (Reference 4) to the AP600 integral effects test facilities.

The overall scaling approach to the integral effects test facilities involves scaling at two levels: top-down and bottom-up scaling.

Top-down scaling involves scaling at a global or system level where the relative influences of various components or processes can be assessed. Top-down scaling is very efficient because it addresses multiple processes with a relatively small number of scaling groups. For an integral effects test facility this macro-level type scaling is well-suited to capture the integral effects of multiple processes.

Bottom-up scaling involves scaling at a local or subsystem level where a more detailed assessment is needed for a specific component or process. This micro-level type scaling is useful to assess separate effects and accomplish the detailed design of a scaled test facility. It is also useful where top-down scaling is not practical.

For the purpose of assessing integral effects test facilities that are already designed (i.e., SPES, OSU, or ROSA) or established, top-down scaling is primarily employed except where impractical or where local effects are deemed to be of high importance in the PIRT (i.e., such as entrainment of liquid in the hot leg to the ADS-4 vent path). Therefore, in this integral effects scaling section, top-down scaling is used extensively. Bottom-up scaling is used only where important phenomena identified in the PIRT are not readily addressed at a system level.

The overall process involved in the scaling is as follows:

1. The SBLOCA event is divided into major phases as identified above. For scaling purposes, it is desirable to subdivide the event into transient and steady-state phases. Each phase should ideally feature some important component or process, which dominates the phase.

2. System level (i.e., top-down) equations (conservation of mass, energy, and momentum) are written addressing important processes (using the PIRT and prior test experience as a guide) involved during the specific phase of the transient. Important processes that are not readily addressed in the system level equation set are addressed with an appropriate model or correlation (i.e., bottom-up).

3. The equations are "combined" at this stage as much as possible to reduce the number of scaling groups that would be obtained and allow a greater number of important phenomena to be directly compared. The equations are also put in a form that highlights the focus of the physical processes on the key parameter of interest such as reactor vessel inventory, pressure, quality, or void fraction. Simplified treatment of phenomena is typically used to achieve this goal. (Refer to each individual scaling sections for further explanation.)

4. The variables in the equations are non-dimensionalized using references values. These reference values may represent a boundary condition, initial condition, range of expected values, or a maximum value such as may be obtained from a steady-state condition. The choice of reference values should render the dimensionless quantities to be of order 1 at the end of this process.

5. The resulting dimensional coefficients in the equations are then normalized using one of the coefficients in the equation. Typically the coefficient associated with the most dominant process is chosen. The end result yields dimensionless π groups, and time constants, τ, or frequencies, ω, (for transient equations).

6. The ratios of dimensionless π groups, time constants, τ, or frequencies, ω, are obtained by comparing test facilities and plant scaling ratios.

7. Acceptance criteria are applied to the key scaling ratios. From this it can be determined which phenomena are acceptably scaled to support code validation and which are distorted.

Steady-state equations are used where the parameter of scaling importance does not change significantly over the phase. For steady-state equations, the scaling process produces only dimensionless π groups, which Zuber refers to as characteristic time ratios. For example; for a steady-state conservation of mass equation, normalized on the mass flow out of the system, we obtain a characteristic time ratio, $\pi_{\dot{m}}$, as shown below.

Starting with the steady-state conservation of mass:

$$\frac{dM}{dt} = \dot{m}_{in} - \dot{m}_{out} = 0 \qquad (4\text{-}1)^*$$

Non-dimensionalizing the mass flows with reference mass flows we obtain:

$$(\dot{m}_{in})_{ref} \dot{m}^+_{in} - (\dot{m}_{out})_{ref} \dot{m}^+_{out} = 0 \qquad (4\text{-}2)$$

Normalizing on the mass flow out of the system, one dimensionless group results:

$$\pi_{\dot{m}} \cdot \dot{m}^+_{in} - \dot{m}^+_{out} = 0 \qquad (4\text{-}3)$$

where $\pi_{\dot{m}} = \left(\frac{\dot{m}_{in}}{\dot{m}_{out}} \right)_{ref}$

Transient equations are used where the parameter of scaling importance changes significantly with time. For transient equations, the scaling process can produce dimensionless π groups and time constants τ or, if the dimensionless π groups are divided through by a time constant, frequencies ω are obtained (i.e., $\omega = \pi/\tau$). A frequency is a ratio of the intensity or strength of transfer of a conserved property relative to the capacity of the receiving volume or mass. A frequency, ω, can also be thought of as the fractional rate of change of the receiving volume or mass by the action of a specific transfer process. Higher frequency represents stronger coupling

*Equation nomenclature is provided on page 4-60.

or interaction, and visa versa. It is the goal of scaling to preserve higher frequency processes between a scaled test facility and prototype. The process of producing dimensionless groups, time constants, and frequencies is demonstrated below.

Starting with the transient conservation of mass:

$$\frac{dM}{dt} = \dot{m}_{in} - \dot{m}_{out} \tag{4-4}$$

For constant density, the above equation can be rewritten as:

$$\rho \cdot \frac{dV}{dt} = \dot{m}_{in} - \dot{m}_{out} \tag{4-5}$$

Non-dimensionalizing the variables in the above equation:

$$(\rho \Delta V)_{ref} \frac{\rho^{+} dV^{+}}{dt} = (\dot{m}_{in})_{ref} \dot{m}_{in}^{+} - (\dot{m}_{out}) \dot{m}_{out}^{+} \tag{4-6}$$

Normalizing on mass flow out, we can obtain a non-dimensional π group, $\pi_{\dot{m}}$, and a time constant, τ:

$$\tau \cdot \frac{\rho^{+} dV^{+}}{dt} = \pi_{\dot{m}} \cdot \dot{m}_{in}^{+} - \dot{m}_{out}^{+} \tag{4-7}$$

where:

$$\pi_{\dot{m}} = \left(\frac{\dot{m}_{in}}{\dot{m}_{out}} \right)_{ref} \tag{4-8}$$

and

$$\tau = \left(\frac{\rho \Delta V}{\dot{m}_{out}} \right)_{ref} \tag{4-9}$$

Now, if we divide through by the time constant, τ, we obtain frequencies instead of a dimensionless group and time constant:

$$\frac{\rho^{+} dV^{+}}{dt} = \left(\frac{\dot{m}_{in}}{\rho \Delta V} \right)_{ref} \cdot \dot{m}_{in}^{+} - \left(\frac{\dot{m}_{out}}{\rho \Delta V} \right)_{ref} \dot{m}_{out}^{+} \tag{4-10}$$

or, this equation can be expressed as:

$$\frac{\rho^{+}dV^{+}}{dt} = \omega_{in} \cdot \dot{m}_{in}^{+} - \omega_{out} \cdot \dot{m}_{out}^{+} \tag{4-11}$$

where:

$$\omega_{in} = \left(\frac{\dot{m}_{in}}{\rho \Delta V}\right)_{ref} \tag{4-12}$$

and

$$\omega_{out} = \left(\frac{\dot{m}_{out}}{\rho \Delta V}\right)_{ref} \tag{4-13}$$

Acceptance Criteria

The acceptance criteria used in assessing the scaling results comparing dimensionless groups, time constants, and frequencies for the test facilities and plants are discussed below.

Dimensionless π Groups

Ideal preservation of all key scaling groups (i.e., $\pi_R = 1.0$) is difficult to attain in scaled test facilities. It is widely recognized that some distortion is inevitable but acceptable as long as it is not significant. Therefore, an acceptance criterion was established in assessing the key scaling ratios of the AP600 test program.

The acceptance criterion used in scaling the test facilities for AP600 was the ratio of important dimensionless π groups between test facility and plant should be within a factor of two of ideal scaling:

$$0.5 \leq \pi_R \leq 2.0 \tag{4-14}$$

where:

$$\pi_R = \pi_{TEST} / \pi_{AP600 \text{ or } AP1000} \tag{4-15}$$

Scaling ratios that fall inside this range are considered acceptable and not significantly distorted. [See the AP600 Scaling and PIRT Closure Report, WCAP-14727 (Reference 4).]

This acceptance criteria is also stated in subsection 21.5.10 of the AP600 FSER, Volume 2, NUREG-1512 (Reference 15) as:

> "Good agreement between a "pi" group value and the AP600 value for the same "pi" group (within a factor of about 2) indicates acceptable scaling of the phenomena or parameter represented by the "pi" group."

This same acceptance criteria is adopted for the AP1000 scaling assessment.

Time Constants and Frequencies

Acceptance criteria for key time constant or frequency ratios was not explicitly established for AP600 transient phases such as ADS depressurization and the ADS-IRWST transition phase. Time constant ratios for important processes should ideally be unity for test facilities such as SPES and ROSA where time is preserved, and should be 1/2 for OSU, which is a time scaled facility. As with dimensionless scaling groups, some distortion associated with key time constant or frequency ratios should be acceptable as long as the distortion is not significant.

The acceptance criteria that will be adopted for assessing AP1000 will be based upon Zuber's concept of scaling frequency. Recall that a frequency (ω) is defined as the ratio of a dimensionless group to time constant (i.e., $\omega = \pi/\tau$). Important frequency ratios should be within a factor of two of ideal scaling. This is done on the basis that to establish similarity between the test facility and plant for a transient, time constants and dimensionless groups in the scaling equation must be preserved. In other words, to achieve similarity, the mathematical solution should be similar and that requires similar coefficients. For example, if scaling the change in reactor vessel inventory (volume) is of interest, the following scaling equation for the test facility and plant could be obtained:

$$\tau_{test} \cdot \frac{\rho^{+} dV^{+}_{vessel,test}}{dt} = \pi_{test} \cdot \dot{m}^{+}_{in,test} - \dot{m}^{+}_{out,test} \tag{4-16}$$

$$\tau_{plant} \cdot \frac{\rho^{+} dV^{+}_{vessel,plant}}{dt} = \pi_{plant} \cdot \dot{m}^{+}_{in,plant} - \dot{m}^{+}_{out,plant} \tag{4-17}$$

In order to achieve similarity between the test and the plant, the coefficients in the equation set above must be similar, since the dimensionless terms are of order one:

$$\pi_{test} \cong \pi_{plant} \tag{4-18}$$

$$\tau_{test} \cong \tau_{plant} \text{ (for time preserved facilities)} \tag{4-19}$$

$$k \cdot \tau_{test} \cong \tau_{plant} \text{ (for time scale facilities)} \tag{4-20}$$

where k = time scale factor

Note that for steady-state equations, only $\pi_{test} \equiv \pi_{plant}$ is required.

Recasting the equations above by dividing by the time constants, the following form in terms of frequencies is obtained:

$$\frac{\rho^{+} dV^{+}_{vessel,test}}{dt} = \omega_{in,test} \cdot \dot{m}^{+}_{in,test} - \omega_{out,test} \cdot \dot{m}^{+}_{out,test} \quad (4\text{-}21)$$

$$\frac{\rho^{+} dV^{+}_{vessel,plant}}{dt} = \omega_{in,plant} \cdot \dot{m}^{+}_{in,plant} - \omega_{out,plant} \cdot \dot{m}^{+}_{out,plant} \quad (4\text{-}22)$$

From the above, it can be seen that the frequencies ($\omega = \pi/\tau$) must be preserved to achieve similarity. Therefore, for a time preserved facility such as SPES or ROSA, where the ideal time constant ratio is 1.0, acceptable scaling is achieved if:

$$0.5 \le (\omega)_R \le 2.0 \quad (4\text{-}23)$$

where $(\omega)_{R-IDEAL} = \frac{(\pi_{test} / \tau_{test})}{(\pi_{plant} / \tau_{plant})} = \left(\frac{\pi_{test}}{\pi_{plant}}\right) \cdot \left(\frac{\tau_{plant}}{\tau_{test}}\right) = (1) \cdot (1) = 1.0$

For a time-scaled facility such as OSU, where the ideal time constant ratio (i.e., $(\tau)_R = \frac{\tau_{OSU}}{\tau_{plant}} = \frac{1}{2}$) is 1/2, acceptable scaling is achieved if:

$$1.0 \le (\omega)_R \le 4.0 \quad (4\text{-}24)$$

where $(\omega)_{R-IDEAL} = \frac{(\pi_{OSU} / \tau_{OSU})}{(\pi_{plant} / \tau_{plant})} = \left(\frac{\pi_{OSU}}{\pi_{plant}}\right) \cdot \left(\frac{\tau_{plant}}{\tau_{OSU}}\right) = (1) \cdot (2) = 2.0$

These acceptance criteria for frequency are based on the same scaling philosophy used in accepting $0.5 < \pi_R < 2$ for AP600 scaling.

The following sections present the scaling assessments for the AP1000 SBLOCA.

4.1.2.1 Blowdown Phase Scaling

As the blowdown phase of a SBLOCA transient is not typically associated with the minimum reactor vessel inventory and the high-ranked processes (i.e., critical break flow and decay heat) involved are not unique to passive plants. This phase received very modest attention in the AP600 scaling analysis. The blowdown phase behavior of the AP600 and AP1000 and the sensitivity of plant behavior to core decay heat is similar to conventional PWR plants since the passive safety systems have virtually no influence on the blowdown phase. This coupled with the ample availability of experimental databases for blowdowns in conventional PWRs, there is

little gained in scaling the blowdown phase for AP600 or AP1000. Therefore, the blowdown phase will not be scaled for AP1000.

4.1.2.2 Natural Circulation Phase Scaling

Top-Down Scaling Analysis of PRHR Natural Circulation

Two-phase natural circulation and PRHR heat transfer are high-ranked PIRT phenomena in this accident phase. PRHR heat transfer is addressed in subsection 4.1.1.3 via the PRHR SET. CMT circulation is addressed in subsection 4.1.1.2 via the CMT SET and later in subsection 4.1.2.4 via CMT injection. PRHR natural circulation is addressed in this section at a top-down level.

Scaling of the PRHR natural circulation phase addresses scaling of two-phase natural circulation at a system level after the natural circulation via the steam generators (which is well known from conventional plants) ceases to dominate. The flow path during natural circulation includes the reactor vessel, the hot leg, the PRHR inlet piping, the PRHR HX, the PRHR outlet piping, the cold leg, and back to the reactor vessel. The fluid is a single-phase liquid from the PRHR HX discharge to the cold leg (steam generator outlet side), to the reactor vessel core where the fluid becomes two-phase, and flows to the PRHR HX inlet via the hot leg. The two-phase mixture discharged from the reactor vessel is condensed in the PRHR HX and returned to the reactor vessel. The recirculation path described can be treated as a closed loop with the condensation effectively occurring at the midpoint elevation of the PRHR (i.e., thermal center) and the boiling effectively occurring at the midpoint of the core. Note that flow paths involving the steam generators are not dominant for energy transport after the blowdown phase when the primary and secondary temperature have reached equilibrium, whereas the PRHR heat sink remains effective at least until the ADS phase. Therefore, only the PRHR circulation is scaled in this phase.

To accomplish the top-down scaling, steady-state conservation of mass, momentum, and energy equations describing the natural circulation path are combined into a single expression. This equation includes the dominant influences such as PRHR gravity head, PRHR flow path hydraulic resistance and core decay power. The influence of subcooling is neglected as water in the RCS is near saturation conditions during this phase.

Quality and pressure determine the state of a two-phase system. Quality is a fundamental parameter of importance to be scaled during this phase as RCS pressure is nearly constant. Therefore, quality was selected as the top-down scaling parameter to evaluate in the natural circulation phase.

Quality should be preserved ($x_R = 1.0$) when property similitude exists such as in full pressure facilities (i.e., SPES and ROSA) and should be scaled when fluid properties are scaled as $x_R \left(\frac{\Delta \rho}{\rho_g} \right)_R = 1.0$ according to Reyes (Reference 1), Ishii and Kotaoka (Reference 17) and Kocamustafaogullari and Ishii (Reference 18). Applying the scaling equation development

for quality for saturated two-phase natural circulation (refer to subsection 4.1.2.6 for details), the following ideal scaling relation can be obtained:

$$\left[x_e\right]_R \cdot \left(\frac{\Delta\rho}{\rho_g}\right)_R = \left[\frac{\left(\frac{Q_{core}}{h_{fg}}\right)^2 \frac{1}{\rho_f}\left[\left(\sum \frac{R}{A^2}\right)_{PRHR\ outlet} + \Phi_{fo}^2 \left(\sum \frac{R}{A^2}\right)_{PRHR\ inlet}\right]}{\rho_f g \left(\Delta Z_{\substack{PRHR \\ core}}\right)}\right]_R^{1/2} \cdot \left(\frac{\Delta\rho}{\rho_g}\right)_R = 1.0 \qquad (4\text{-}25)$$

Using appropriate reference values for AP600, AP1000, OSU, and SPES; the following scaling ratios are obtained:

[

Natural Circulation Phase – Quality Relation					

]a,b,c

From the scaling ratios above, it can be seen that SPES is sufficiently scaled to both AP600 and AP1000. OSU, on the other hand, is not well scaled to AP600 or AP1000 from a top-down perspective for the natural circulation phase. Therefore, the codes should be benchmarked against the separate effects test and SPES for the Natural Circulation phase rather than OSU. Refer to the SET section (4.1.1.3) for additional details on PRHR scaling. The distortion in OSU appears to be associated with PRHR flow path resistance. The OSU flow resistance produces a mass flow rate which is too small relative to AP600 and AP1000 and results in a quality that is much higher than required by the scaling relation applied by Reyes. In order to satisfy core power, a much higher quality than desired results.

Bottom-Up Scaling Analysis

CMT Balance Line Flow Composition

CMT balance line flow composition is important as it influences CMT draining, and therefore, when the ADS actuation setpoint in the CMT is reached, the flow composition in the CMT balance line is dependent upon the flow pattern in the cold leg to which it is connected and phase separation at the cold leg to CMT balance line tee connection. Therefore, cold leg flow pattern and phase separation at the cold leg to CMT balance line tee connection will be scaled from the bottom-up perspective below.

Cold Leg Flow Pattern

Modified Froude number is a dominant parameter used by Taitel-Dukler (Reference 19) in establishing flow regime boundaries for two-phase flow in horizontal pipe flow. Reyes used this approach in scaling horizontal pipe flow in OSU. The Froude number used by Taitel-Dukler is defined as follows:

$$F_r = \frac{j_g}{\sqrt{gd}}\left(\frac{\rho_g}{\rho_f - \rho_g}\right)^{1/2} \tag{4-26}$$

Preserving Froude number results in the following:

$$(\pi_{Fr})_R = \left[\frac{j_g}{\sqrt{d}}\left(\frac{\rho_g}{\rho_f - \rho_g}\right)^{1/2}\right]_R \tag{4-27}$$

The superficial velocity, j_g, in the cold leg is expressed as:

$$(j_g)_{CL} = \left(\frac{Q_g}{A}\right)_{CL} \tag{4-28}$$

An estimate of the volumetric flow rate of the gas phase in the RCS loop piping, Q_g, for scaling purposes can be obtained from a steady-state balance in the reactor core for saturated conditions:

$$Q_g = \frac{q_{core}}{\rho_g \cdot h_{fg}} \tag{4-29}$$

The Froude number scaling ratio for facilities where pressure similitude exists, such as SPES and ROSA, becomes:

$$(\pi_{Fr})_R = \left[\frac{q_{core}}{d_{CL}^{5/2}}\right]_R \tag{4-30}$$

Using appropriate reference values for AP600, AP1000, OSU, and SPES, the following scaling ratios are obtained:

Natural Circulation Phase – Froude Number – Cold Leg					

a,b,c

Both SPES and OSU are sufficiently scaled to AP600 and AP1000.

Phase Separation at Cold Leg to CMT Balance Line Tee

When a two-phase flow encounters a T-junction with a vertical upward branch (i.e., CMT balance line) connected to the top of a main pipe (i.e., cold leg), the branch quality (x_{branch}) is, in general, different from the quality in the main pipe (x_{main}) due to phase separation. Phase separation is influenced by:

- Inertial and buoyancy forces. The lower density phase preferentially enters a top-vertical branch.
- Flow pattern in the main pipe upstream of the T-junction.

There is currently no general or top-down method for predicting this two-phase flow phenomenon, however, some experimental work (References 20 and 21) address phase separation.

A correlation relating branch to main pipe quality for a top-vertical branch for a non-stratified upstream flow regime has been developed by Seeger et al. (Reference 20) and supported by Mudde et al. (Reference 21):

$$\frac{x_{branch}}{x_{main}} = \left(\frac{G_{branch}}{G_{main}}\right)^{-0.8} \tag{4-31}$$

where $G = \dot{m} / A$ = mass flux.

Preserving the relation between branch and main pipe quality:

$$(\pi_x)_R = \left(\frac{x_{branch}}{x_{main}}\right)_R = \left[\left(\frac{\dot{m}_{branch}}{\dot{m}_{main}}\right)\cdot\left(\frac{A_{main}}{A_{branch}}\right)\right]_R^{-0.8} = \left[\left(\frac{\dot{m}_{branch}}{\dot{m}_{main}}\right)\cdot\left(\frac{d_{main}}{d_{branch}}\right)^2\right]_R^{-0.8} \tag{4-32}$$

Putting this in terms of the CMT balance line (i.e., branch) and cold leg (i.e., main):

$$(\pi_x)_R = \left[\left(\frac{\dot{m}_{\substack{\text{CMT} \\ \text{balance} \\ \text{line}}}}{\dot{m}_{CL}} \right) \cdot \left(\frac{d_{CL}}{d_{\substack{\text{CMT} \\ \text{balance} \\ \text{line}}}} \right)^2 \right]_R^{-0.8} \tag{4-33}$$

For approximate preservation of resistance and gravity head in the CMT flow path relative to the main reactor coolant piping, the flow distribution should be approximately preserved so that the scaling ratio simplifies to:

$$(\pi_x)_R = \left[\left(\frac{d_{CL}}{d_{\substack{\text{CMT} \\ \text{balance} \\ \text{line}}}} \right)^2 \right]_R^{-0.8} \tag{4-34}$$

Using appropriate reference values for AP600, AP1000, OSU, and SPES, the following scaling ratios are obtained:

Phase Separation at Cold Leg to CMT Balance Line Tee					

a,b,c

Both SPES and OSU are acceptably scaled to AP600 and AP1000.

4.1.2.3 ADS Phase Scaling

Depressurization of the RCS is crucial in a SBLOCA transient for a passive plant as it allows gravity injection for long term core cooling. The function of the ADS-1/2/3 in the AP600 and AP1000 designs is to provide rapid high-pressure venting of steam from the upper volume of the RCS. As shown in Figure 4.1-1, the ADS-1/2/3 vent path is connected to the top of the pressurizer and receives steam from the RCS volume via the hot leg and surge line. The ADS-4 vent paths are connected to the top of each hot leg and are designed to maintain depressurization of the RCS at low pressure by venting steam produced by core decay heat from the reactor vessel.

The AP600 scaling analysis (Reference 4) found that the dominant mass, energy, and momentum effects during this phase of the transient are associated with ADS vent path. For scaling purposes, the RCS could be treated at a system level as a simple steam-liquid control volume vented via the ADS.

4.1.2.3.1 Top-Down Scaling Analysis

Depressurization of the Reactor Coolant System via ADS-1/2/3

The parameter of primary interest in the depressurization phase is reactor coolant system pressure. Therefore, the rate of pressure change (RPC) equation is used to scale the ADS depressurization process from a top-down perspective. Transient scaling is used, since the pressure is changing significantly with time.

AP600 Scaling analyses by Wulff (Reference 2) and Reyes (Reference 1) found that mass and energy injected into the RCS during the ADS phase (i.e., associated with $\dot{m}_{in}$) from the core makeup tanks or accumulators is small relative to the ADS discharge flow and energy (i.e., associated with $\dot{m}_{out}$). Therefore, as the ADS discharge flow and energy are dominant, the boundary of the RCS volume is rigid, and the ADS largely vents steam from the pressurizer during the early stages of the ADS phase (i.e., the pressurizer and upper regions of the RCS are drained) the rate of pressure change equation [per Moody (Reference 22), Yadigaroglou (Reference 23), or Reyes (Reference 24)] can be simplified to the ideal gas form for the ADS phase as:

$$\left(\frac{V_{RCS}}{\frac{\text{steam volume}}{(\gamma-1)}}\right)\frac{dp_{RCS}}{dt}_{\text{steam volume}} = \dot{m}_{\underset{\text{steam}}{\text{core}}}\, h_g - \dot{m}_{\underset{\text{steam}}{\text{ADS}}}\, h_g \qquad (4\text{-}35)$$

The PRHR heat exchanger does provide some steam condensation at the onset of the ADS phase, but very quickly diminishes as the ADS is actuated. The ADS rapidly reduces the RCS pressure and hence the temperature difference across the PRHR heat exchanger. In addition, the reduction in RCS pressure increases the steam specific volume and results in a decrease in mass flow rate to the PRHR heat exchanger.

The rate of pressure change equation parameters can be non-dimensionalized and put into the following form:

$$\frac{1}{(\gamma-1)}\cdot\frac{dp^{+}_{RCS}}{dt}_{\text{steam volume}} = \left[\frac{\dot{m}_{\underset{\text{steam}}{\text{core}}}\cdot h_g}{(V\Delta p)_{\underset{\text{steam volume}}{RCS}}}\right]_{Ref}\cdot \dot{m}^{+}_{\underset{\text{steam}}{\text{core}}}\, h^{+}_g - \left[\frac{\dot{m}_{\underset{\text{steam}}{\text{ADS}}}\cdot h_g}{(V\Delta p)_{\underset{\text{steam volume}}{RCS}}}\right]_{Ref}\cdot \dot{m}^{+}_{\underset{\text{steam}}{\text{ADS}}}\, h^{+}_g \qquad (4\text{-}36)$$

The coefficients associated with the dimensionless terms on the right-hand side of the above equation represent process frequencies. The above equation can be re-expressed as:

$$\frac{1}{(\gamma-1)}\cdot\frac{dp^{+}_{\substack{RCS\\ steam\ volume}}}{dt}=\omega_{\substack{core\ steam\\ -RCS\ stm\ vol}}\cdot\dot{m}^{+}_{\substack{core\\ steam}}\,h^{+}_{g}-\omega_{\substack{ADS\ steam\\ -RCS\ stm\ vol}}\cdot\dot{m}^{+}_{\substack{ADS\ steam\\ -RCS\ stm\ vol}}\cdot h^{+}_{g} \tag{4-37}$$

where

$$\omega_{\substack{core\ steam\\ -RCS\ stm\ vol}}=\left[\frac{\dot{m}_{\substack{core\\ steam}}\cdot h_g}{(V\cdot\Delta p)_{\substack{RCS\\ steam\\ volume}}}\right]_{Ref} \tag{4-38}$$

and

$$\omega_{\substack{ADS\ steam\\ -RCS\ stm\ vol}}=\left[\frac{\dot{m}_{\substack{ADS\\ steam}}\cdot h_g}{(V\cdot\Delta p)_{\substack{RCS\\ steam\\ volume}}}\right]_{Ref} \tag{4-39}$$

Now, for similarity, the frequencies between the scaled test facility and plants should be scaled.

Steam mass flow from core heat, $\dot{m}_{\substack{core\\ steam}}$, can be estimated from a steady-state energy balance on the core for saturated conditions:

$$\dot{m}_{\substack{core\\ steam}}=\frac{q_{core}}{h_{fg}} \tag{4-40}$$

Steam mass flow out the ADS, $\dot{m}_{\substack{ADS\\ steam}}$, can be estimated from the equation for critical flow of an ideal gas per Moody (Reference 22):

$$\dot{m}_{\substack{ADS\\ steam}}=G_c A_{ADS}=\left(\frac{2}{\gamma+1}\right)^{\frac{\gamma+1}{2(\gamma-1)}}\left[\gamma\cdot\rho_{g_{inlet}}\cdot p_{inlet}\right]^{1/2}\cdot A_{ADS} \tag{4-41}$$

Using appropriate values for AP600, AP1000, OSU, and SPES; the following scaling ratios are obtained.

ADS Phase – Core Steam to RCS Steam Volume						a,b,c

ADS Phase – ADS-1/2/3 Steam Vent to RCS Steam Volume						a,b,c

SPES is acceptably scaled to AP600 and AP1000 for the ADS-1/2/3 depressurization and should be used for code validation. As OSU is just outside the acceptance criteria, it may be used to support code validation and should be sufficient to set up initial conditions for the ADS to IRWST transition phase.

4.1.2.3.2 Bottom-Up Scaling Analysis – Surge Line Pressure Drop

During the initial stages of ADS depressurization, only steam is vented via ADS-1/2/3 as the upper region of the RCS is voided and the ADS is connected to the top of the pressurizer. The venting of steam has a rapid and substantial impact on reducing the pressure in the RCS.

Steam venting from the RCS via the ADS must flow through the surge line into the pressurizer, which is connected to AD-1/2/3. The pressure drop through the surge line is a moderately important phenomenon for AP1000.

To preserve the pressure drop through the surge line, the resistance of the surge line (i.e., $[R_{SL} = fL/d + K]_R$ must be preserved. In OSU, the length to diameter ratio and surge line layout is preserved relative to AP600. As the surge line length to diameter ratio in AP1000 is the same as AP600, it should be preserved relative to OSU as well. The surge line length to diameter ratio is not ideally preserved in SPES.

In later stages of ADS depressurization, a two-phase mixture will flow through the surge line into the pressurizer. During this time, the pressure drop will further depend upon flow regime in the surge line. However, flow pattern transitions are very difficult to scale and preserve; especially in a reduced pressure test facility (Schwartzbeck and Kocamustafaogullari, Reference 25), as the transition is very dependent upon density. In OSU, Reyes found that some flow patterns such as the slug-annular flow regime transition were possibly distorted with respect to AP600. Therefore, it is expected that some distortion may exist with respect to AP1000 as well. A scaling analysis of flow pattern transitions was not performed for SPES. However, it should be less of a challenge to preserve flow pattern transitions in SPES, as pressure similitude exists with respect to AP600 and AP1000 and flow pattern transitions are largely dependent upon density.

In conclusion, although there may be some distortion of flow regime transition in the surge line of SPES and OSU, it should only affect the later stages of ADS depressurization when a two-phase mixture is discharged. As it is well known that venting of the gas phase has a higher impact on RCS pressure than discharging of the liquid phase, surge line pressure drop should be acceptably scaled for the steam venting regime and therefore the data from the test facilities can be used during the ADS phase for code validation.

4.1.2.4 ADS-IRWST Transition

4.1.2.4.1 Top-Down Scaling Analysis of CMT and IRWST Injection

Reactor Vessel Inventory

Transient scaling is used because the parameter of interest, the reactor vessel inventory, is changing significantly with time. Reactor vessel inventory is among the parameters of highest importance during a small-break LOCA, since if reactor vessel inventory is maintained, so is core cooling. The typical SBLOCA for the AP600 experiences minimum vessel inventory during the transition period between ADS actuation and IRWST injection. Scaling of the reactor vessel inventory refers to the liquid phase as the mass associated with steam at low pressure is very small compared to the liquid phase. Additionally, the ability of the gas phase to remove additional core decay heat is small relative to that of the liquid inventory. Therefore, vessel liquid inventory was used as the key system parameter for top-down scaling in the ADS-IRWST transition phase.

The dominant top-down processes affecting reactor vessel liquid inventory during this phase of a SBLOCA include:

- Core decay heat depletion of liquid inventory in the vessel, and steam venting via the ADS.

- Liquid inventory replenishment from the CMTs and IRWST (the accumulators have already discharged at much higher RCS pressure).

The CMTs provide short-term inventory replenishment while the IRWST provides longer-term replenishment. Liquid inventory replenishment via the IRWST in this phase is closely coupled to the reactor vessel pressure, which in turn is largely determined by steam venting via the ADS paths. Inventory replenishment via the CMTs is largely independent of vessel pressure or venting via the ADS paths.

Typically in SBLOCAs, CMT injection occurs before IRWST injection as the CMTs are much less sensitive to reactor vessel pressure. They can inject at high RCS pressure as well as low pressure. The IRWST on the other hand cannot inject until at least one CMT reaches its low-level set point (to open the ADS Stage 4 and the IRWST injection valves) and the differential pressure between the reactor vessel and containment decreases to less than the available IRWST gravity head.

During the AP600 licensing process, the ACRS review focused on the processes related to "triggering" reactor vessel inventory replenishment after the ADS is actuated. CMT injection and the triggering of IRWST injection are discussed below.

Description of CMT Injection and "Trigger" for IRWST Injection

CMT Injection

The core makeup tanks operate on fluid density difference between the CMT and discharge piping and the cold leg balance line. As the CMTs are connected to a pressure balance line from the cold leg, their operation is largely insensitive to RCS pressure (pressure effects are addressed via scaling of the rate of pressure change equation). CMT injection (see Figure 4.1-7) is generally very steady as seen in the AP600 test and analysis program.

IRWST Injection

The IRWST trigger depends upon gravity head and pressure difference as mentioned above. The IRWST trigger is "pulled" when the gravity head of the liquid in the IRWST exceeds the pressure difference between the RCS and containment:

$$\rho_f g [Z_{IRWST} - Z_{DVI}] > [p_{RCS} - p_{CONT}] \qquad (4\text{-}42)$$

The RCS pressure is dominated by the ADS venting processes (during this transition period). ADS venting is influenced by entrainment and phase separation in the vent paths. Also, when the pressurizer is draining back into the hot leg, the effectiveness of ADS-1/2/3 venting is reduced and liquid entrainment in ADS-4 increases. These processes are local effects scaled in more detail from a bottom-up perspective. (Figures 4.1-8 and 4.1-9 illustrate IRWST injection – pressurizer draining and pressurizer drained, respectively.)

ADS-IRWST Transition Subphases

During the ADS-IRWST transition, there will be a period where CMT injection will dominate reactor vessel inventory replenishment followed by a period where CMT injection ends and

IRWST injection dominates. Since this is the most crucial period of a SBLOCA, both of the following subphases are scaled as the ADS finishes depressurization of the RCS and the transition to long-term gravity injection from the IRWST is made:

- CMT injection dominant
- IRWST injection dominant

Subphase – Core Makeup Tank Injection Dominant

Reactor Vessel Inventory

The transient conservation of mass equation written for the reactor vessel inventory can be expressed as follows:

$$\frac{dM_{vessel}}{dt} = \dot{m}_{CMT} - \dot{m}_{core} \tag{4-43}$$

The contribution of the break on the liquid inventory is not dominant compared with core decay heat depletion and removal via the ADS vent flow at this point in the SBLOCA transient and is therefore not included in the scaling of this transition phase.

Estimation of CMT Mass Flow from Steady Momentum Balance

During this subphase, the core makeup tanks are in the draining (i.e., injection) mode. That is, the cold legs and balance lines are voided (recirculation mode has ceased) as is the upper region of the core makeup tank itself. When the CMT is the dominant source of injection into the reactor vessel, the conservation of momentum for the draining mode consists of a flow path from the CMT to the reactor vessel via the DVI line. As the balance line equalizes the pressure between the RCS and the CMT, the steady conservation of momentum equation for this flow path reduces to a balance of the CMT gravity head and the flow path resistance expressed as follows:

$$\rho_f g[Z_{CMT} - Z_{DVI}] = \left[\left(\sum \frac{R}{A^2}\right)_{DVI}^{CMT}\right] \frac{\dot{m}_{CMT}^2}{2\rho_f} \tag{4-44}$$

Rearranging the above to obtain an expression for $\dot{m}_{CMT}$ results in the following:

$$\dot{m}_{CMT} = \left[\frac{2\rho_f^2 g[Z_{CMT} - Z_{DVI}]}{\left(\sum \frac{R}{A^2}\right)_{DVI}^{CMT}}\right]^{1/2} \tag{4-45}$$

Estimation of Core Flow from Steady Energy Balance

As core decay heat is about constant at this point in the transient, a steady-state energy balance can be applied to the reactor vessel as follows:

$$q_{core} = \dot{m}_{core}\left(h_{out} - h_{in}\right) = \dot{m}_{core}\left(\Delta h_{sub} + x_{exit} h_{fg}\right) \tag{4-46}$$

Rearranging the above energy equation, an expression for the core mass flow $\dot{m}_{core}$ can be obtained:

$$\dot{m}_{core} = \frac{q_{core}}{\left(\Delta h_{sub} + x_{exit} h_{fg}\right)} \tag{4-47}$$

To scale reactor vessel inventory when CMT injection is dominant, the mass flows obtained from the conservation of momentum and energy equations are inserted into the conservation of vessel inventory equation to obtain the following:

$$\rho_f \frac{dV_{\substack{vessel\\liquid}}}{dt} = \left[\frac{2\rho_f^2 g(Z_{CMT} - Z_{DVI})}{\left(\sum \frac{R}{A^2}\right)_{\substack{CMT\\DVI}}}\right]^{1/2} - \frac{q_{core}}{\Delta h_{sub} + x_{exit} h_{fg}} \tag{4-48}$$

The above equation can be non-dimensionalized to obtain the following form:

$$\left(\rho_f \Delta V_{\substack{vessel\\liquid}}\right)_{ref} \frac{\rho^+ dV^+_{\substack{vessel\\liquid}}}{dt} = \left(\dot{m}_{CMT}\right)_{ref} \dot{m}^+_{CMT} - \left(\dot{m}_{core}\right)_{Ref} \dot{m}^+_{core} \tag{4-49}$$

$$\frac{\rho^+ dV^+_{\substack{vessel\\liquid}}}{dt} = \left(\frac{\dot{m}_{CMT}}{\rho_f \cdot \Delta V_{\substack{vessel\\liquid}}}\right)_{Ref} \dot{m}^+_{CMT} - \left(\frac{\dot{m}_{core}}{\rho_f \cdot \Delta V_{\substack{vessel\\liquid}}}\right)_{Ref} \dot{m}^+_{core} \tag{4-50}$$

$$\frac{\rho^+ dV^+_{\substack{vessel\\liquid}}}{dt} = \omega_{\substack{CMT\\-vessel\\liquid}} \cdot \dot{m}^+_{CMT} - \omega_{\substack{core\\-vessel\\liquid}} \cdot \dot{m}^+_{core} \tag{4-51}$$

Now, core mass flow can be estimated from a steady-state energy balance on the reactor core:

$$\dot{m}_{core} = \frac{q_{core}}{\Delta h_{sub} + x_{exit} h_{fg}} \tag{4-52}$$

The CMT mass flow can be estimated from a steady-state injection:

$$\dot{m}_{CMT} = \left[\frac{2\rho_f^2 g[Z_{CMT} - Z_{DVI}]}{\left(\sum \frac{R}{A^2} \right)_{DVI}^{CMT}} \right]^{1/2} \tag{4-53}$$

From this, the frequencies become:

$$\omega_{\substack{CMT \\ -vessel \\ liquid}} = \frac{\left[\frac{2\rho_f^2 g(Z_{CMT} - Z_{DVI})}{\left(\sum \frac{R}{A^2} \right)_{DVI}^{CMT}} \right]_{Ref}^{1/2}}{\left(\rho_f \cdot \Delta V_{\substack{vessel \\ liquid}} \right)_{Ref}} \tag{4-54}$$

$$\omega_{\substack{core \\ -vessel \\ liquid}} = \frac{\left[\frac{q_{core}}{\Delta h_{sub} + x_{exit} h_{fg}} \right]_{Ref}}{\left(\rho_f \cdot \Delta V_{\substack{vessel \\ liquid}} \right)_{Ref}} \tag{4-55}$$

[

ADS-IRWST Transition					

a,b,c]

ADS-IRWST Transition					

a,b,c

The scaling values in the above table are based upon no subcooling and preservation of quality (i.e., for $\Delta h_{sub}=0$; $x_e=1.0$).

The scaling results indicate that CMT injection relative to vessel inventory is sufficiently scaled in SPES and OSU. Therefore, both test facilities can be used for code validation with respect to CMT injection during this phase of the transient.

Subphase – IRWST Injection Dominant

The dominant processes affecting reactor vessel inventory during this subphase of a SBLOCA transient include core decay power boil-off of inventory in the vessel and inventory replenishment from the IRWST. The CMTs are drained or nearly drained at this point. Unlike the CMTs, IRWST injection is very dependent upon the pressure difference between the reactor vessel and containment. Reactor vessel pressure is controlled largely by the ADS-4 vent paths and the rate of steam generation by core decay heat. In the early or initial stages of IRWST injection, ADS venting performance is influenced by entrainment in the ADS-4 vent path and countercurrent draining of liquid in the pressurizer back to the hot leg. Entrainment into ADS-4 and pressurizer draining will be addressed later.

Reactor Vessel Inventory

For this subphase, top-down scaling of reactor vessel inventory was selected as the dominant parameter to be scaled. The transient conservation of mass equation written for the reactor vessel liquid inventory can be expressed as follows:

$$\frac{dM_{\substack{vessel\\liquid}}}{dt} = \dot{m}_{IRWST} - \dot{m}_{core} \qquad (4\text{-}56)$$

From the above conservation equation, the change in vessel inventory can be scaled from the IRWST mass flow and core mass flow. To scale core mass flow, a steady energy balance on the core is used. To scale IRWST mass flow, steady conservation of momentum from the IRWST to the reactor vessel is used.

Core Mass Flow Estimated from Steady-State Energy Balance

As core decay heat is nearly constant at this point in the transient, a steady energy balance can be applied to the reactor vessel as follows:

$$q_{core} = \dot{m}_{core}(h_{out} - h_{in}) = \dot{m}_{core}(\Delta h_{sub} + x_{exit} h_{fg}) \tag{4-57}$$

Rearranging the above energy equation, an expression for the core mass flow $\dot{m}_{core}$ can be obtained:

$$\dot{m}_{core} = \frac{q_{core}}{(\Delta h_{sub} + x_{exit} h_{fg})} \tag{4-58}$$

IRWST Mass Flow Estimated from Steady Momentum Balance

During this phase of a SBLOCA transient, the IRWST is in the draining (injection mode). When the IRWST is the dominant source of injection into the reactor vessel, the conservation of momentum consists of a flow path from the IRWST to the reactor vessel via the DVI line. The steady conservation of momentum equation for this flow path is a balance of the IRWST gravity head, pressure difference between the reactor vessel and containment and the IRWST-DVI flow path resistance as follows:

$$\rho_f g[Z_{IRWST} - Z_{DVI}] - [p_{RCS} - p_{CONT}] = \left[\left(\sum \frac{R}{A^2}\right)_{\substack{IRWST \\ DVI}}\right] \frac{\dot{m}^2_{IRWST}}{2\rho_f} \tag{4-59}$$

The backpressure associated with the RCS (i.e., p_{RCS}) can be estimated from the gravity head associated with the liquid hold-up (in the pressurizer) above the reactor vessel. Therefore,

$$p_{RCS} \equiv \rho_f g\left[Z_{PZR} - Z_{\substack{PZR \\ BOT}}\right] + p_{\substack{PZR \\ steam\ space}} \tag{4-60}$$

With a small steam flow through the ADS-1/2/3 path due to CCFL in the surge line, the pressure drop from the pressurizer steam space to the ADS-1/2/3 discharge is small such that $p_{\substack{PZR \\ steam\ space}} \equiv p_{CONT}$. Therefore, equation (4-59) becomes:

$$\rho_f g\left\{[Z_{IRWST} - Z_{DVI}] - \left[Z_{PZR} - Z_{\substack{PZR \\ BOT}}\right]\right\} = \frac{\dot{m}^2_{IRWST}}{2\rho_f}\left(\sum \frac{R}{A^2}\right)_{\substack{IRWST \\ DVI}} \tag{4-61}$$

Rearranging the above to obtain an expression for $\dot{m}_{IRWST}$ results in the following:

$$\dot{m}_{IRWST} = \left[\frac{2\rho_f \left[\rho_f g(Z_{IRWST} - Z_{DVI}) - \rho_f g(Z_{PZR} - Z_{HL})\right]}{\left(\sum \frac{R}{A^2}\right)_{DVI}^{IRWST}} \right]^{1/2} \tag{4-62}$$

To scale these dominant processes, the conservation of momentum and energy equations can be combined into a single conservation of vessel inventory equation of the following form:

$$\rho_f \frac{dV_{\substack{vessel \\ liquid}}}{dt} = \left[\frac{\left[\rho_f g(Z_{IRWST} - Z_{DVI}) - \rho_f g(Z_{PZR} - Z_{HL})\right] 2\rho_f}{\left(\sum \frac{R}{A^2}\right)_{DVI}^{IRWST}} \right]^{1/2} - \frac{q_{core}}{\Delta h_{sub} + x_{exit} h_{fg}} \tag{4-63}$$

The above equation can be non-dimensionalized to obtain the following form:

$$\left(\rho_f \Delta V_{\substack{vessel \\ liquid}}\right)_{Ref} \frac{\rho^+ dV^+_{\substack{vessel \\ liquid}}}{dt} = \left(\dot{m}_{IRWST}\right)_{Ref} \dot{m}^+_{IRWST} - \left(\dot{m}_{core}\right)_{Ref} \dot{m}^+_{core} \tag{4-64}$$

$$\frac{\rho^+ dV^+_{\substack{vessel \\ liquid}}}{dt} = \left(\frac{\dot{m}_{IRWST}}{\rho_f \cdot \Delta V_{\substack{vessel \\ liquid}}} \right)_{Ref} \dot{m}^+_{IRWST} - \left(\frac{\dot{m}_{core}}{\rho_f \cdot \Delta V_{\substack{vessel \\ liquid}}} \right)_{Ref} \dot{m}^+_{core} \tag{4-65}$$

$$\frac{\rho^+ dV^+_{\substack{vessel \\ liquid}}}{dt} = \omega_{\substack{IRWST \\ -vessel \\ liquid}} \cdot \dot{m}^+_{IRWST} - \omega_{\substack{core \\ -vessel \\ liquid}} \cdot \dot{m}^+_{core} \tag{4-66}$$

Again, core mass flow can be estimated from a steady-state energy balance on the reactor core:

$$\dot{m}_{core} = \frac{q_{core}}{\Delta h_{sub} + x_{exit} h_{fg}} \tag{4-67}$$

The IRWST mass flow can be estimated from steady-state injection:

$$\dot{m}_{IRWST} = \left[\frac{[\rho_f g (Z_{IRWST} - Z_{DVI}) - \rho_f g (Z_{PZR} - Z_{HL})] 2\rho_f}{\left(\sum \frac{R}{A^2} \right)_{\substack{IRWST \\ DVI}}} \right]^{1/2} \quad (4\text{-}68)$$

From this, the frequencies become:

$$\omega_{\substack{IRWST \\ -vessel \\ liquid}} = \frac{\left[\frac{[\rho_f g (Z_{IRWST} - Z_{DVI}) - \rho_f g (Z_{PZR} - Z_{HL})] 2\rho_f}{\left(\sum \frac{R}{A^2} \right)_{\substack{IRWST \\ DVI}}} \right]^{1/2}_{Ref}}{\left(\rho_f \cdot \Delta V_{\substack{vessel \\ liquid}} \right)_{Ref}} \quad (4\text{-}69)$$

$$\omega_{\substack{core \\ -vessel \\ liquid}} = \frac{\left[\frac{q_{core}}{\Delta h_{sub} + x_{exit} \cdot h_{fg}} \right]_{Ref}}{\left(\rho_f \cdot \Delta V_{\substack{vessel \\ liquid}} \right)_{Ref}} \quad (4\text{-}70)$$

[

ADS-IRWST Transition					

] a,b,c

ADS-IRWST Transition					

a,b,c

The scaling results indicate that IRWST injection relative to reactor vessel inventory is sufficiently scaled in OSU and SPES relative to AP600 and AP1000.

Vessel Depressurization via ADS-4

The pressure associated with the steam volume of the RCS is important as it acts as backpressure to IRWST injection. The pressure change associated with the ADS-4 venting process is scaled from a top-down perspective using the RPC equation and treating the steam volume as an ideal gas as follows:

$$\left[\frac{V}{(\gamma-1)}\right]_{\substack{RCS\\steam\\volume}} \frac{dp_{\substack{RCS\\steam\ volume}}}{dt} = \dot{m}_{\substack{core\\steam}} \cdot h_g - \dot{m}_{\substack{ADS-4\\steam}} \cdot h_g \qquad (4\text{-}71)$$

The RPC equation can be non-dimensionalized as follows:

$$\frac{1}{(\gamma-1)} \cdot \frac{dp^+_{\substack{RCS\\steam\ volume}}}{dt} = \left[\frac{\dot{m}_{\substack{core\\steam}} \cdot h_g}{(V\Delta p)_{\substack{RCS\\steam\\volume}}}\right]_{Ref} \cdot \dot{m}^+_{\substack{core\\steam}} \cdot h^+_g - \left[\frac{\dot{m}_{ADS-4} \cdot h_g}{(V\Delta p)_{\substack{RCS\\steam\\volume}}}\right]_{Ref} \cdot \dot{m}^+_{ADS-4} \cdot h^+_g \qquad (4\text{-}72)$$

The above equation can be re-expressed as follows:

$$\frac{1}{(\gamma-1)} \cdot \frac{dp^+_{\substack{RCS\\steam\ volume}}}{dt} = \omega_{\substack{core\ steam\\-RCS\ stm\ vol}} \cdot \dot{m}^+_{\substack{core\\steam}} \cdot h^+_g - \omega_{\substack{ADS-4\\-RCS\ stm\ vol}} \cdot \dot{m}^+_{ADS} \cdot h^+_g \qquad (4\text{-}73)$$

where the coefficients represent frequencies:

$$\omega_{\substack{\text{core steam}\\ \text{–RCS stm vol}}} = \left[\frac{\dot{m}_{\substack{\text{core}\\ \text{steam}}} \cdot h_g}{(V\Delta p)_{\substack{\text{RCS}\\ \text{steam vol}}}} \right]_{Ref} \tag{4-74}$$

and

$$\omega_{\substack{\text{ADS–4}\\ \text{–RCS stm vol}}} = \left[\frac{\dot{m}_{\text{ADS–4}} \cdot h_g}{(V\Delta p)_{\substack{\text{RCS}\\ \text{steam vol}}}} \right]_{Ref} \tag{4-75}$$

Core steam flow can be estimated from a steady-state energy balance on the reactor core:

$$\dot{m}_{\substack{\text{core}\\ \text{steam}}} = \frac{q_{\text{core}}}{h_{fg}} \tag{4-76}$$

ADS-4 steam flow can be estimated from the steady-state equation for critical flow of an ideal gas:

$$\dot{m}_{\text{ADS–4}} = G_c A_{\text{ADS–4}} = \left(\frac{2}{\gamma+1} \right)^{\frac{\gamma+1}{2(\gamma-1)}} \left[\gamma \cdot \rho_{g_{\text{inlet}}} \cdot p_{\text{inlet}} \right]^{1/2} \cdot A_{\text{ADS–4}} \tag{4-77}$$

For non-critical, steady-state, compressible flow of an ideal gas (with negligible body force term for gas):

$$\dot{m}_{\text{ADS–4}} = \left\{ \frac{\Delta P_{\text{inlet–outlet}}}{\frac{\left(\sum \frac{R}{A^2} \right)_{\text{ADS–4}}}{2\rho_g} + \left[\frac{1}{(\rho_g A^2)_{\substack{\text{ADS–4}\\ \text{outlet}}}} - \frac{1}{(\rho_g A^2)_{\substack{\text{ADS–4}\\ \text{inlet}}}} \right]} \right\}^{1/2} \tag{4-78}$$

Δp is approximately preserved as pressure similitude exists during this phase of the transient.

$V_{\substack{\text{RCS}\\ \text{steam}\\ \text{volume}}}$ represents upper head/plenum/hot leg/steam generators.

For critical flow and pressure similitude, $\omega_{\substack{ADS-4 \\ -RCS \\ stm\ vol}}$ reduces to a simple ADS-4 vent area to vessel steam volume ratio:

$$\omega_{\substack{ADS-4 \\ -RCS\ stm\ vol}} = \frac{A_{ADS-4}}{V_{RCS\ stm\ vol}} \tag{4-79}$$

Similarly, $\omega_{\substack{core\ stm \\ -RCS\ stm\ vol}}$ can be reduced to a core power to steam volume ratio:

$$\omega_{\substack{core\ stm \\ -RCS\ stm\ vol}} = \frac{q_{core}}{V_{RCS\ stm\ vol}} \tag{4-80}$$

For non-critical flow and pressure similitude:

$$\omega_{\substack{ADS-4 \\ -RCS\ stm\ vol}} = \frac{1}{\left\{\frac{\left(\sum \frac{R}{A^2}\right)_{ADS-4}}{2\rho_g} + \left[\frac{1}{\left(\rho_g A^2\right)_{\substack{ADS-4 \\ outlet}}} - \frac{1}{\left(\rho_g A^2\right)_{\substack{ADS-4 \\ inlet}}}\right]\right\}^{1/2} \cdot V_{\substack{RCS \\ stm\ vol}}} \tag{4-81}$$

Using appropriate reference values for OSU, SPES, AP600, and AP1000; the following scaling ratios are obtained:

[

ADS – IRWST					

]a,b,c

ADS – IRWST					

a,b,c

ADS – IRWST					

a,b,c

From the above scaling ratios, it can be seen that OSU and SPES are acceptably scaled to AP600 and AP1000 for ADS-4 critical flow and with respect to core power. Therefore, these test facilities can be used for code validation while ADS-4 flow is choked.

When ADS-4 flow is non-critical, only OSU can be used for code validation as SPES is distorted due to the oversized ADS-4 vent paths.

NRC-Sponsored Tests at OSU

The NRC-sponsored tests at the OSU test facility include some tests that lend additional support for safety analysis code validation for an uprated version of AP600.

The first noteworthy test is that designated as NRC-20. NRC-20 represents an AP600 design basis accident with 20 percent higher core decay power. Though it is not sufficient to represent the AP1000 core decay power, it is of interest in uprating the AP600.

The second, more noteworthy, test is designated as NRC-25. NRC-25 is actually a series of ten tests called "core uncovery tests." In this test series, the RCS is drained to the hot leg level, the IRWST is pressurized to simulate the AP600 gravity head, and only the IRWST and ADS-4 vents are then used to provide passive core cooling. In addition, multiple ADS-4 failures are taken to simulate beyond design basis accidents for AP600. This test series is of interest to AP1000, since as will be shown below, they may represent IRWST injection for an AP1000 design basis accident.

As shown earlier, the top-down scaling relation for quality during IRWST injection, where the two-phase resistance dominates, is as follows:

$$[x_e]_R = \left(\frac{q_{core}}{\rho_f \cdot h_{fg}}\right)_R^2 \left(\frac{\Delta\rho}{\rho_g}\right)_R \frac{\left[\left(\sum \frac{R}{A^2}\right)_{2\phi}\right]_R}{(\Delta Z)_R} \qquad (4\text{-}82)$$

For pressure similitude and gravity head preserved in this series of tests, the scaling relations reduces to:

$$[x_e]_R = (q_{core})_R^2 \left[\left(\sum \frac{R}{A^2}\right)_{2\phi}\right]_R \qquad (4\text{-}83)$$

An NRC-25 test, which simulates only 2 of 4 ADS-4 vent paths available in OSU, appears to acceptably simulate IRWST injection for an AP1000 design basis accident with 3 of 4 ADS-4 vent paths available as shown below:

a,b,c

[ ]

Therefore, the NRC-25 OSU tests, with 2 of 4 ADS-4 vent paths available, could be used for code validation for AP1000.

4.1.2.4.2 Bottom-Up Scaling Analysis

Hot Leg Flow Pattern

Hot leg flow pattern transition between stratified and non-stratified flow is an important local phenomenon as this flow regime influences pressure drop and entrainment in the ADS vent paths. Although it is a very complex phenomenon, a simple scaling approach similar to that taken by Reyes for OSU can be used by scaling the hot leg using a modified Froude number. The modified Froude number is a dominant parameter used by Taitel-Dukler in establishing flow regime boundaries for two-phase flow in horizontal pipe flow. The Froude number used by Taitel-Dukler is defined as follows:

$$Fr = \frac{j_g}{\sqrt{gd}}\left(\frac{\rho_g}{\rho_f - \rho_g}\right)^{1/2} \qquad (4\text{-}84)$$

Preserving Froude number results in the following:

$$(\pi_{Fr})_R = Fr_{Ratio} = 1 \tag{4-85}$$

As pressure similitude exists between the test facilities and plants during this phase of the transient, the Froude number ratio simplifies to the following:

$$(\pi_{Fr})_R = \left[\frac{j_g}{\sqrt{d}}\right]_R \tag{4-86}$$

The superficial velocity, j_g, in the hot leg is expressed as:

$$(j_g)_{HL} = \left(\frac{Q_g}{A}\right)_{HL} \tag{4-87}$$

An estimate of the volumetric flow rate of the gas phase in the hot leg, Q_g, for scaling purposes can be obtained from a steady-state energy balance on the reactor core. The steam flow rate exiting the core into the hot leg for saturated conditions in the core results in:

$$Q_g = \frac{q_{core}}{\rho_g h_{fg}} \tag{4-88}$$

Therefore, the Froude number ratio (for pressure similitude conditions) becomes:

$$(\pi_{Fr})_R = \left[\frac{q_{core}}{d_{HL}^{5/2}}\right]_R \tag{4-89}$$

Using appropriate reference values for AP600, AP1000, OSU and SPES, the scaling ratios in the following table are obtained:

ADS-IRWST Transition Phase – Froude Number – Hot Leg					

a,b,c

Both OSU and SPES are well scaled to AP600. OSU and SPES are within the acceptance criteria with respect to AP1000.

Entrainment from Hot Leg into ADS-4

Entrainment of liquid from the hot leg into the ADS-4 vent path is an important local phenomenon. Entrainment influences the distribution of liquid mass in the system as well as the pressure drop in the hot leg and ADS-4 vent paths.

The process of entrainment itself is very complex, however, the onset of liquid entrainment from large tanks or pipes to a vertical offtake (with stratified flow pattern in the main pipe) has been correlated with Froude number and a geometric ratio of the level of the liquid phase measured from the top of the main pipe (L_g) to the diameter ($d_{offtake}$) of the offtake as follows (for example, see Schrock et al., Reference 26 and Zuber, Reference 27):

$$\frac{u_g\sqrt{\rho_g}}{\sqrt{g(\rho_f-\rho_g)L_g}} \geq 5.7\left(\frac{L_g}{d_{offtake}}\right)^{3/2} \tag{4-90}$$

This translates into the following scaling relation:

$$\left[\frac{u_g\sqrt{\rho_g}}{\sqrt{g(\rho_f-\rho_g)L_g}}\right]_R\left(\frac{d_{offtake}}{L_g}\right)_R^{3/2}=1 \tag{4-91}$$

As pressure similitude exists between the test facilities and the plants during this phase; entrainment scaling relation reduces to:

$$\left[\frac{u_g}{\sqrt{L_g}}\right]_R\left[\frac{d_{offtake}}{L_g}\right]_R^{3/2}=1.0 \tag{4-92}$$

or

$$\left[\frac{u_g\cdot d_{offtake}^{3/2}}{L_g^{\,2}}\right]_R=1.0 \tag{4-93}$$

The velocity of steam in the offtake can be estimated from a steady-state energy balance on the reactor core:

$$u_g=\frac{q_{core}}{\rho_g\cdot h_{fg}\cdot A_{offtake}}=\frac{q_{core}}{\rho_g\cdot h_{fg}\cdot A_{ADS-4}} \tag{4-94}$$

The level of the liquid phase in the main pipe is difficult to estimate, but it can be ranged over the main pipe diameter, which in this case is the hot leg diameter d_{HL}.

The entrainment scaling correlation then becomes (again noting that pressure similitude exists):

$$\left[\frac{q_{core}}{d^{1/2}_{\substack{ADS-4\\inlet}} \cdot d^{2}_{HL}}\right]_R = 1.0 \qquad (4\text{-}95)$$

a,b,c

Entrainment Onset Scaling Relation					

OSU is well scaled to AP600 and AP1000. SPES is distorted.

Countercurrent Flow in the Surge Line and Pressurizer Draining

Countercurrent flow in the surge line is an important local phenomenon since it influences the draining rate of the pressurizer subsequent to refilling during ADS-1/2/3 operation. The countercurrent flow in the pressurizer-surge line influences the pressure in the upper head/upper plenum region of the reactor vessel which in turn may impact the IRWST injection.

Scaling countercurrent flow in the surge line involves scaling the Kutateladze (K*) number as the piping is sufficiently large so as not be influenced by diameter as in the Wallis number. The Kutateladze number is defined as:

$$K_i^* = \frac{\rho_i^{1/2} j_i}{\left((\rho_f - \rho_g) g \sigma\right)^{1/4}} \qquad (4\text{-}96)$$

where i refers to the liquid or gas phase.

During this phase of a small-break LOCA transient where the pressurizer is poorly vented as the ADS-1/2/3 path is "plugged" by a column of water above the sparger in the IRWST (until the IRWST drains sufficiently), the mode of pressurizer draining can be described for scaling purposes as an equal volume replacement process (i.e., $j_f = j_g$). Based upon this, the Kutateladze number scaling can be developed below.

Starting from the Kutateladze flooding relation:

$$K_g^{*1/2} + K_f^{*1/2} = 1.79 \tag{4-97}$$

We can obtain the following by applying equal volume replacement ($j_g = j_f$):

$$\frac{j_g (\rho_f^{1/4} + \rho_g^{1/4})^2}{[\Delta\rho g\sigma]^{1/4}} = 3.2 \tag{4-98}$$

This results in the following scaling relation for the surge line:

$$\left[\frac{j_g (\rho_f^{1/4} + \rho_g^{1/4})^2}{[\Delta\rho\sigma]^{1/4}}\right]_R = 1.0 \tag{4-99}$$

As pressure similitude exists between the test facilities and the plant during this phase of the transient, the scaling relation for the surge line becomes:

$$[(j_g)_{SL}]_R = [(j_f)_{SL}]_R = 1.0 \tag{4-100}$$

The above scaling relation simply states that the superficial velocity and hence the Kutateladze number is preserved (for equal volume replacement draining) in the test facilities and plants as pressure similitude exists.

Pressurizer Draining (After Refill During ADS Phase)

The pressurizer experiences a series of periodic drain and refill cycles during the ADS-IRWST transition phase. The AP600 integral effects test facilities demonstrated that this pressurizer drain process is controlled by very complex and dynamic interactions involving the compressibility of the steam volume in the reactor vessel, counter-current flow in the surge line, and entrainment in the ADS-4 vent paths.

This phenomenon has been evaluated by Bessette and DiMarzo (Reference 28). It was found that the periodic pressurizer drain behavior occurs in ROSA-AP600 and OSU. SPES may experience only a few cycles. Bessette and DiMarzo reached the following conclusions:

- The pressurizer drain process is distorted in SPES and OSU, as it occurs too rapidly relative to AP600. In SPES, this is likely due to the oversized ADS-4 vent paths. In OSU, this is likely due to the oversized surge line.

- ROSA-AP600 provides a reasonable representation of the pressurizer drain/IRWST injection phenomena.

- The pressurizer drain phenomenon does not impact safety of the plant, since it is due to an excessive amount of liquid inventory above the ADS-4 offtake and reactor vessel.

As AP1000 has the same surge line size and configuration as AP600 and the ADS-4 vent is scaled to handle the increased core power, similar behavior (as well represented in ROSA-AP600) to AP600 is expected.

4.1.2.5 IRWST Injection Phase Scaling

The physical parameter selected for top-down scaling in this phase is core exit quality, since quality impacts the thermodynamic state, the two-phase flow regime and pressure drop.

4.1.2.5.1 Top-Down Scaling Analysis of IRWST Injection

The IRWST injection phase can be scaled as a two-phase natural circulation process at a system level. The system during IRWST injection includes the IRWST, direct vessel injection line, reactor vessel and ADS vent. Referring to Figure 4.1-9, the natural circulation flow path during IRWST injection consists of a single-phase liquid path from the IRWST through the direct vessel injection (DVI) line to the downcomer of the reactor vessel, through the reactor vessel core where the fluid becomes a two-phase mixture, and out the ADS vent paths (two-phase mixture) via the hot legs. The two-phase mixture discharged from the ADS vents is condensed inside containment and returned to the IRWST or sump.

Steady conservation of mass, momentum, and energy equations describing the IRWST injection path are combined into one expression. Parallel flow paths in the DVI and ADS lines are combined into single equivalent flow paths in the momentum equation. The result is essentially the same form as that used by Reyes (Reference 1) and Todreas and Kazimi (Reference 29) and Duffey and Sursock (Reference 30). This equation applied to AP600, AP1000, OSU and SPES includes the dominant influences such as IRWST head, DVI and ADS line hydraulic resistance and core decay power.

In order to develop top-down, system level equations useful for scaling, the two-phase region of the flow path (i.e., core, upper vessel region, ADS vents, etc.) is treated as uniform (well-mixed) as the equilibrium quality is used for this region. This approach was used by Reyes (Reference 1) in scaling OSU. Trying to account for spatial distribution of quality, even a simple linear distribution of quality in the reactor core, in the two-phase region results in a hybrid of mathematical forms (power and logarithmic) associated with quality in the two-phase natural circulation scaling equation. The mixture of mathematical forms makes it difficult to isolate important parameters such as quality for scaling purposes.

The influence of subcooling is not small during IRWST injection (especially during the initial period of injection) as water temperature in the IRWST can be in the range of about 100° to 212°F. Although the influence of subcooling should be approximately preserved as property similitude exists between AP600, AP1000, OSU and SPES during IRWST injection, subcooling will be included in the scaling equations for IRWST injection.

The state of a two-phase system can be determined by two thermodynamic properties such as pressure and quality or void fraction. As pressure similitude exists during this phase of an SBLOCA transient, quality and void fraction will be scaled. The scaling relation for core exit quality is derived from a top-down analysis and evaluated below. Void fraction in the core will be addressed from a bottom-up (local level) in the next section as it is more difficult to scale from a top-down approach.

Conservation of Mass

The mass flow through the reactor vessel is steady or approximately constant during the IRWST injection phase, therefore the conservation of mass is simply:

$$\dot{m} = \text{constant} \tag{4-101}$$

Conservation of Momentum

The conservation of momentum can be expressed for a two-phase natural circulation system during IRWST injection as follows:

$$g\rho_L\left[Z_{IRWST} - Z_{\substack{core\\inlet}}\right] - g\bar{\rho}_L\left[Z_{\substack{core\\2\phi}} - Z_{\substack{core\\inlet}}\right] - g\bar{\rho}_m\left[Z_{IRWST} - Z_{\substack{core\\2\phi}}\right] = \left(\frac{\dot{m}^2}{2\rho_f}\right)\left[\left(\sum\frac{R}{A^2}\right)_{DVI} + \Phi_{fo}^2\left(\sum\frac{R}{A^2}\right)_{ADS}\right] \tag{4-102}$$

where:

$$R = {}^{fL}\!/_{d} + K \tag{4-103}$$

$Z_{\substack{core\\2\phi}}$ = elevation in core where the two-phase region begins (i.e., boiling)

Φ_{fo}^2 = two-phase multiplier

$\bar{\rho}_L$ = average liquid density from core inlet to core elevation where 2ϕ region begins. As liquid density does not vary significantly in the expected range, it will be treated as ρ_f (i.e., $\rho_L \approx \bar{\rho}_L \approx \rho_f$).

The average mixture density for the two-phase region is defined in terms of equilibrium quality x_e obtained from an energy balance. As the entire two-phase region is treated as a uniform region, the equilibrium quality is therefore the same as the exit quality x_{exit}.

$$\bar{\rho}_m = \frac{\rho_f}{1 + x_{exit}\left(\frac{\Delta\rho}{\rho_g}\right)} \tag{4-104}$$

The elevation in the core where the two-phase region begins can be expressed as follows:

$$Z_{\substack{core \\ 2\phi}} = \frac{\dot{m}\left(Z_{\substack{core \\ outlet}} - Z_{\substack{core \\ inlet}}\right)\Delta h_{sub}}{q_{core}} + Z_{\substack{core \\ inlet}} \tag{4-105}$$

substituting $\dot{m} = \frac{q_{core}}{x_{exit} h_{fg} + \Delta h_{sub}}$ we obtain:

$$Z_{\substack{core \\ 2\phi}} = \frac{\left(Z_{\substack{core \\ outlet}} - Z_{\substack{core \\ inlet}}\right)\Delta h_{sub}}{x_{exit} h_{fg} + \Delta h_{sub}} + Z_{\substack{core \\ inlet}} \tag{4-106}$$

Conservation of Energy

As core decay power is essentially constant during sump injection, the steady conservation of energy equation can be written as follows:

$$q_{core} = \dot{m}\left(h_{\substack{core \\ outlet}} - h_{\substack{core \\ inlet}}\right) = \dot{m}\left[\left(h_f + x_{exit} h_{fg}\right) - h_L\right] = \dot{m}\left[\Delta h_{sub} + x_{exit} h_{fg}\right] \tag{4-107}$$

Rearranging to solve for mass flow, we obtain:

$$\dot{m} = \frac{q_{core}}{x_{exit} h_{fg} + \Delta h_{sub}} \tag{4-108}$$

Substituting the conservation of mass and energy equations into the conservation of momentum equation and using the approximation $\rho_L \approx \bar{\rho}_L \approx \rho_f$:

$$g\rho_f\left[Z_{IRWST} - Z_{\substack{core \\ 2\phi}}\right] - g\bar{\rho}_m\left[Z_{IRWST} - Z_{\substack{core \\ 2\phi}}\right] = \left(\frac{q_{core}}{x_{exit} h_{fg} + \Delta h_{sub}}\right)^2 \frac{1}{2\rho_f}\left[\left(\sum \frac{R}{A^2}\right)_{DVI} + \Phi_{fo}^2\left(\sum \frac{R}{A^2}\right)_{ADS}\right] \tag{4-109}$$

Multiplying both sides of the above equation by $\left[x_e h_{fg} + \Delta h_{sub}\right]^2\left[1 + x_{exit}\left(\frac{\Delta\rho}{\rho_g}\right)\right]$ and collecting like terms in x_e we obtain:

$$x_e^3\left[\rho_f \cdot g\left(Z_{IRWST} - Z_{\substack{core\\inlet}}\right)h_{fg}^2\right] + x_e^2\left[h_{fg}\Delta h_{sub}\left\{\rho_f g\left[2\left(Z_{IRWST} - Z_{\substack{core\\inlet}}\right) - \left(Z_{\substack{core\\outlet}} - Z_{\substack{core\\inlet}}\right)\right]\right\}\right]$$

$$+ x_e\left[\Delta h_{sub}^2\left\{\rho_f \cdot g\left[\left(Z_{IRWST} - Z_{\substack{core\\inlet}}\right) - \left(Z_{\substack{core\\outlet}} - Z_{\substack{core\\inlet}}\right)\right]\right\} - \frac{q_{core}^2}{2\rho_f}\left\{\left(\sum\frac{R}{A^2}\right)_{DVI} + \Phi_{fo}^2\left(\sum\frac{R}{A^2}\right)_{ADS}\right\}\right]$$

$$-\frac{q_{core}^2}{2\rho_f}\left(\frac{\rho_g}{\Delta\rho}\right)\left[\left(\sum\frac{R}{A^2}\right)_{DVI} + \Phi_{fo}^2\left(\sum\frac{R}{A^2}\right)_{ADS}\right] = 0 \qquad (4\text{-}110)$$

Dividing by $h_{fg}^2\, g\rho_f\left[Z_{IRWST} - Z_{\substack{core\\inlet}}\right]$ and performing some algebra, the following polynomial form of the two-phase natural circulation equation is obtained:

$$x_e^3 + x_e^2\frac{\left[\Delta h_{sub}\left\{g\left[2\left(Z_{IRWST} - Z_{\substack{core\\inlet}}\right) - \left(Z_{\substack{core\\outlet}} - Z_{\substack{core\\inlet}}\right)\right]\right\}\right]}{h_{fg}\left[Z_{IRWST} - Z_{\substack{core\\inlet}}\right]}$$

$$+ x_e\left[\left(\frac{\Delta h_{sub}}{h_{fg}}\right)^2\frac{\left[\left(Z_{IRWST} - Z_{\substack{core\\inlet}}\right) - \left(Z_{\substack{core\\outlet}} - Z_{\substack{core\\inlet}}\right)\right]}{\left(Z_{IRWST} - Z_{\substack{core\\inlet}}\right)} - \frac{1}{2}\left(\frac{q_{core}}{\rho_f h_{fg}}\right)^2\frac{\left[\left(\sum\frac{R}{A^2}\right)_{DVI} + \Phi_{fo}^2\left(\sum\frac{R}{A^2}\right)_{ADS}\right]}{g\left[Z_{IRWST} - Z_{\substack{core\\inlet}}\right]}\right]$$

$$-\frac{\frac{q_{core}^2}{2\rho_f}\left(\frac{\rho_g}{\Delta\rho}\right)\left[\left(\sum\frac{R}{A^2}\right)_{DVI} + \Phi_{fo}^2\left(\sum\frac{R}{A^2}\right)_{ADS}\right]}{h_{fg}^2\,\rho_f \cdot g\left(Z_{IRWST} - Z_{\substack{core\\inlet}}\right)} = 0 \qquad (4\text{-}111)$$

The third order polynomial in x_{exit} can be recast as:

$$x_{exit}^3 + \phi_a x_{exit}^2 + \phi_b x_{exit} - \phi_c = 0 \qquad (4\text{-}112)$$

where the coefficients are defined as:

$$\phi_a = \frac{\Delta h_{sub}}{h_{fg}} \frac{\left[2\left(Z_{IRWST} - Z_{\substack{core \\ inlet}}\right) - \left(Z_{\substack{core \\ outlet}} - Z_{\substack{core \\ inlet}}\right)\right]}{\left(Z_{IRWST} - Z_{\substack{core \\ inlet}}\right)} \tag{4-113}$$

$$\phi_b = \frac{\left(\frac{\Delta h_{sub}}{h_{fg}}\right)^2 \frac{\left[\left(Z_{IRWST} - Z_{\substack{core \\ inlet}}\right) - \left(Z_{\substack{core \\ outlet}} - Z_{\substack{core \\ inlet}}\right)\right]}{\left(Z_{IRWST} - Z_{\substack{core \\ inlet}}\right)} - \frac{1}{2}\left(\frac{q_{core}}{\rho_f h_{fg}}\right)^2 \left[\left(\sum \frac{R}{A^2}\right)_{DVI} + \Phi_{fo}^2 \left(\sum \frac{R}{A^2}\right)_{ADS}\right]}{g\rho_f \left[Z_{IRWST} - Z_{\substack{core \\ inlet}}\right]} \tag{4-114}$$

$$\phi_c = \frac{\frac{1}{2}\left(\frac{q_{core}}{\rho_f h_{fg}}\right)^2 \left(\frac{\rho_g}{\Delta\rho}\right)\left[\left(\sum \frac{R}{A^2}\right)_{DVI} + \Phi_{fo}^2 \left(\sum \frac{R}{A^2}\right)_{ADS}\right]}{g\rho_f \left[Z_{IRWST} - Z_{\substack{core \\ inlet}}\right]} \tag{4-115}$$

The cubic root solution to the third order polynomial equation above does not result in a form that is easily used for scaling. Applying catastrophe theory similar to Reyes (Reference 1) in the OSU scaling report can circumvent this problem. Catastrophe theory holds that a scaling factor β exists such that the following relation can be made:

$$[x_{exit}]_R = \frac{1}{\beta} = [\phi_b]_R^{1/2} \tag{4-116}$$

$$[x_e]_R = \left[\left(\frac{\Delta h_{sub}}{h_{fg}}\right)^2 \frac{\left[\left(Z_{IRWST} - Z_{\substack{core \\ inlet}}\right) - \left(Z_{\substack{core \\ outlet}} - Z_{\substack{core \\ inlet}}\right)\right]}{\left(Z_{IRWST} - Z_{\substack{core \\ inlet}}\right)} - \frac{1}{2}\left(\frac{q_{core}}{\rho_f \cdot h_{fg}}\right)^2 \frac{\left[\left(\sum \frac{R}{A^2}\right)_{DVI} + \Phi_{fo}^2 \left(\sum \frac{R}{A^2}\right)_{ADS}\right]}{g \cdot \left[Z_{IRWST} - Z_{\substack{core \\ inlet}}\right]}\right]_R^{1/2} \tag{4-117}$$

For situations where two-phase resistance is dominant, the above scaling can be simplified to:

$$[x_e]_R = \left(\frac{q_{core}}{\rho_f \cdot h_{fg}}\right)_R^2 \cdot \left(\frac{\Delta\rho}{\rho_g}\right)_R \left[\frac{\left(\sum \frac{R}{A^2}\right)_{2\phi}}{\left(Z_{IRWST} - Z_{\substack{core \\ inlet}}\right)}\right]_R \left[2g\left(\frac{\Delta h_{sub} \cdot \rho_f}{q_{core}}\right)^2 \frac{\left[\left(Z_{IRWST} - Z_{\substack{core \\ inlet}}\right) - \left(Z_{\substack{core \\ outlet}} - Z_{\substack{core \\ inlet}}\right)\right]}{\Phi_{fo}^2 \left(\sum \frac{R}{A^2}\right)_{2\phi}} - 1\right]_R \quad (4\text{-}118)$$

The above scaling relation for quality is very similar to that derived for sump injection. It contains a density ratio, gravity head to resistance ratio, and a core power to enthalpy ratio. The difference is the additional term, which includes the influence of subcooling. Notice that this scaling relation becomes identical with that derived for saturated conditions where subcooling is neglected.

Using appropriate reference values for AP600, AP1000, OSU, and SPES the following scaling ratios are obtained:

IRWST Injection Phase Natural Circulation – Quality Relation					

a,b,c

From the scaling ratios above, it can be seen that OSU quality is sufficiently well scaled to AP600 and AP1000 from a top-down perspective. SPES is not well scaled to AP600 and AP1000 as the ADS-4 resistance is distorted. Therefore, code validation should be based on OSU for this phase of the transient.

4.1.2.5.2 Bottom-Up Scaling Analysis of IRWST Injection

To scale void fraction in the reactor core, the Yeh correlation is used:

$$\alpha = 0.925\left(\frac{\rho_g}{\rho_f}\right)^{0.24}\left(\frac{j_g}{V_{bcr}}\right)^a\left(\frac{j_g}{j_g + j_f}\right)^{0.6} \quad (4\text{-}119)$$

where V_{bcr} is defined as:

$$V_{bcr} = 1.53\left(\frac{\sigma g \Delta\rho}{\rho_f^2}\right)^{1/4} \quad (4\text{-}120)$$

and the value of exponent a is 0.67 if $j_g/V_{bcr} < 1$
0.47 if $j_g/V_{bcr} \geq 1$

An average exponent (a) of 0.57 will be used to cover the entire range for scaling purposes. For applications where the superficial liquid velocity is small, the void fraction correlation shown above can be simplified as follows:

$$\alpha = 0.925\left(\frac{\rho_g}{\rho_f}\right)^{0.24}\left(\frac{j_g}{V_{bcr}}\right)^{0.57} \tag{4-121}$$

Preserving the void fraction between the test facility and the full scale plant results in the following ideal scaling ratio:

$$\pi_R = (\alpha)_R = 1 \tag{4-122}$$

For saturated core inlet conditions and a uniform axial core power profile, the superficial gas velocity in the reactor core can be expressed as follows:

$$j_g(Z) = \frac{q_{core} \cdot Z}{\rho_g h_{fg} L_{core} A_{core}} = \frac{q_{core}}{V_{core}} \cdot \frac{Z}{\rho_g h_{fg}} \tag{4-123}$$

Substituting the above expression for superficial gas velocity into the simplified Yeh correlation, the following scaling relation for void fraction is obtained:

$$(\alpha)_R = \left(\frac{\rho_g}{\rho_f}\right)_R^{0.24}\left(\frac{\left(\frac{q_{core} \cdot Z}{V_{core}\rho_g h_{fg}}\right)}{V_{bcr}}\right)_R^{0.57} \tag{4-124}$$

The resulting scaling relation consists of a density ratio and ratios of superficial gas velocity j_g to V_{bcr}. As property similitude exists, the density ratio and V_{bcr} should be automatically preserved. Therefore, the scaling relation reduces to:

$$(\alpha)_R = \left(\frac{q_{core} \cdot Z}{V_{core}}\right)_R^{0.57} \tag{4-125}$$

IRWST Injection Phase – Core Exit Void Fraction				a,b,c

The core exit void fraction in OSU is adequately scaled to AP600 and AP1000. SPES bottom-up scaling was not assessed for the phase, as the top-down scaling results were distorted.

4.1.2.6 Sump Injection Phase Scaling

4.1.2.6.1 Top-Down Scaling Analysis of Sump Injection

The core exit quality is considered the important parameter, since this quality impacts the thermodynamic state, the two-phase flow regime, and pressure drop. The sump injection phase can be scaled as a two-phase natural circulation loop at a system level. Referring to Figure 4.1-10, the system during sump injection includes the containment sump, direct vessel injection (DVI) line, reactor vessel and ADS vent paths. The natural circulation loop during sump injection consists of a single-phase liquid path from the containment sump through the DVI line to the downcomer of the reactor vessel, through the reactor vessel core where the fluid becomes a two-phase mixture. The two-phase mixture discharged from the ADS vents is condensed inside containment and returned to the containment sump. This recirculation path can be treated as a closed loop with boiling effectively occurring at the entrance of the core and the condensation effectively occurring at the elevation of the sump flood-up level (for top-down scaling purpose).

Steady-state conservation of mass, momentum, and energy equations describing the sump circulation path are combined into one expression. Parallel flow paths in the DVI and ADS lines are combined into single equivalent flow paths in the momentum equation. The result is essentially the same form as that used by Reyes (Reference 1), Todreas and Kazimi (Reference 29), and Duffey and Sursock (Reference 30). This equation when applied to AP600, AP1000, and OSU includes the dominant integral effects of sump gravity head, DVI and ADS line hydraulic resistance and core decay heat.

In order to develop top-down, system level equations useful for scaling, the two-phase region of the recirculation path (core, upper vessel region, ADS vents, etc.) is treated as uniform (well-mixed) as the equilibrium quality is used for this region. This approach was used by Reyes (Reference 1) in scaling OSU. Trying to account for spatial distribution of quality, even a simple linear distribution of quality in the reactor core region, results in a "hybrid" of mathematical forms (power and logarithmic) associated with quality in the two-phase natural circulation scaling equation. The mixture of mathematical forms makes it difficult to isolate important parameters such as quality for scaling purposes.

The influence of subcooling is small in the sump injection phase as near saturation conditions exist in the containment. Any subcooling should be approximately preserved as property similitude exists between AP600, AP1000, and OSU during sump injection. Subcooling can therefore be neglected in the scaling equations for sump injection.

Quality

The state of a two-phase system in thermodynamic equilibrium can be determined from two properties such as pressure and quality (or void). As pressure similitude exists between OSU

and AP600 or AP1000 during this phase and pressure is nearly constant, the scaling focuses on the quality and void fraction associated with two-phase natural circulation system. To preserve similarity between the OSU test facility and AP600 or AP1000, quality and void fraction should be preserved ($x_R = 1.0$ and $\alpha_R = 1.0$ for pressure similitude; see Reference 1). The scaling relation for quality is derived from a top-down perspective and evaluated below. Scaling void fraction is more difficult to accomplish from a top-down approach, therefore, it will be addressed from a bottom-up perspective (local level) in the next section.

Conservation of Mass

The mass flow through the two-phase natural circulation path is steady during the sump injection phase, therefore the conservation of mass is simply:

$$\dot{m} = (\rho A u)_{ref} = \text{constant} \tag{4-126}$$

Conservation of Momentum

The conservation of momentum can be expressed for a two-phase natural circulation system during sump injection as follows:

$$g\rho_f\left[Z_{sump} - Z_{\substack{core\\inlet}}\right] - g\bar{\rho}_m\left[Z_{sump} - Z_{\substack{core\\inlet}}\right] = \left(\frac{\dot{m}^2}{2\rho_f}\right)\left[\left(\sum\frac{R}{A^2}\right)_{DVI} + \Phi_{fo}^2\left(\sum\frac{R}{A^2}\right)_{ADS}\right] \tag{4-127}$$

where:

$$R = {}^{fL}/_{d} + K \tag{4-128}$$

Φ_{fo}^2 = two-phase multiplier

The average mixture density for the two-phase region is defined in terms of equilibrium quality x_e obtained from an energy balance. As the entire two-phase region is treated as a uniform region, the equilibrium quality is therefore the same as the core exit quality x_{exit} and average mixture density can be expressed as follows:

$$\bar{\rho}_m = \frac{\rho_f}{1 + x_{exit}\left(\frac{\Delta\rho}{\rho_g}\right)} \tag{4-129}$$

Conservation of Energy

As core decay power is essentially constant during sump injection, the steady conservation of energy equation can be written as follows (no subcooling as discussed above):

$$q_{core} = \dot{m}\left(h_{\substack{core \\ outlet}} - h_{\substack{core \\ inlet}} \right) = \dot{m}\left[\left(h_f + x_{exit} h_{fg} \right) - h_f \right] = \dot{m} x_{exit} h_{fg} \tag{4-130}$$

Rearranging to solve for mass flow, we obtain:

$$\dot{m} = \frac{q_{core}}{x_{exit} h_{fg}} \tag{4-131}$$

Substituting the conservation of mass and energy equations into the conservation of momentum equation:

$$g\rho_f \left[Z_{sump} - Z_{\substack{core \\ inlet}} \right] - g\bar{\rho}_m \left[Z_{sump} - Z_{\substack{core \\ inlet}} \right] = \left(\frac{q_{core}}{x_{exit} h_{fg}} \right)^2 \frac{1}{2\rho_f} \left[\left(\sum \frac{R}{A^2} \right)_{DVI} + \Phi_{fo}^2 \left(\sum \frac{R}{A^2} \right)_{ADS} \right] \tag{4-132}$$

Multiplying both sides of the above equation by $x_{exit}^2 \left[1 + x_{exit} \left(\frac{\Delta\rho}{\rho_g} \right) \right]$ and collecting like terms in x_{exit} we obtain:

$$x_{exit}^3 \left(\frac{\Delta\rho}{\rho_g} \right) g\rho_f \left[Z_{sump} - Z_{\substack{core \\ inlet}} \right] - x_{exit} \left(\frac{q_{core}}{h_{fg}} \right)^2 \left(\frac{\Delta\rho}{\rho_g} \right) \frac{1}{2\rho_f} \left[\left(\sum \frac{R}{A^2} \right)_{DVI} + \Phi_{fo}^2 \left(\sum \frac{R}{A^2} \right)_{ADS} \right] - \left(\frac{q_{core}}{h_{fg}} \right)^2 \frac{1}{2\rho_f} \left[\left(\sum \frac{R}{A^2} \right)_{DVI} + \Phi_{fo}^2 \left(\sum \frac{R}{A^2} \right)_{ADS} \right] = 0 \tag{4-133}$$

Dividing by $\left(\frac{\Delta\rho}{\rho_g} \right) g\rho_f \left[Z_{sump} - Z_{\substack{core \\ inlet}} \right]$ and performing some algebra, the following polynomial form of the two-phase natural circulation equation is obtained:

$$x_{exit}^3 + x_{exit} \left[\frac{-\left(\frac{q_{core}}{h_{fg}} \right)^2 \frac{1}{2\rho_f} \left[\left(\sum \frac{R}{A^2} \right)_{DVI} + \Phi_{fo}^2 \left(\sum \frac{R}{A^2} \right)_{ADS} \right]}{g\rho_f \left[Z_{sump} - Z_{\substack{core \\ inlet}} \right]} \right] - \frac{\left(\frac{q_{core}}{h_{fg}} \right)^2 \left(\frac{\rho_g}{\Delta\rho} \right) \frac{1}{2\rho_f} \left[\left(\sum \frac{R}{A^2} \right)_{DVI} + \Phi_{fo}^2 \left(\sum \frac{R}{A^2} \right)_{ADS} \right]}{g\rho_f \left[Z_{sump} - Z_{\substack{core \\ inlet}} \right]} = 0 \tag{4-134}$$

The third order polynomial in x_{exit} can be recast as:

$$x_{exit}^3 + \phi_a x_{exit}^2 + \phi_b x_{exit} - \phi_c = 0 \tag{4-135}$$

where the coefficients are:

$$\phi_a = 0$$

$$\phi_b = \frac{-\left(\frac{q_{core}}{h_{fg}}\right)^2 \frac{1}{2\rho_f}\left[\left(\sum \frac{R}{A^2}\right)_{DVI} + \Phi_{fo}^2\left(\sum \frac{R}{A^2}\right)_{ADS}\right]}{g\rho_f\left[Z_{sump} - Z_{\substack{core \\ inlet}}\right]} \tag{4-136}$$

$$\phi_c = \frac{\left(\frac{q_{core}}{h_{fg}}\right)^2 \left(\frac{\rho_g}{\Delta\rho}\right)\frac{1}{2\rho_f}\left[\left(\sum \frac{R}{A^2}\right)_{DVI} + \Phi_{fo}^2\left(\sum \frac{R}{A^2}\right)_{ADS}\right]}{g\rho_f\left[Z_{sump} - Z_{\substack{core \\ inlet}}\right]} \tag{4-137}$$

As the coefficient $\phi_a = 0$ and the coefficient $\phi_c << \phi_b x_e$ (an order of magnitude less) at low pressure (<100 psia) and quality $x_e > 0.05$; the third order polynomial simplifies to:

$$x_{exit}^3 = \phi_b x_{exit} \tag{4-138}$$

$$x_{exit} = (\phi_b)^{1/2} \tag{4-139}$$

Applying the above relation, the top-down scaling relation for quality can be obtained:

$$[x_{exit}]_R = (\phi_b)_R^{1/2} = \left(\frac{q_{core}}{h_{fg}}\right)_R \left[\frac{\frac{1}{\rho_f}\left[\left(\sum \frac{R}{A^2}\right)_{DVI} + \Phi_{fo}^2\left(\sum \frac{R}{A^2}\right)_{ADS}\right]}{\rho_f g\left(Z_{sump} - Z_{\substack{core \\ inlet}}\right)}\right]_R^{1/2} = 1.0 \tag{4-140}$$

The scaling relation for quality contains a gravity head to hydraulic resistance ratio and a core power to enthalpy ratio.

The above scaling relation can also be put in an alternate form to which brings out a power to effective flow area ratio if desired:

$$[x_e]_R = \left(\frac{q_{core}}{A_{eff}}\right)_R \left(\frac{1}{h_{fg}}\right)_R \left[\frac{\frac{1}{\rho_f}\left[(\Sigma R)_{DVI} + \Phi_{fo}^2 (\Sigma R)_{ADS}\right]}{\rho_f g\left(Z_{sump} - Z_{\substack{core \\ inlet}}\right)}\right]_R^{1/2} = 1.0 \tag{4-141}$$

As the test facility (OSU) and plants will be fully depressurized during sump injection, property similitude exists and therefore the density and enthalpy ratios will be automatically preserved ($[\rho_f]_R = 1.0$ and $[h_{fg}]_R = 1.0$). Therefore, the scaling relation reduces to a gravity head to resistance ratio and core power ratio as follows:

$$[x_{exit}]_R = (q_{core})_R \left[\frac{\left[\left(\sum \frac{R}{A^2} \right)_{DVI} + \Phi_{fo}^2 \left(\sum \frac{R}{A^2} \right)_{ADS} \right]}{\left(Z_{sump} - Z_{\substack{core \\ inlet}} \right)} \right]_R^{1/2} = 1.0 \qquad (4\text{-}142)$$

The above scaling relation for quality requires an estimate of the two-phase multiplier Φ_{fo}^2. Applying the homogeneous equilibrium model, the two-phase multiplier can be estimated as follows (see Todreas, Reference 29):

$$\Phi_{fo}^2 \approx \frac{\rho_f}{\rho_m} = \left[1 + x_e \left(\frac{\Delta\rho}{\rho_g} \right) \right] \qquad (4\text{-}143)$$

As the two-phase multiplier is a function of quality, the scaling relation for quality shown above is therefore an implicit form with respect to quality:

$$[x_{exit}]_R = \left(\frac{q_{core}}{h_{fg}} \right)_R \left[\frac{\frac{1}{\rho_f} \left[\left[\left(\sum \frac{R}{A^2} \right)_{DVI} + \left(\sum \frac{R}{A^2} \right)_{ADS} \right] + x_{exit} \left(\frac{\Delta\rho}{\rho_g} \right) \left(\sum \frac{R}{A^2} \right)_{ADS} \right]}{\rho_f \cdot g \left(Z_{sump} - Z_{\substack{core \\ inlet}} \right)} \right]_R^{1/2} = 1.0 \qquad (4\text{-}144)$$

An explicit form of this relation is more difficult to obtain. However, for situations where the two-phase component of resistance in the two-phase region is dominant relative to the single phase resistance of both single phase and two phase regions, which is the case for $\left\{ x_e \left(\frac{\Delta\rho}{\rho_g} \right) \left(\sum \frac{R}{A^2} \right)_{2\phi} >> \left(\sum \frac{R}{A^2} \right)_{1\phi} + \left(\sum \frac{R}{A^2} \right)_{2\phi} \right\}$ AP600 and AP1000 during sump injection, the following explicit form can be obtained:

$$[x_e]_R = \left(\frac{q_{core}}{\rho_f h_{fg}} \right)^2 \left(\frac{\Delta\rho}{\rho_g} \right)_R \frac{\left[\left(\sum \frac{R}{A^2} \right)_{2\phi} \right]_R}{(\Delta Z)_R} \qquad (4\text{-}145)$$

By applying the following substitutions in the above scaling relation: $q_{core} = x_e \dot{m} h_{fg}$ and $\dot{m} = \rho_f A_{ref} u_{ref}$ (where $\dot{m}$ represents the mass flow at some reference location in the system such as the core inlet) we can obtain an alternate form:

$$[x_e]_R \left(\frac{\Delta\rho}{\rho_g}\right)_R \cdot \left[\frac{u_{ref}}{(\Delta Z)^{1/2}}\right]_R^2 \cdot (F_{2\phi})_R = 1.0 \qquad (4\text{-}146)$$

It can be seen that this top-down scaling relation contains several scaling relations obtained by Ishii (References 19 and 20).

$$[x_e]_R \cdot \left(\frac{\Delta\rho}{\rho_g}\right)_R = 1.0 \qquad (4\text{-}147)$$

$$(F_{2\phi})_R = 1.0 \qquad (4\text{-}148)$$

$$\text{where } F_{2\phi} = \left(\sum \frac{R}{A^2}\right)_{2\phi} A_{ref}^2 \qquad (4\text{-}149)$$

$$(u_{ref})_R = [\Delta Z]_R^{1/2} \qquad (4\text{-}150)$$

This is a significant result in that it provides a compact, top-down framework to relate a subset of the scaling laws obtained by Ishii for two-phase natural circulation where the two-phase resistance dominates and the system is at low pressure.

Using appropriate reference values for AP600, AP1000 and OSU, the following scaling ratios are obtained:

[

Sump Injection Phase – Quality Relation			

] a,b,c

From the scaling ratios shown in the previous table, it can be seen that quality is well scaled between OSU and AP600 as well as AP1000 from a top-down perspective. Therefore, OSU can be used for code validation during sump injection. The sump injection portion of AP600 was not modeled in SPES.

Alternate Derivation of Two-Phase Natural Circulation Top-Down Scaling Relation Under Saturated Fluid Conditions

Starting with the combined conservation of mass, momentum, and energy equation for two-phase natural circulation:

$$g\rho_f[\Delta Z]-g\left[\frac{\rho_f}{1+x_e\dfrac{\Delta\rho}{\rho_g}}\right][\Delta Z]=\frac{1}{2\rho_f}\frac{q_{core}^2}{x_e^2h_{fg}^2}\left[\left(\sum\frac{R}{A^2}\right)_{1\phi}+\Phi_{fo}^2\left(\sum\frac{R}{A^2}\right)_{2\phi}\right] \tag{4-151}$$

Multiply the above equation by $x_e^2\left[1+x_e\left(\dfrac{\Delta\rho}{\rho_g}\right)\right]$:

$$\left\{x_e^3\left(\frac{\Delta\rho}{\rho_g}\right)+x_e^2\right\}g\cdot\rho_f\cdot\Delta Z-x_e^2g\rho_f\Delta Z=\left[1+x_e\left(\frac{\Delta\rho}{\rho_g}\right)\right]\frac{q_{core}^2}{2\rho_f\cdot h_{fg}^2}\left(\sum\frac{R}{A^2}\right)_{1\phi}+\left[1+x_e\left(\frac{\Delta\rho}{\rho_g}\right)\right]^2\frac{q_{core}^2}{2\rho_f\cdot h_{fg}^2}\left(\sum\frac{R}{A^2}\right)_{2\phi} \tag{4-152}$$

$$x_e^3\left(\frac{\Delta\rho}{\rho_g}\right)\cdot g\cdot\rho_f\cdot\Delta Z=\frac{q_{core}^2}{2\rho_f\cdot h_{fg}^2}\left[\left(\sum\frac{R}{A^2}\right)_{1\phi}+\left(\sum\frac{R}{A^2}\right)_{2\phi}\right]+\frac{q_{core}^2}{2\rho_f\cdot h_{fg}^2}\left[x_e\left(\frac{\Delta\rho}{\rho_g}\right)\left(\sum\frac{R}{A^2}\right)_{1\phi}+2x_e\left(\frac{\Delta\rho}{\rho_g}\right)\left(\sum\frac{R}{A^2}\right)_{2\phi}\right]$$

$$+\frac{q_{core}^2}{2\rho_f\cdot h_{fg}^2}\left[x_e^2\left(\frac{\Delta\rho}{\rho_g}\right)^2\left(\sum\frac{R}{A^2}\right)_{2\phi}\right] \tag{4-153}$$

Collecting like terms we obtain:

$$x_e^3\left\{\left(\frac{\Delta\rho}{\rho_g}\right)\cdot g\cdot\rho_f\cdot\Delta Z\right\}-x_e^2\left\{\left(\frac{\Delta\rho}{\rho_g}\right)^2\frac{q_{core}^2}{2\rho_f\cdot h_{fg}^2}\cdot\left(\sum\frac{R}{A^2}\right)_{2\phi}\right\}-x_e\left\{\frac{q_{core}^2}{2\rho_f\cdot h_{fg}^2}\left(\frac{\Delta\rho}{\rho_g}\right)\left[\left(\sum\frac{R}{A^2}\right)_{1\phi}+2\left(\sum\frac{R}{A^2}\right)_{2\phi}\right]\right\}$$

$$-\frac{q_{core}^2}{2\rho_f\cdot h_{fg}^2}\left[\left(\sum\frac{R}{A^2}\right)_{1\phi}+\left(\sum\frac{R}{A^2}\right)_{2\phi}\right]=0 \tag{4-154}$$

Dividing by $\left(\frac{\Delta\rho}{\rho_g}\right) g \cdot \rho_f \Delta Z$, we obtain:

$$x_e^3 - x_e^2\left\{\left(\frac{\Delta\rho}{\rho_g}\right)\cdot\frac{q_{core}^2}{2\rho_f \cdot h_{fg}^2}\cdot\frac{\left(\sum\frac{R}{A^2}\right)_{2\phi}}{g\cdot\rho_f\cdot\Delta Z}\right\} - x_e\left\{\frac{q_{core}^2}{2\rho_f \cdot h_{fg}^2}\cdot\frac{\left(\sum\frac{R}{A^2}\right)_{1\phi}+2\left(\sum\frac{R}{A^2}\right)_{2\phi}}{g\cdot\rho_f\cdot\Delta Z}\right\}$$

$$-\frac{q_{core}^2}{2\rho_f \cdot h_{fg}^2}\frac{\left[\left(\sum\frac{R}{A^2}\right)_{1\phi}+\left(\sum\frac{R}{A^2}\right)_{2\phi}\right]}{g\cdot\rho_f\cdot\Delta Z}=0 \qquad (4\text{-}155)$$

The third order polynomial in x_e can be expressed as follows:

$$x_e^3 + \phi_a x_e^2 + \phi_b x_e + \phi_c = 0 \qquad (4\text{-}156)$$

where the coefficients are defined as:

$$\phi_a = -\left(\frac{\Delta\rho}{\rho_g}\right)\cdot\frac{q_{core}^2}{2\cdot\rho_f\cdot h_{fg}^2}\cdot\frac{\left(\sum\frac{R}{A^2}\right)_{2\phi}}{g\cdot\rho_f\cdot\Delta Z} \qquad (4\text{-}157)$$

$$\phi_b = -\frac{q_{core}^2}{2\cdot\rho_f\cdot h_{fg}^2}\cdot\frac{\left(\sum\frac{R}{A^2}\right)_{1\phi}+2\left(\sum\frac{R}{A^2}\right)_{2\phi}}{g\cdot\rho_f\cdot\Delta Z} \qquad (4\text{-}158)$$

$$\phi_c = -\frac{q_{core}^2}{2\cdot\rho_f\cdot h_{fg}^2}\cdot\frac{\left(\sum\frac{R}{A^2}\right)_{1\phi}+\left(\sum\frac{R}{A^2}\right)_{2\phi}}{g\cdot\rho_f\cdot\Delta Z} \qquad (4\text{-}159)$$

Now, applying the scaling relationships between coefficients as reported by Reyes (Reference 31):

$$[x_e]_R = (\phi_a)_R = (\phi_b)_R^{1/2} \tag{4-160}$$

$$[x_e]_R = (\phi_a)_R = \left(\frac{\Delta\rho}{\rho_g}\right)_R \cdot \left(\frac{q_{core}}{\rho_f \cdot h_{fg}}\right)_R^2 \left[\frac{\left(\sum \frac{R}{A^2}\right)_{2\phi}}{\Delta Z}\right]_R \tag{4-161}$$

It is important to note that this is the same result obtained earlier, where the two-phase resistance dominates.

$$[x_e]_R = (\phi_b)_R^{1/2} = \left(\frac{q_{core}}{\rho_f \cdot h_{fg}}\right)_R \left[\frac{\left(\sum \frac{R}{A^2}\right)_{total} + \left(\sum \frac{R}{A^2}\right)_{2\phi}}{\Delta Z}\right]_R^{1/2} \tag{4-162}$$

where:

$$\left(\sum \frac{R}{A^2}\right)_{total} = \left(\sum \frac{R}{A^2}\right)_{1\phi} + \left(\sum \frac{R}{A^2}\right)_{2\phi} \tag{4-163}$$

Now, set $[x_e]_R = [x_e]_R$ or $(\phi_a)_R = (\phi_b)_R^{1/2}$ (4-164)

$$\left(\frac{\Delta\rho}{\rho_g}\right)_R \left(\frac{q_{core}}{\rho_f \cdot h_{fg}}\right)_R^2 \left[\frac{\left(\sum \frac{R}{A^2}\right)_{2\phi}}{\Delta Z}\right]_R = \left(\frac{q_{core}}{\rho_f \cdot h_{fg}}\right)_R \left[\frac{\left(\sum \frac{R}{A^2}\right)_{total} + \left(\sum \frac{R}{A^2}\right)_{2\phi}}{\Delta Z}\right]_R^{1/2} \tag{4-165}$$

Dividing by the right-hand side, we obtain the following relation:

$$\left(\frac{\Delta\rho}{\rho_g}\right)_R \left(\frac{q_{core}}{\rho_f \cdot h_{fg}}\right)_R \frac{\left[\left(\sum \frac{R}{A^2}\right)_{2\phi}\right]_R}{\left[\left(\sum \frac{R}{A^2}\right)_{total} + \left(\sum \frac{R}{A^2}\right)_{2\phi}\right]_R^{1/2}} \left(\frac{1}{\Delta Z}\right)_R^{1/2} = 1.0 \tag{4-166}$$

Now, as $x_e = \frac{q_{core}}{\dot{m} \cdot h_{fg}} = \frac{q_{core}}{\rho_f A_c u_c \cdot h_{fg}}$ by definition then, the quantity $\frac{q_{core}}{\rho_f \cdot h_{fg}} = x_e \cdot A_c u_c$ can be replaced in the equation above. (4-167)

Making this substitution results in the following:

$$\left(\frac{\Delta\rho}{\rho_g}\right)_R (x_e \cdot A_c u_c)_R \frac{\left[\left(\sum \frac{R}{A^2}\right)_{2\phi}\right]_R}{\left[\left(\sum \frac{R}{A^2}\right)_{total} + \left(\sum \frac{R}{A^2}\right)_{2\phi}\right]_R^{1/2}} \left(\frac{1}{\Delta Z}\right)_R^{1/2} = 1.0 \quad (4\text{-}168)$$

Multiplying by $\left(\frac{A_c}{A_c}\right)_R$:

$$(x_e)_R \left(\frac{\Delta\rho}{\rho_g}\right)_R \left(\frac{u_c}{\Delta Z^{1/2}}\right)_R \cdot \left[\left(\sum \frac{R}{A^2}\right)_{2\phi}\right]_R (A_c)_R \cdot \left(\frac{A_c}{A_c}\right)_R \frac{1}{\left[\left(\sum \frac{R}{A^2}\right)_{total} + \left(\sum \frac{R}{A^2}\right)_{2\phi}\right]_R^{1/2}} = 1.0 \quad (4\text{-}169)$$

The reference area, A_c can be absorbed into the resistance terms to result in friction numbers as follows:

$$(x_e)_R \cdot \left(\frac{\Delta\rho}{\rho_g}\right)_R \cdot \left(\frac{u_c}{\Delta Z^{1/2}}\right)_R \cdot \left[\left(\sum \frac{R}{A^2}\right)_{2\phi} \cdot A_c^2\right]_R \frac{1}{\left\{\left[\left(\sum \frac{R}{A^2}\right)_{total} + \left(\sum \frac{R}{A^2}\right)_{2\phi}\right] \cdot A_c^2\right\}_R^{1/2}} = 1.0 \quad (4\text{-}170)$$

$$(x_e)_R \cdot \left(\frac{\Delta\rho}{\rho_g}\right)_R \cdot \left(\frac{u_c}{\Delta Z^{1/2}}\right)_R \cdot \frac{[F_{2\phi}]_R}{[F_{total} + F_{2\phi}]_R^{1/2}} = 1.0 \quad (4\text{-}171)$$

The above scaling relation contains several scaling relations obtained by Ishii as shown below:

$$(x_e)_R \cdot \left(\frac{\Delta\rho}{\rho_g}\right)_R = 1.0 \quad (4\text{-}172)$$

$$[F_{2\phi}]_R = 1.0 \quad (4\text{-}173)$$

$$\left[\frac{u_c}{\Delta Z^{1/2}}\right]_R = 1.0 \Rightarrow (u_c)_R = \left(\Delta Z^{1/2}\right)_R \quad (4\text{-}174)$$

$$\left[F_{total} + F_{2\phi}\right]_R^{1/2} = 1.0 \tag{4-175}$$

$$\Rightarrow \left[F_{total} + F_{2\phi}\right]_R = 1.0 \Rightarrow \left[F_{total}\right]_R = 1.0 \Rightarrow \left[F_{1\phi}\right]_R = 1.0 \text{ as } \left[F_{2\phi}\right]_R = 1.0 \tag{4-176}$$

4.1.2.6.2 Bottom-Up Scaling Analysis

Refer to subsection 4.1.2.5.2 for IRWST injection phase scaling of void fraction, as it applies here too.

4.1.2.7 IET Scaling Conclusions

4.1.2.7.1 Conclusions By Phase

Blowdown

Blowdown is not an important phase for a SBLOCA as there is sufficient core cooling and inventory during this phase. The phenomena involved in the blowdown phase are well known for AP600 and AP1000 as they behave similar to a conventional plant for which there is ample test data. For these reasons, scaling of the blowdown phase is not as important as for other phases such as the ADS to IRWST transition phase.

Scaling of the blowdown for the AP600 test program indicated that it was well scaled from an integral effects level in SPES. OSU does not scale the blowdown phase as well, however, this was not critical for OSU as its primary function is to provide data at low pressure during the IRWST and sump injection phases where most of the effects of the blowdown on initial conditions of subsequent phases are swept from primary system once the ADS is actuated.

Since the AP1000 power to volume ratio relative to AP600 is not preserved, the blowdown phase scaling for AP1000 to the test facilities is impacted. However, as mentioned above, this is not serious as the blowdown phase is not critical for the SBLOCA transient for AP600 or AP1000 and the phenomena is already well understood and supported by an established test data base.

Natural Circulation

The two-phase natural circulation scaling focussed on the PRHR HX as natural circulation associated with the steam generators is brief in AP600 and AP1000. In addition, natural circulation in the AP600 and AP1000 steam generators is similar to conventional plants and is well understood and supported by ample test data.

The two-phase natural circulation process with the PRHR HX dominant is well represented in the SPES facility for AP600 but is distorted in OSU. The quality relation is not as well-scaled in SPES for AP1000 as the power level is low. However, the scaling of quality is within the acceptance criteria. Therefore, SPES can be used for code validation for the high pressure two-phase natural circulation phase.

The distortion seen in two-phase natural circulation at high pressure at OSU is not serious since OSU is intended primarily to provide data at low pressure IRWST and sump injection. Finally, while the operation of the PRHR HX does have some influence on the SBLOCA event it is not of high importance for a SBLOCA as it is not needed for energy removal or inventory recovery. The primary function of the PRHR HX is energy removal for non-LOCA events.

ADS

This phase is important in that it supports depressurization to allow long-term cooling. The scaling results show that the key scaling groups (derived from the RPC equation) are acceptably scaled in SPES relative to AP600 and AP1000. Therefore, SPES can be used for code validation from an integral effects perspective.

ADS to IRWST Transition

This is the most critical phase of an SBLOCA transient as it typically experiences the minimum reactor vessel inventory. Consequently, scaling reactor vessel inventory is the primary focus.

The key scaling ratio associated with inventory replenishment when CMT injection is dominant is well scaled in OSU and SPES relative to AP600 and AP1000.

Similarly, the key scaling ratio associated with inventory replenishment when IRWST injection is dominant is well scaled in OSU and SPES relative to AP600 and AP1000.

However, with respect to pressure in the RCS (which is important to IRWST injection), only OSU is well scaled to AP600 and AP1000. SPES is distorted.

Therefore, OSU can be used for code validation for this phase from an integral test perspective.

IRWST and Sump Injection

The two-phase natural circulation process for AP600 and AP1000 is well represented in the OSU test facility at the integral effects level. This is shown by the very favorable results of scaling the core exit quality from a top-down perspective. Scaling of void fraction in the core (based upon the Yeh correlation) while not ideal is acceptable for integral effects simulation. Therefore, OSU can be used for code validation.

The SPES facility is not well scaled to AP600 or AP1000 for IRWST injection as the ADS-4 vent path resistance is distorted. The SPES facility was not designed to simulate sump injection.

Equation Symbols

Symbol	Definition
A	area
d	diameter
e	specific internal energy
E	energy
f	friction factor
F	friction number
Fr	Froude Number
g	gravitational acceleration
G	mass flux
h	specific enthalpy
j	superficial velocity
K*	Kutateladze Number
L	length
$\dot{m}$	mass flow rate
M	mass
p	pressure
q	heat transfer rate, or power
Q	volumetric flow rate
R	resistance
u	velocity
υ	specific volume
V	volume
x	quality
Z	elevation
α	void fraction
γ	ratio of specific heats (c_p/c_v)
ε	dilation
π	non-dimensional scaling group
ρ	density

Symbol	Definition
σ	surface tension
τ	time constant
Γ	mass transfer rate
Φ_{fo}^2	two-phase multiplier
Subscripts	
ADS steam	automatic depressurization system steam
bcr	critical bubble rise
c	critical
CMT	core makeup tank
core	core
core steam	core steam
DVI	direct vessel injection
e	exit or equilibrium
eff	effective
exit	exit
f	liquid
fo	liquid only
g	gas
HL	hot leg
IRWST	in-containment refueling water storage tank
j	phase, liquid or gas
PZR	pressurizer
RCS UH/UP	reactor coolant system upper head/upper plenum
R	ratio
Ref	reference
SL	surge line
sub	subcooled
sump	sump
sys	system
vessel	reactor vessel

Symbol	Definition
vessel liquid	reactor vessel liquid
1ϕ	single-phase
2ϕ	two-phase
Superscripts	
+	indicates non-dimensional quantity

Table 4.1-1 Summary of Dominant Phenomena and Processes of an SBLOCA Transient

Blowdown	Natural Circulation	ADS	ADS-IRWST Transition	IRWST Injection	Sump Injection
Break flow (critical)----------→					
		ADS flow----------→ (critical)	ADS flow (subsonic) ----------→		
Core Decay Heat ----------→					
	Natural Circulation				
			IRWST gravity injection -------→		Sump gravity injection
	CMT drain/injection ----------→				
	CMT balance line flow composition				
	Phase separation in CMT balance line - Cold leg tee				
		Pressurizer refill/drain -------→			
		Surge line pressure drop and CCFL			
			Entrainment in UH/UP, Hot Leg, and ADS paths -----→		
			Hot leg flow pattern transition ----------→		

Table 4.1-2 Comparison of Key ADS Parameters a,b,c

Table 4.1-3 CMT Scaling Groups a,b,c

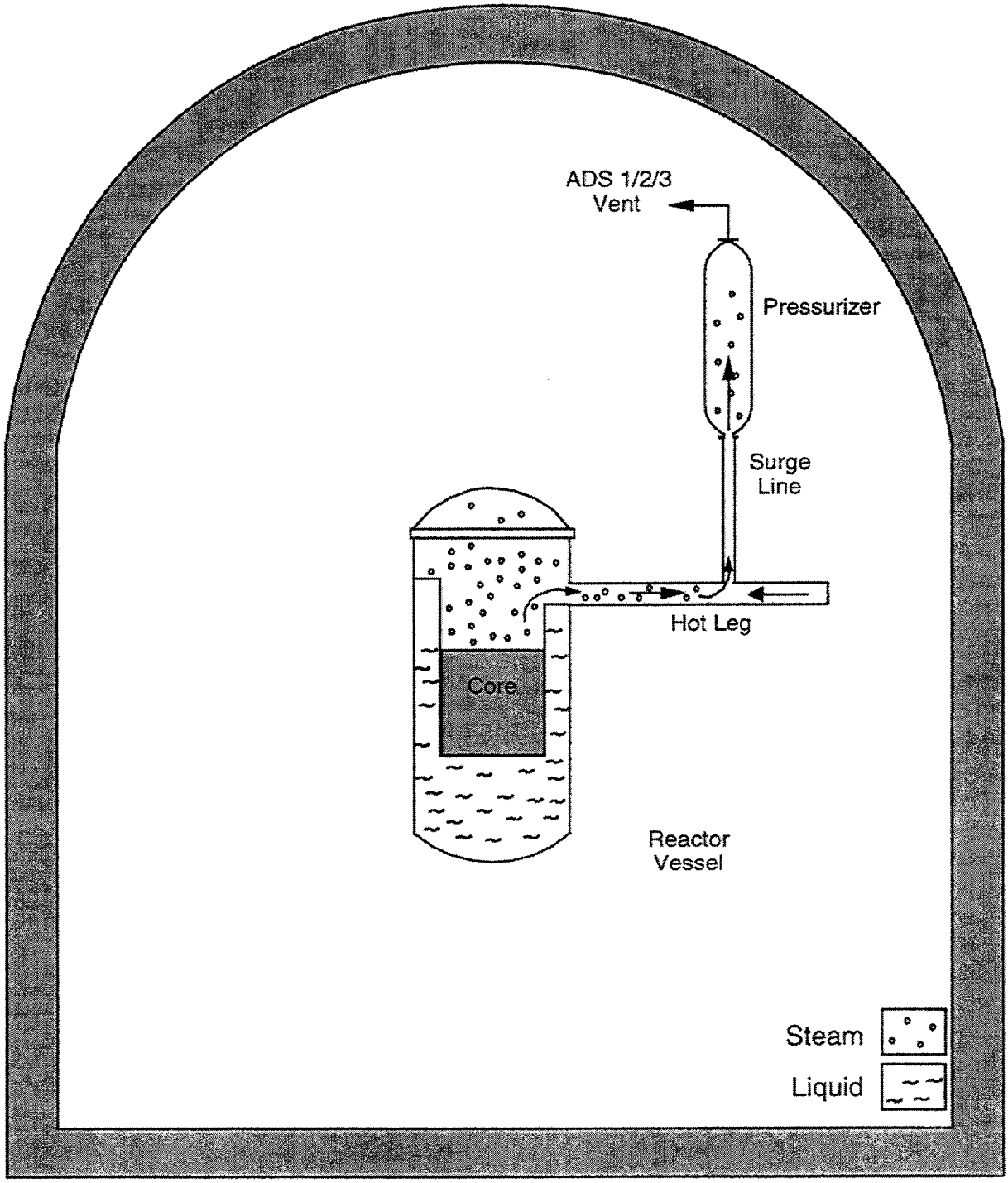

Figure 4.1-1 Automatic Depressurization System Function

a,b,c

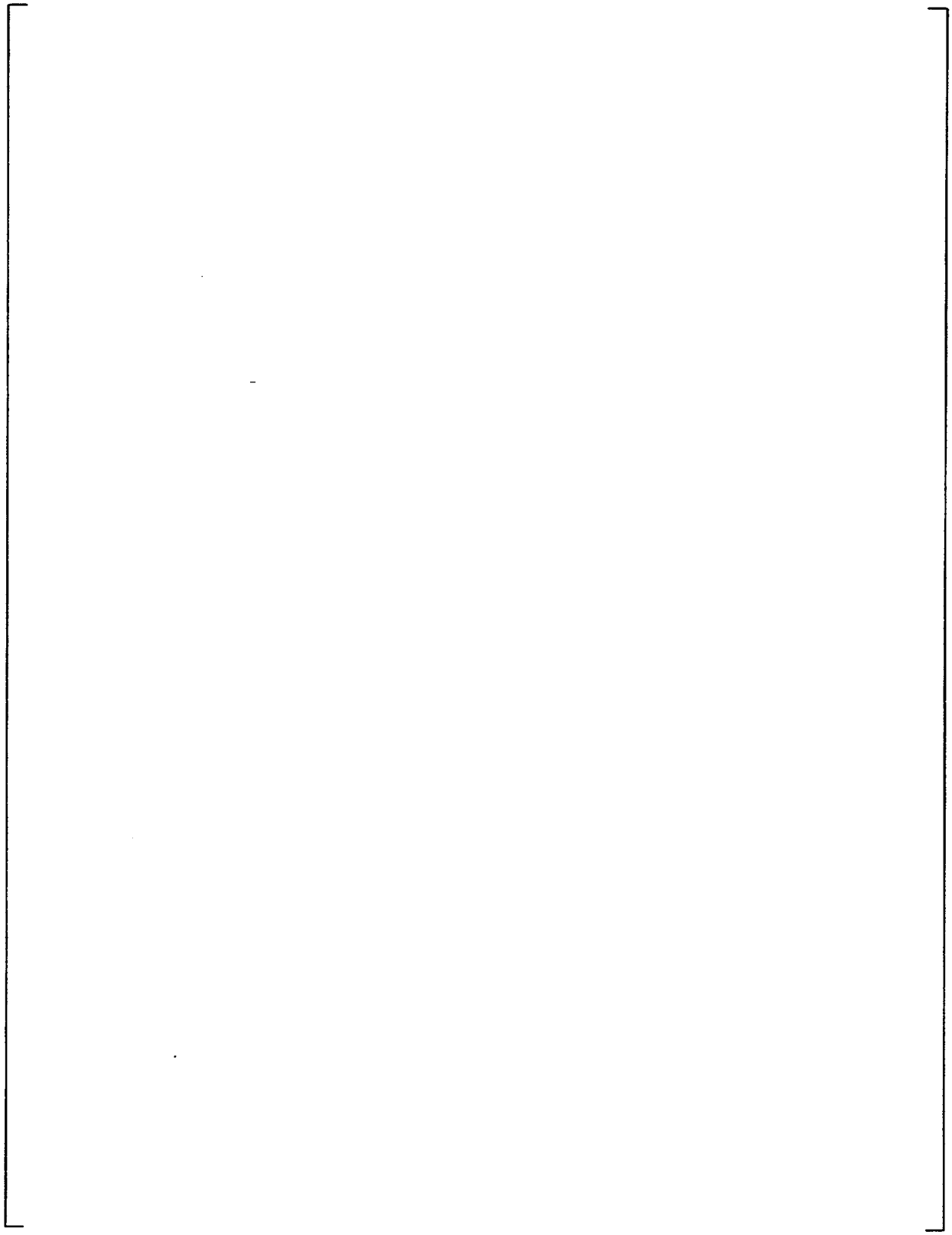

Figure 4.1-2 Typical Pressure Profile – 2-in. Cold Leg Break – SPES-2

a,b,c

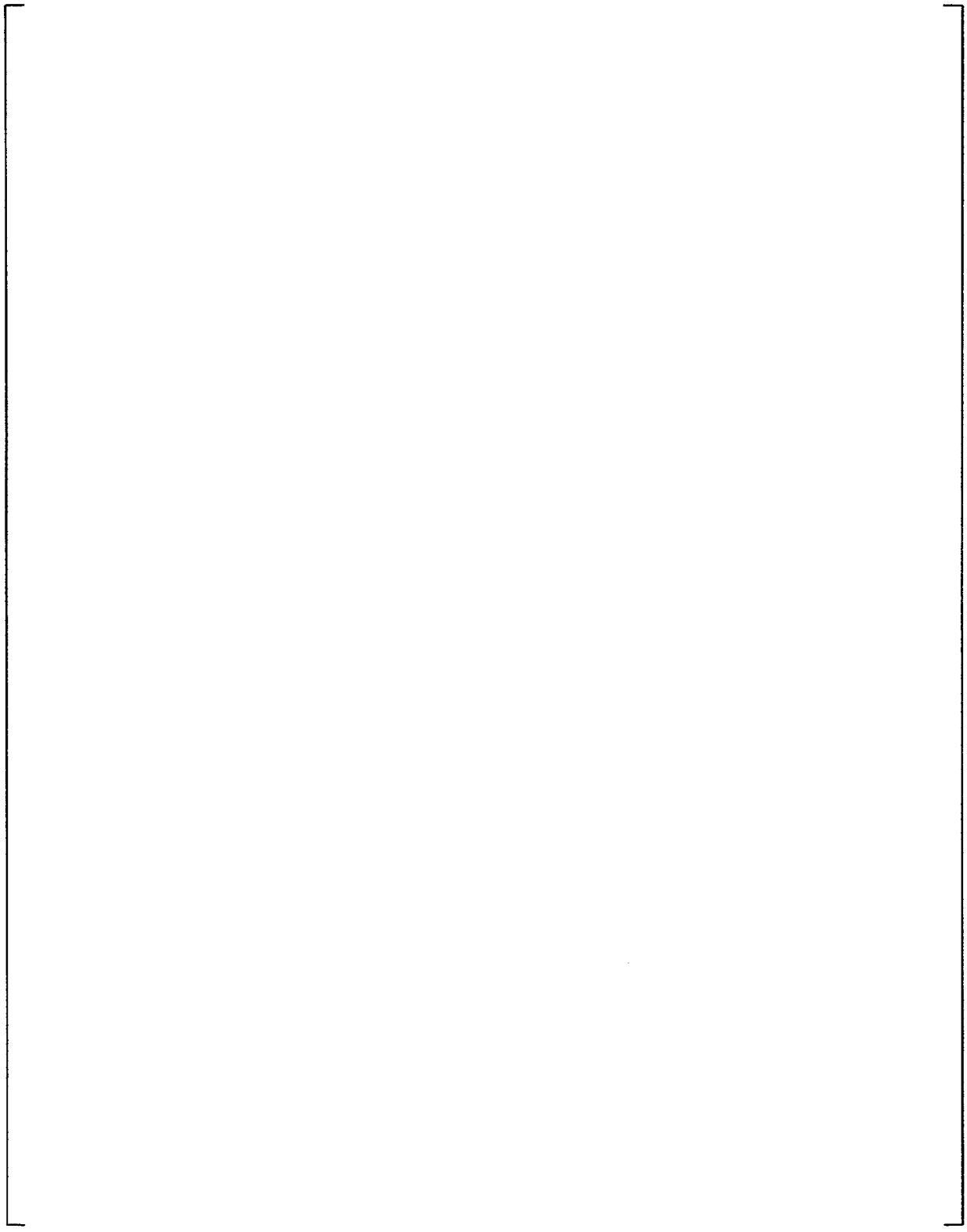

Figure 4.1-3 AP600/AP1000 PRHR HX Heat Flux

a,b,c

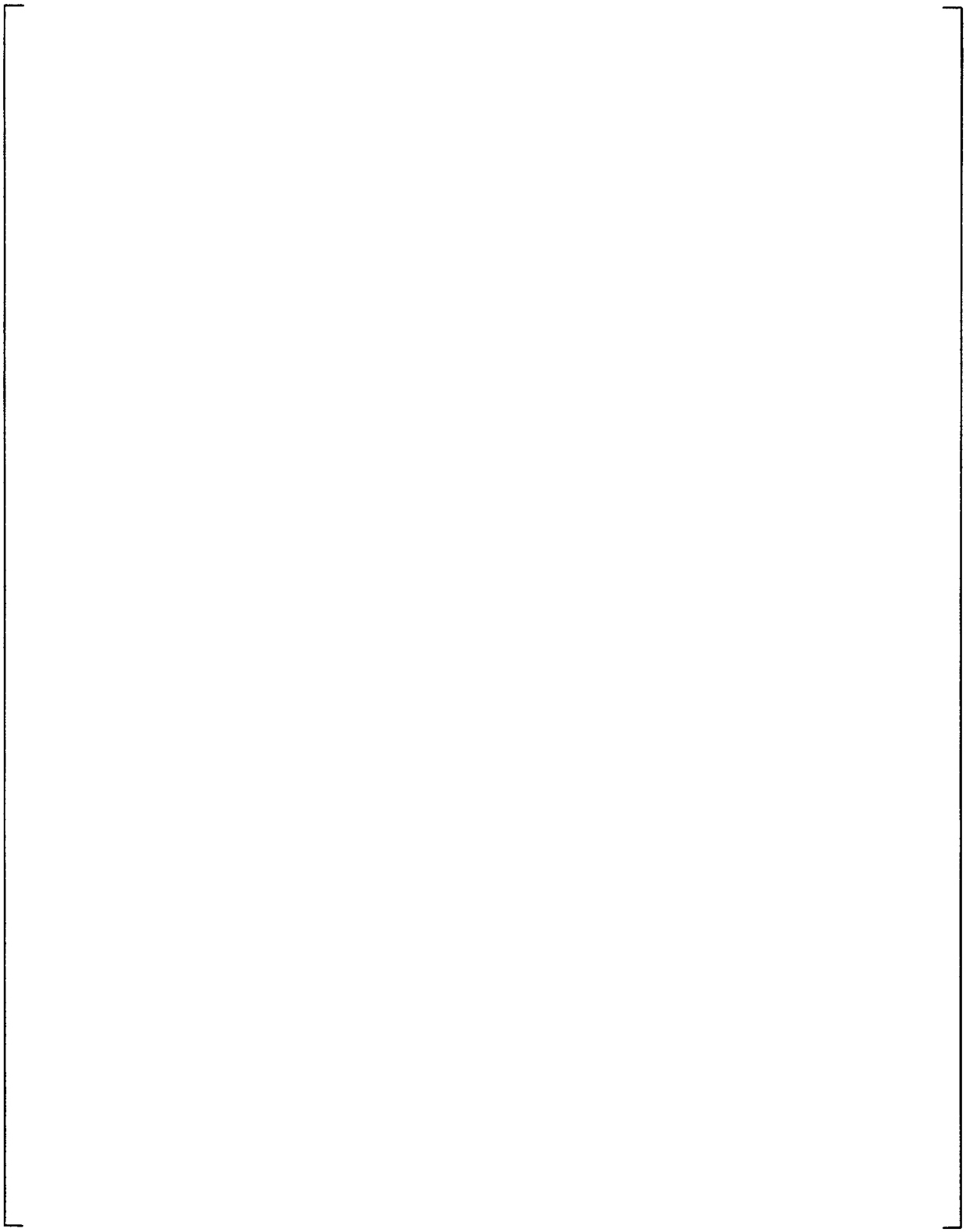

Figure 4.1-4 Comparison of AP600 and AP1000 for Loss of Power Events

a,b,c

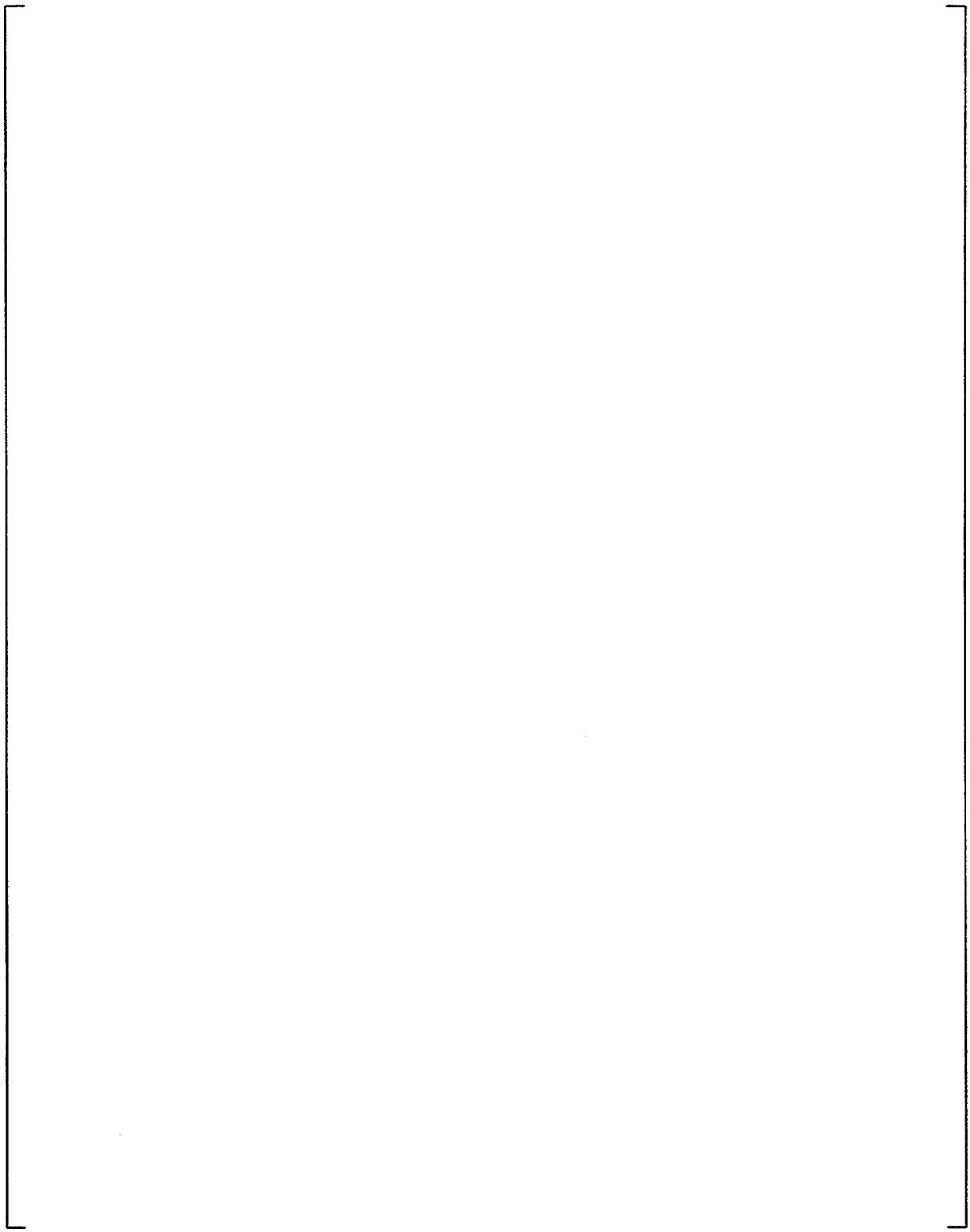

Figure 4.1-5 Comparison of AP600 and AP1000 for Loss of Normal Feedwater Events

a,b,c

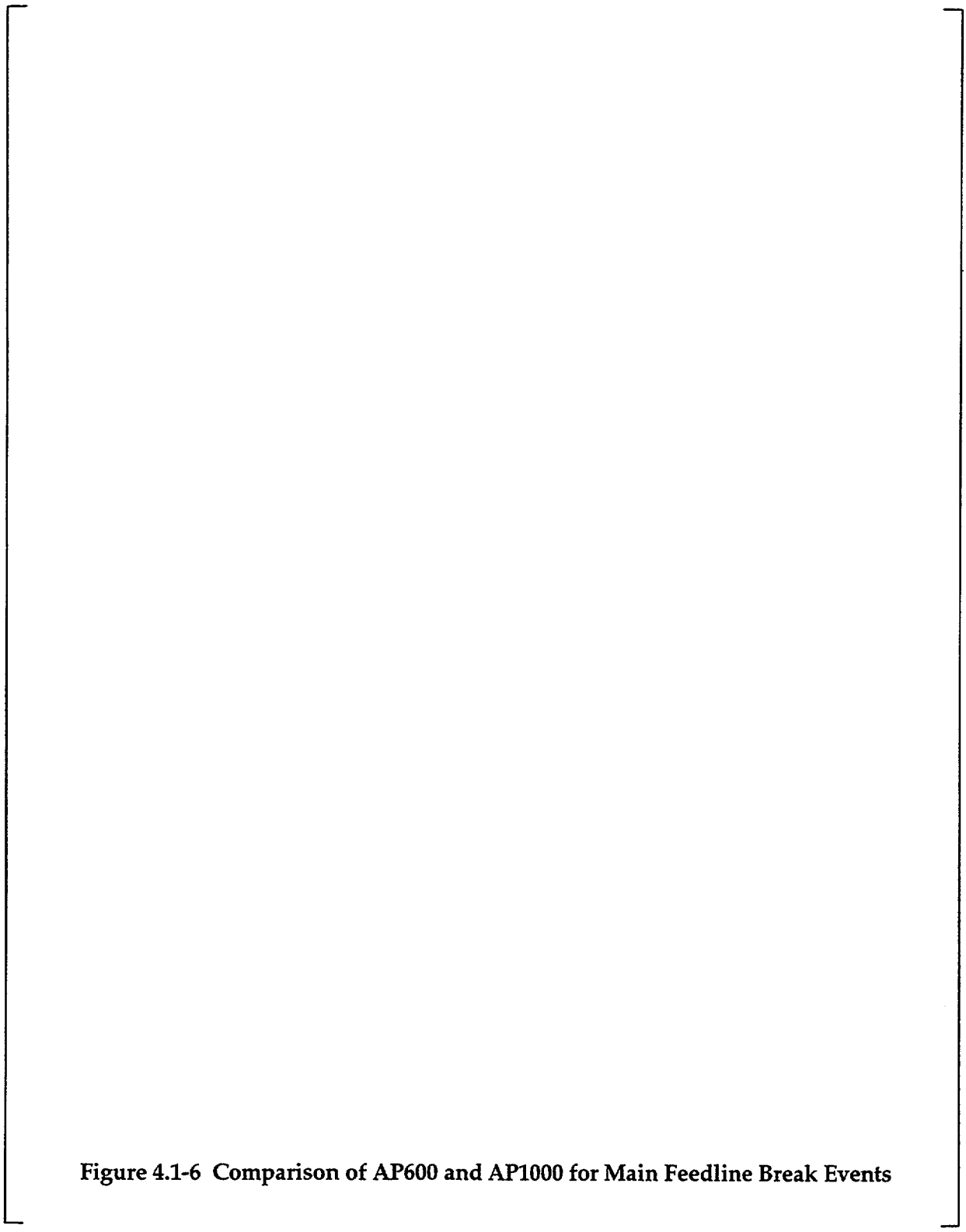

Figure 4.1-6 Comparison of AP600 and AP1000 for Main Feedline Break Events

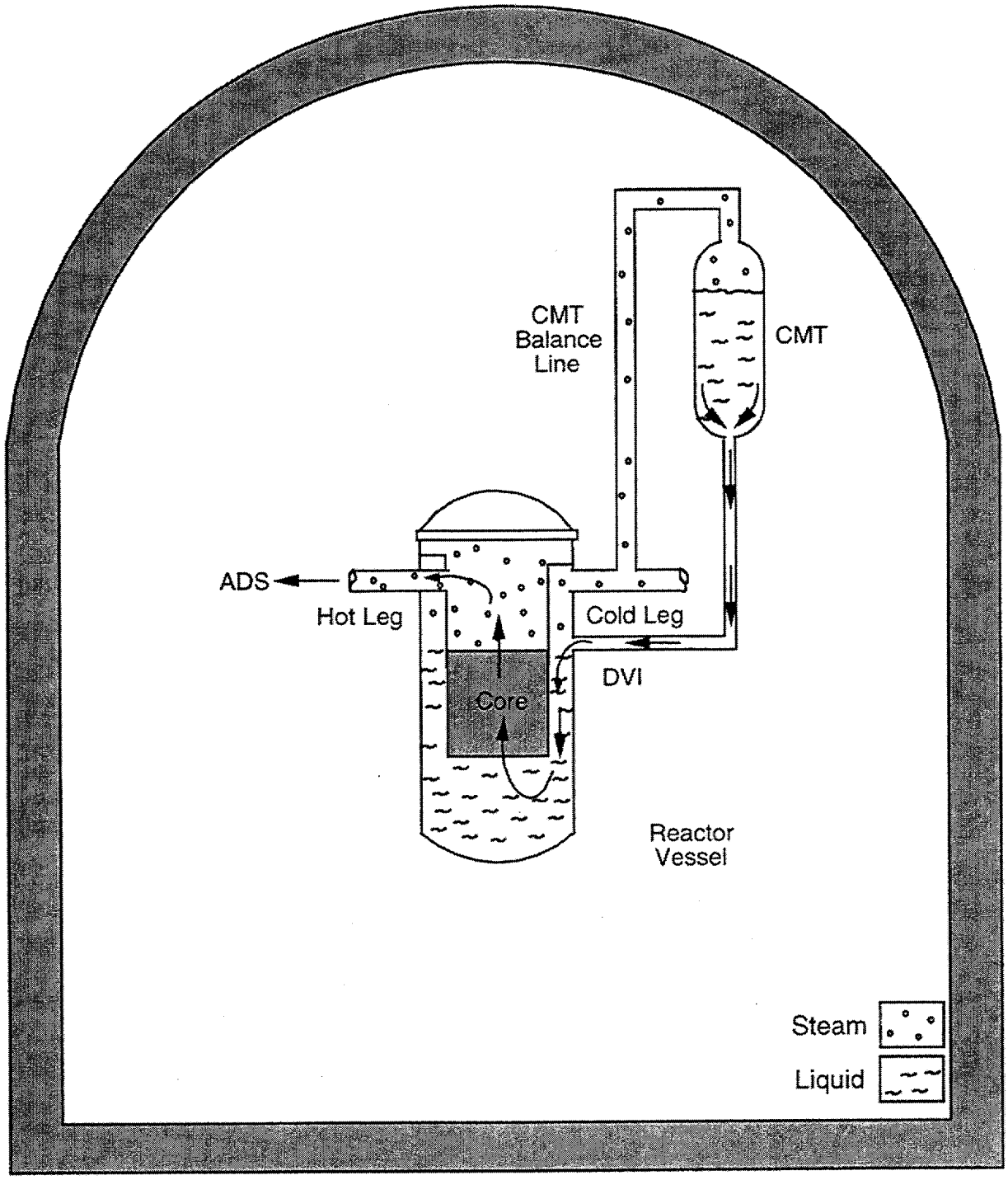

Figure 4.1-7 CMT Injection

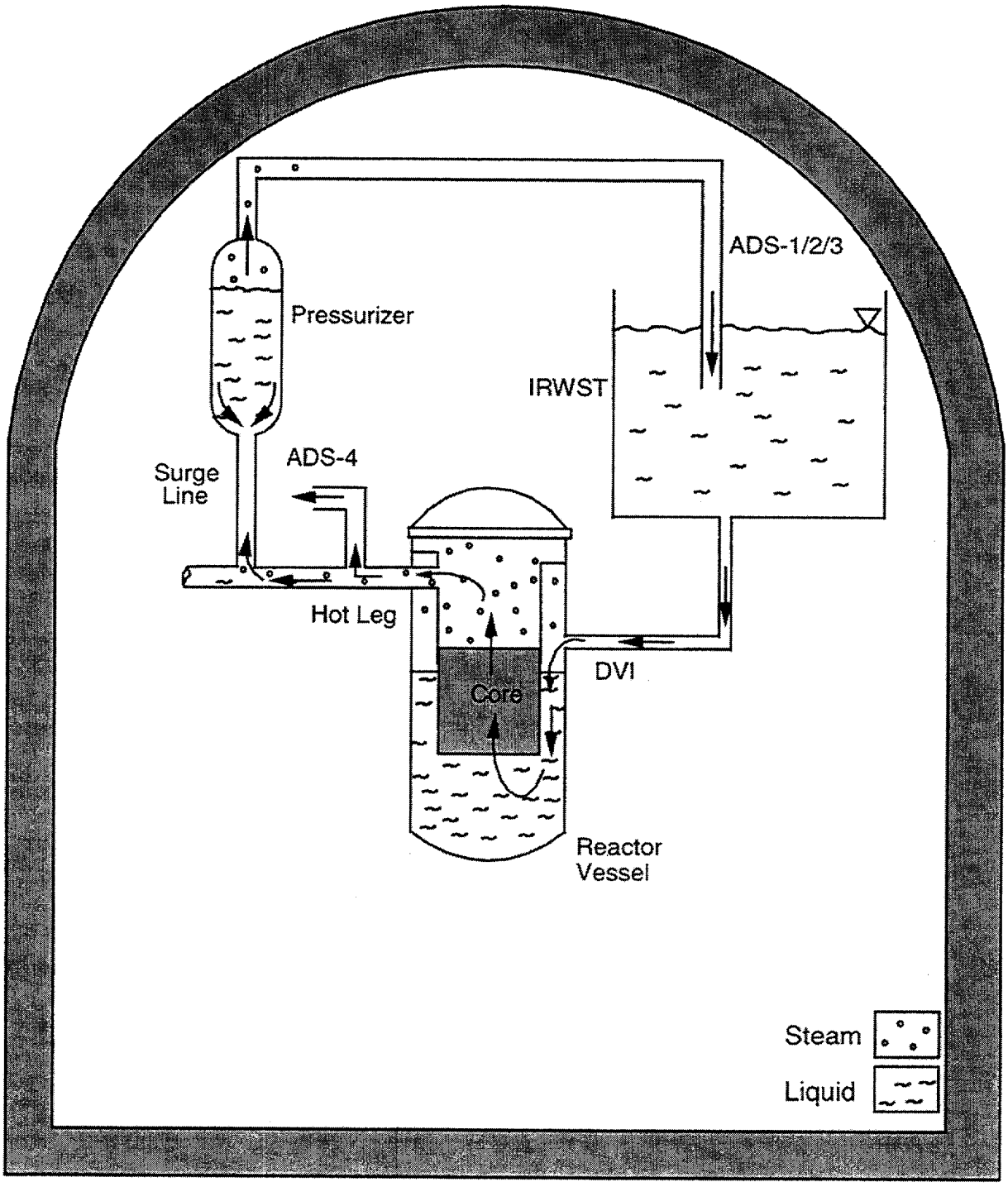

Figure 4.1-8 IRWST Injection (Pressurizer Draining)

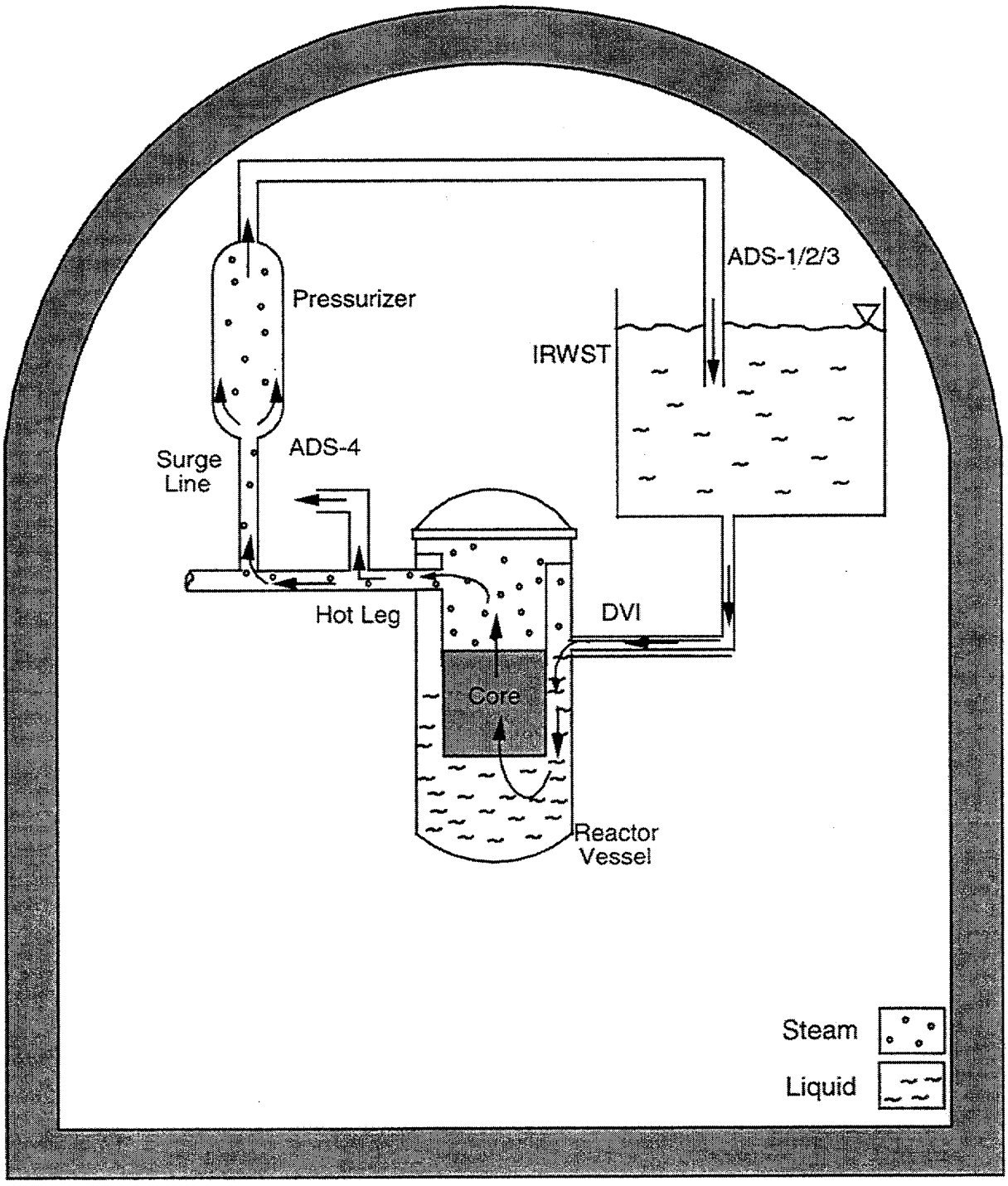

Figure 4.1-9 IRWST Injection (Pressurizer Drained)

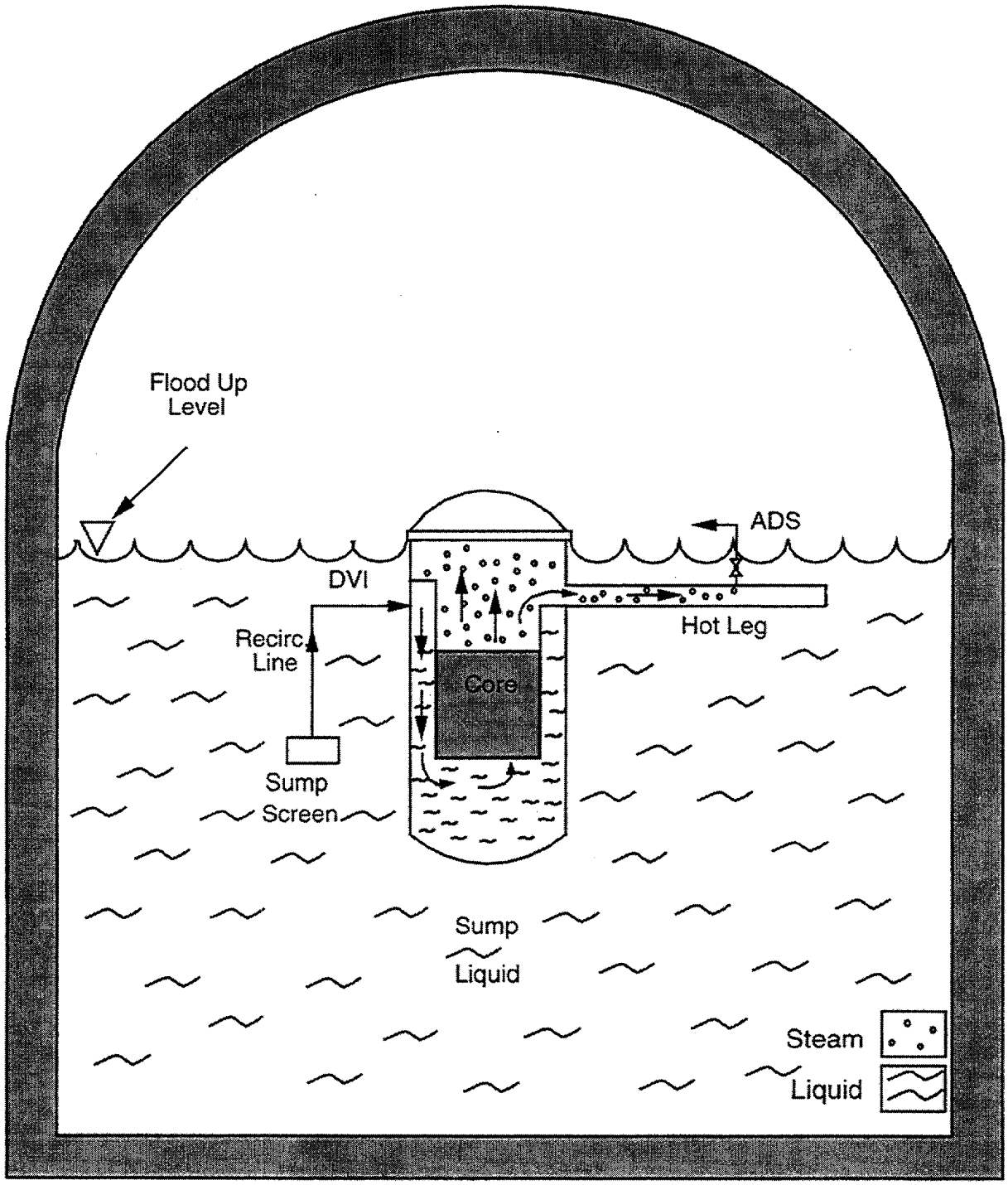

Figure 4.1-10 Sump Injection

4.2 CONTAINMENT PERFORMANCE PHENOMENA

The transport processes and components that affect the containment pressure response following a DBA are identified and ranked according to importance in a phenomena identification and ranking table (PIRT). The AP600 containment PIRT was documented in WCAP-14812, Rev. 1 (Reference 32). The high ranked phenomena in the AP600 PIRT were: the break source, condensation on the inside surfaces of the containment, evaporation from the outside surface of the containment shell, natural circulation flow through the PCS cooling air annulus, in-containment circulation and stratification, inter-compartment flow, source fog, and liquid film stability on the outside surface. As described in Section 2.2, the AP1000 design differences do not affect the results of the AP600 containment PIRT.

After identifying the important phenomena for determining the containment pressure response, a series of tests were developed to provide scalable data for validating the containment evaluation model. The Westinghouse-supported test data for validating the AP600 containment evaluation model were obtained from the following sources:

- Water Distribution Tests – a full-scale section of the containment dome that was used to determine the effectiveness of the water distribution weirs and to provide an estimate of the water coverage on the dome and at the top containment sidewall as a function of the applied water flow rate.

- PCS Air Flow Tests – a forced draft, scaled section of the PCS downcomer, air inlets, riser and exhaust chimney that was used to provide data on the frictional loss coefficient.

- Dry/Wet Flat Plate Tests – a forced draft test section to provide convection and evaporation data needed to validate the heat and mass transfer correlations.

- University of Wisconsin Condensation Tests – a forced draft test section to provide data to validate condensation heat and mass transfer on the inside of the containment surface.

- Small Scale Tests – a steady-state, forced draft test facility to provide integrated internal condensation, external evaporation and water distribution data needed to validate the heat and mass transfer correlations.

- Large Scale Tests (LST) – a steady-state, forced draft test facility to provide integrated internal condensation, external evaporation and water distribution data needed to validate the heat and mass transfer correlations.

In addition to data from the Westinghouse-supported tests, data from other sources was used to validate and qualify the AP600 containment evaluation model. These sources included various published heat transfer papers (Gilliland and Sherwood, and Eckert and Diagalia) and various containment test facilities (HDR, NUPEC, CVTR, and others).

The effects of the AP1000 design differences on the use of this test data for validation of the AP1000 containment evaluation model are evaluated below.

LST Scaling Comparison

The LST was designed to provide steady-state heat and mass transfer data from a dimensional 1/8-scale AP600 containment vessel. A top-down scaling assessment was presented in Section 10.2 of WCAP-14845, Rev. 3 (Reference 33) to determine the extent to which data from the LST could be used for code and model validation. The AP600/LST scaling assessment considered both the blowdown transient and quasi-steady-state phases of the event.

A similar scaling assessment was performed for AP1000. A comparison of the transient phase LST, AP600, and AP1000 time constant and scaling ratios is presented in Table 4.2-1.

The LST is not well scaled to model the blowdown transient condensation and convective energy transfer (π_{COND}, π_{CONV}) for either AP600 or AP1000. The reason for this is that the LST steam mass flow rate was not large enough to simulate the blowdown break energy release rates associated with a large LOCA or MSLB in the AP600 or AP1000. Therefore, the LST should not be used as a system level representation of the AP600 or AP1000 transient response.

In the quasi-steady-state phase of the event, the mass and energy sources and sinks are approximately equal. That is, the steam released by the break is condensed on the shell. The break energy is conducted through the shell and is transferred to the PCS riser via sensible heating and evaporation of the water film, convection, and radiation from the surface of the external shell.

As shown in WCAP-14845, Rev. 3 (Reference 33), the LST system level phenomena were well scaled for AP600 in the quasi-steady-state phase. Component level distortions in the LST were addressed by using local measurements of temperature, concentration, and velocity from the LST. Therefore, the steady-state LST data was determined to be acceptable for use as a source of separate effects data for internal condensation, above-deck steam distribution, external heat transfer, and external water coverage.

Heat and Mass Transfer Constitutive Relations

The containment and reactor coolant system design changes made to create the AP1000 affect the top end of the range for some of the dimensionless parameters that are used in the heat and mass transfer constitutive relations. A comparison of the parameter ranges is shown in Table 4.2-2. The ranges of the Pr and Sc numbers remain the same for the AP1000, but the top end of the ranges for $\Delta\rho/\rho$, Re_d, Gr_d, and the film Re number increase.

The $\Delta\rho/\rho$ value represents the density difference between the bulk containment air/steam mixture and air/steam mixture at the film surface. The containment $\Delta\rho/\rho$ value increases as the:

- containment pressure and temperature increase,
- amount of air above the operating deck decreases, and
- internal PCS shell film temperature decreases.

Due to the larger steam generators in AP1000, a higher pressure, more steam rich environment above the operating deck is expected during a large MSLB event than was predicted for AP600. This causes the slight increase in the estimated $\Delta\rho/\rho$ value for AP1000 over AP600.

The Re_d value is dependent on the annulus air/steam properties and buoyancy driven flow rate. The Re_d value increases as the:

- annulus air/steam velocity increases,
- riser air/steam density increases, and
- riser air/steam viscosity decreases.

Although the annulus hydraulic diameters and flow areas are the same for AP600 and AP1000, the increase in shell height causes the buoyancy driven flow rate to be higher in AP1000. This results in an increase in the estimated Re_d value for AP1000.

The Gr_d value is dependent on the annulus air/steam and evaporating liquid film properties. The Gr_d value increases as the:

- external PCS film temperature increases, and
- riser air/steam temperature decreases.

The AP1000 shell area is 47-percent larger than AP600 while the core power is over 75-percent higher. Therefore, due to the higher steam production rate compared to the shell area, the PCS shell heat flux is expected to be higher for AP1000. Although the shell thickness increased slightly (by about 8 percent), the higher shell heat flux results in a higher external film temperature and consequently an increase in the estimated Gr_d value for AP1000.

The film Re number is dependent on the film flow rate and coverage fraction. The film Re value increases as the:

- film flow rate increases, and
- film coverage fraction decreases.

The film flow rate on the inside of containment is less than outside due to film removal at the crane rail and stiffener ring, and the fact that the inside film flow rate starts at zero at the top of the dome and increases as the film flows downward. Therefore, the film Re number is bounded by the external value.

The initial AP1000 external PCS water flow rate is approximately 7-percent higher than AP600. The external shell coverage fraction is determined by the weir/dam distribution system and flow rate. Since the PCS flow rate is only slightly higher, the external shell coverage fraction should be approximately the same as AP600. Since the AP1000 shell diameter remains the same as AP600, the film Re number should only be about 10-percent higher than AP600. It is noted that the initial high external PCS water flow rate is maintained for 3 hours, while the peak containment pressure for the LBLOCA and MSLB events is reached at <1 hour. After 3 hours, the PCS water flow rate is reduced to more closely correspond with the core decay heat. These

higher AP1000 flow rates result in the AP1000 having higher water coverage than AP600, and therefore better use of the applied water than AP600.

A number of separate effects tests were performed to validate the heat and mass transfer correlations over the range of AP600 operating parameters. Data from the Wisconsin Condensation Tests and the Westinghouse Large Scale Tests were used to validate the condensation mass transfer correlation. Data from Gilliland and Sherwood and the Westinghouse Flat Plate Tests were used to validate the evaporation mass transfer correlation. A more complete description of the separate effects heat and mass transfer tests along with an evaluation of the data is given in WCAP-14326, Rev. 3 (Reference 34).

The LST condensation mass transfer data and Sherwood number correlation are shown in Figure 4.2-1. The range of $\Delta\rho/\rho$ covered by the LST is slightly less than the operating range of AP1000, however, the upper value of the AP1000 range for $\Delta\rho/\rho$ is covered by the Wisconsin Condensation Tests. Figure 4.2-1 shows the LST data agree with the selected free convection mass transfer correlation.

The Westinghouse wet flat plate test forced convection mass transfer data and Sherwood number correlation are shown in Figure 4.2-2. The range of Re_d covered by the wet flat plate tests is slightly less than the operating range of AP1000, however, the upper value of the AP1000 range for Re_d is covered by data from the dry flat plate tests. Figure 4.2-2 shows the test data agree with the selected forced convection mass transfer correlation.

The concrete shield building and metal structures within the chimney are potential heat sinks for the heated air and evaporated steam coming from the riser. The heat and mass transfer in the chimney is a low ranked phenomena in both the AP600 and AP1000 PIRT. The upper values for both the AP600 and AP1000 chimney Re_d and Gr_d numbers are not covered by the test data. Therefore, the standard Uchida correlation is used for calculating heat and mass transfer to the heat sinks within the chimney region of both the AP600 and AP1000 containment evaluation models.

In summary, the test program covered the upper range of both the AP600 and AP1000 dimensionless parameters for the selected heat and mass transfer correlations for condensation on the inside of the shell and evaporation/convection on the outside of the shell in the important riser region of the annulus. Therefore, the use of bounded heat and mass transfer correlations for condensation and evaporation is reasonable for both the AP600 and AP1000 evaluation models.

Internal Circulation/Mixing

Internal circulation and mixing are highly ranked phenomena in the PIRT. Circulation and mixing affect the distribution of steam within the containment, which in turn affects the condensation rate on the internal heat sinks and the PCS shell. A detailed assessment of circulation and mixing for AP600 is documented in Section 9 of WCAP-14407 (Reference 35).

The size, location, and direction of the break flow (jet or plume) can influence circulation and mixing inside containment. During blowdown, the high kinetic energy of a large break can significantly mix the containment atmosphere. Breaks located in the lower compartments can potentially mix more of the containment volume than breaks located above the operating deck. Breaks directed upward and away from obstructions can entrain a significant amount of air and drive circulation throughout containment.

For break jets and plumes within containment, the ratio of inertia forces and buoyant forces influences the entrainment and mixing of surrounding gases. The volumetric Froude (Fr_v) number is the ratio of inertia to gravity forces. If the Fr_v number is greater than the Peterson stability limit, inertia forces dominate. This promotes circulation and better mixing within containment.

The Fr_v number is greater than the Peterson stability limit for both AP1000 and AP600 during blowdown, even though the AP1000 containment is taller than AP600. Therefore, the containment volume above the break elevation is expected to be well mixed during blowdown.

The post-blowdown Fr_v value is much less than 1.0 for both AP600 and AP1000. Therefore, a break plume, by itself, will not significantly mix the containment atmosphere after blowdown is complete.

Condensation on the dome and vertical walls of the containment shell also influences the circulation and mixing within containment. Condensation cools the air/steam mixture near the shell surface and creates negatively buoyant plumes.

Condensation on the walls results in a cool, air-rich boundary layer plume that falls down along the wall. Condensation on the dome results in cool air-rich plumes that fall down from the dome. Warm plumes of steam and air travel upward as the cooler air-rich mixture fills the lower part of containment. The cooler, air-rich wall and dome plumes interact with the warmer steam-rich plumes to mix the containment volume above the operating deck.

The Grashof (Gr) number (the ratio of the buoyancy to viscous forces) or Raleigh (Ra) number (a product of the Gr and Pr numbers) is used when considering the interaction between the warm rising plumes and the cooler falling plumes. The characteristic length in the wall Gr number is the diameter of containment. The characteristic length in the dome Gr number is the containment height.

The diameter of the AP1000 containment shell is the same as AP600. Therefore, the wall Gr number for the two plants should not be significantly different. The dome Gr number for AP1000 would increase since the containment shell is taller and the temperature and/or density difference between the top and bottom of containment could be higher.

Separate effects tests, cited in Section 9 of WCAP-14407 (Reference 35), have shown that with dome Gr numbers greater than 10^4, turbulent mixing occurs. For both AP600 and AP1000, the dome $Gr > 2 \times 10^{13}$. So, with the combination of a rising plume of steam from the fourth stage

ADS and condensation on the dome and walls, the containment atmosphere above the operating deck should be well mixed.

In addition to the separate effects tests cited in Reference 35, data from several international containment test facilities was examined for application to the mixing and circulation phenomena within the passive (externally cooled) containment design. In particular, test E11.4 at the HDR test facility demonstrated the affect of external cooling on mixing within the open volume above the operating deck. For HDR test E11.4, the steam release into a lower-level compartment promoted global circulation and homogenized the containment atmosphere. Application of the external sprays caused a decrease in the containment pressure and a reduction in the axial temperature gradient. The external spray also promoted a more uniform gas concentration.

In order to address concerns with atmospheric mixing that were raised during the AP600 Design Certification Program, an alternative analysis methodology was pursued to independently assess the degree of mixing for large volumes mixed by thermal gradients. CFD models representing the AP600 and AP1000 dome region volumes were created using the StarCD code (version 3.100A) to numerically determine the effects of the increased height on mixing above the operating deck. The vertical walls and ceilings in the model were maintained at a relatively cold temperature (to simulate the cooling effect of the PCS) while the floor was kept hot (to simulate the heating effect of a break plume). In both cases, the analysis considered heat transfer to/from dry air.

The AP600 dome region was modeled as a vertical slice 40 meters wide (x-direction) and 40 meters high (y-direction). The thickness of the slice was 0.4 meters. Two layers/slabs (each 0.2 m thick) of control volume cells were applied in the z direction (resulting in a 3D numerical model). Two sets of grids (coarse and fine) were applied to the x and y directions. The coarse grid (see Figure 4.2-3a) had a maximum cell size of 0.4 m x 0.4 m, and a minimum cell size of 0.004 m x 0.004 m in the corners and near the vertical and horizontal boundaries. The total number of applied cells was 492,296 (246,148 in each slab/layer). The fine grid (see Figure 4.2-3c) had maximum and minimum cell sizes of 0.1 m x 0.1 m and 0.001 m x 0.001 m, respectively. The majority of the cells close to the solid wall boundaries were 0.004 m along the boundary and 0.001 m wide. Total number of cells was 940,448 (470,224 in each slab/layer).

The AP1000 dome region was modeled as a vertical slice 40 meters wide and 48 meters high. The coarse grid had maximum and minimum cell sizes of 0.2 m x 0.2 m and 0.001 m x 0.001 m, respectively (see Figure 4.2-3b). The majority of the cells close to the solid wall boundaries were 0.004 m along the boundary and 0.002 m wide. The two slabs/layers in the z direction were each 0.1 m thick, each. The total number of cells was 700,968 (350,484 in each slab/layer). The fine mesh configuration for the AP1000 dome region was the same as the one used for the AP600 calculations. The total number of cells was 1,066,528 (533,264 in each slab/layer).

The vertical walls and ceilings were maintained at a constant temperature of 366.3 K; the floors were maintained at 394.1 K. A no slip velocity boundary condition was used for all (vertical and horizontal) walls. The symmetry boundary conditions were used for all variables at x-y boundary planes (at z = 0.2 m and z = -0.2 m), so that both slabs of the cells in the z direction are

expected to be the same. The initial velocities were all set equal to zero. The initial internal air temperature was set to 380.2 K (which corresponds to the mean value of the hot and cold wall boundary temperatures).

All air properties were constant (μ = 1.81e-05 kg/ms, C_p = 1006 J/kgK, k = 0.02637 W/mK), except density which is a function of temperature, as for an ideal gas.

The applied temperatures and properties of the dry air result in Grashof numbers of $Gr_{W=20\,m}$ = 1.75 x 10^{13}, $Gr_{H=40\,m}$ = 1.40 x 10^{14} and $Gr_{H=48\,m}$ = 2.42 x 10^{14}, based on the model radius and heights, respectively. These values are approximately the same as would be expected in the AP600 and AP1000 dome regions during the long term cooling phase of a large LOCA event.

The gravity acceleration of g = –9.81 m/s^2 was applied in the y direction. The standard k-ε, high Reynolds number turbulence model was applied for all calculations. The turbulence model coefficients that were applied in StarCD for this model were C_μ = 0.09, C_{e1} = 1.44, C_{e2} = 1.92, C_{e3} = 1.44, C_{e4} = -0.33, κ = 0.419, σ = 1, σ_ε = 1.219 and σ_h = 0.9.

The first order upwind numerical scheme was used for all variables. Relaxation factors for velocities, turbulence kinetic energy and turbulence dissipation rate were 0.7, for temperature 0.95, and 0.2 for pressure. The number of sweeps and residual tolerance for all equations (except for pressure) was 100 and 0.1, respectively. They were 1000 and 0.05 for pressure. The SIMPLE solving procedure was applied.

The residual histories for each calculation are presented in Figure 4.2-4. The residuals for mass balance decreased three orders of magnitude in all cases after 1000 iterations. However, the decrease of the residuals for other equations was slower. This could be due to the fact that StarCD presents after 10 iterations relative residuals for the cases when there is no inflow, or outflow from the domain. In fact residuals are normalized with the residuals obtained in the tenth iteration.

The temperature and velocity fields obtained with the coarse and fine meshes for the AP600 configuration are presented in Figures 4.2-5 and 4.2-6. As expected, the cold boundary layers near vertical walls and hot rising plume in the middle of the dome are present. The resulting velocity field suggests low velocities exist between the downward flowing boundary layers (near the vertical walls) and the rising plume (close to the vertical axis). The core of the dome region is at an almost uniform temperature (within 2 K) due to the mixing caused by entrainment in the boundary layers and the rising plume. The rising plume is almost able to reach the ceiling, so the entire volume is affected by air circulation.

The results for the AP1000 configuration are presented in Figures 4.2-7 and 4.2-8. The flow pattern and velocity values are similar to the AP600 geometry. The AP1000 model also predicts a nearly uniform temperature field (within 2 K) in the core of the dome region. Due to the presence of the cold downward plumes, the central (hot) rising plume departs from the vertical axis and does not penetrate as close to the dome ceiling as in the AP600 case.

The coarse mesh predicts almost symmetrical flow and temperature fields throughout the entire calculation (for all iterations). On the other hand, the finer mesh predicts movement of the plume around the vertical axis and a change in the thickness and velocities in the boundary layers located near the vertical walls due to the detachment of the cold downward plumes from the dome ceiling. Figure 4.2-9 presents intermediate results from the fine mesh case to illustrate this behavior.

The way in which relaxation of the equations is implemented in the SIMPLE solving procedure produces results similar to those that would be predicted with a transient calculation. So, the results shown in Figure 4.2-9 could be considered as output of a quasi-transient run. Increasing the number of iterations does not result in a stable/steady-state solution with the fine mesh. This indicates the mixing process is very turbulent.

The StarCD results are in qualitative agreement with the separate effects tests, cited in Section 9 of WCAP-14407. The separate effects test has shown that with dome Gr_H numbers greater than 10^4 (for enclosure with cold lid and hot floor) turbulent mixing occurs, and flow is unstable due to the presence of hot uprising, and cold falling plumes. The turbulent mixing for enclosures with opposite vertical walls at different temperatures starts at $Gr_W = 10^6$, resulting in well mixed core region and stable flow pattern with high velocities predominantly in the boundary layer regions near the walls.

The applied boundary conditions for the StarCD analysis are in fact a combination of the boundary conditions of the referenced separate effects tests if the vertical uprising plume is considered a hot boundary of the cold vertical walls. The StarCD results show the effects of the combination of both boundary condition configurations.

In reality the presence of steam with smaller molecular weight will increase mixing in the AP600 and AP1000 (if released at the lower levels) because the buoyancy forces will be stronger than in the case of pure/dry air. The moving condensation film near the vertical walls will improve mixing and entrainment into the boundary layer. Also, vertical boundary layers with higher ratio of heavier air than in the air-steam mixture in the dome core will produce additional buoyancy forces.

Steam condensation will be more efficient near the top of the dome than on the vertical sidewalls, because the lighter steam will find it easier to penetrate and displace the air-rich layer close to the ceiling walls. The top of the dome has an elliptical slope (it is not horizontal as in the presented models). The sloped shell surface will provide a path for film condensate removal and additional entrainment in the boundary layer. Detachment of the film condensate in the center of the dome, in the form of falling droplets, or rivulets (depending on the surface tension/wetting angle between the condensate and ceiling wall), is possible and this would additionally improve mixing and heat transfer below the ceiling.

Therefore, based on the results of scaleable separate effects tests and a comparison of the numerical simulation results for conditions representing the long term post-LOCA cooling period, the region above the operating deck in both the AP600 and AP1000 should be well mixed. This allows the region to be reasonably modeled using a lumped parameter volume.

The effects of internal circulation and mixing on the containment pressure calculation are bounded in the AP600 DBA containment evaluation model. The evaluation model assumes perfect mixing above the operating deck, ignores heat and mass transfer to conductors inside dead-ended compartments, ignores heat and mass transfer to floors (horizontal surfaces), and uses a bounded, free-convection correlation for calculating the heat and mass transfer to the internal surface of the containment shell. This same approach will be used in the AP1000 DBA containment evaluation model.

Liquid Film Coverage Fraction

Liquid film coverage fraction is also a highly ranked phenomenon in the PIRT. The liquid film coverage fraction affects the evaporation rate on the external PCS shell.

The liquid film coverage fraction is dependent on the PCS water flow rate and the weir distribution system. Water from the PCS tank is delivered to a distribution bucket located just above the center of the dome. Water is metered from the bucket to eight divider plates that extend to the first set of weirs. The water fills the dams behind the weirs, and eventually spills over numerous V-notches in the weirs. The runoff from this first set of weirs covers the top half of the dome before filling the dams behind the second set of weirs. Water eventually spills over the V notches in the second set of weirs to be distributed over the lower half of the dome and vertical sidewall of the shell.

The AP1000 water distribution system is identical to the AP600 system but, the initial PCS water flow rate is slightly higher ([ ]^{a,b,c} vs. [ ]^{a,b,c} for AP600).

The amount of water required for evaporative heat removal from the PCS shell decreases as the core decay heat decreases. Therefore, the PCS flow rate was designed to vary over time.

As shown in the Water Distribution Tests (see Figure 5-4 of WCAP-14407, Rev. 3), the liquid film coverage fraction below the second weir on the containment shell decreases linearly as the delivered PCS flow rate becomes less than about 220 gpm. Using this information, the AP1000 coverage fraction just below the second weir should be >90 percent for the first 4 hours and >80 percent over the next 7 hours.

The estimates for the maximum and minimum values of the AP600 and AP1000 film coverage parameters during a DBA are tabulated in Table 4.2-3. The range of film coverage parameters is compared with the composite test data range from the PCS tests.

For evaluating film stability on the AP600 and AP1000 shell surface, it is important for the test data to cover the higher range of heat flux and the lower range of the sidewall film Reynolds number. Films with high Reynolds number values at low heat flux are more stable than films with low Reynolds number values at high heat flux. The maximum tested heat flux is about 50-percent higher than the estimated maximum AP1000 value. Tests were run at low film flow rates and to dryout, so the lower range of film Reynolds numbers is also covered.

For the AP1000, it is theoretically possible for the film temperature to reach the boiling point if the containment pressure and temperature were to remain at design values for an extended period of time. The existing PCS test data does not cover this possibility, however, there are no known design basis events which are predicted to result in external film boiling.

The AP1000 containment response to both a large LOCA and a large MSLB event was modeled with WGOTHIC; the results of these analyses are presented in Reference 14. The calculated containment peak pressure and temperature for the large MSLB event were higher than AP600, and like AP600, the peak occurred before steady-state PCS flow was established. The above-deck internal heat sinks and containment shell (without evaporation of the PCS flow) were able to absorb enough energy to stop the increase and begin decreasing the containment pressure for the large MSLB event. The containment pressure continued to decrease after the break flow was terminated and PCS flow was established. The PCS film temperature increased to over 200°F, but it was not predicted to reach the boiling point.

Summary of Conclusions

- Due to its relatively low and constant steam injection flow rate, the LST was not well scaled to model the blowdown transient condensation and convective energy transfer (π_{COND}, π_{CONV}) for either AP600 or AP1000. However, the steady-state LST data was determined to be acceptable for use as a source of separate effects data for internal condensation, above-deck steam distribution, external heat transfer, and external water coverage.

- The values for the AP600 and AP1000 dimensionless parameters used in scaling the heat and mass transfer correlations were compared to the values from the AP600 PCS test program. The AP600 PCS test program dimensionless parameter values for the selected heat and mass transfer correlations for condensation on the inside of the shell and evaporation/convection on the outside of the shell in the important riser region of the annulus covered both the AP600 and AP1000 operating range values.

- Based on Fr number scaling of the break jet, the volume above the operating deck in both the AP600 and AP1000 is expected to be well mixed during the blowdown portion of a DBA event. Based on the HDR E11.4 test results, scalable separate effects test data and the CFD analysis results presented in this report, this same volume is expected to be well mixed during the long-term heat removal phase of the DBA event, when condensation on the shell is occurring. Therefore, the use of a lumped parameter node to model the volume above the operating deck is acceptable.

- The operating ranges of the AP600 and AP1000 film coverage parameters were compared with the range of the PCS test data. The test data covered the operating range of the important film coverage parameters (minimum Re and maximum heat flux) for both AP600 and AP1000.

Table 4.2-1 Transient Phase Scaling Parameter Comparison

a,b,c

Table 4.2-2 Operating Range Comparison for AP600 and AP1000 Heat and Mass Transfer Parameters

a,b,c

Table 4.2-3 Comparison of the Range of Film Coverage Parameters

a,b,c

a,b,c

Figure 4.2-1 Condensation Mass Transfer Comparison

a,b,c

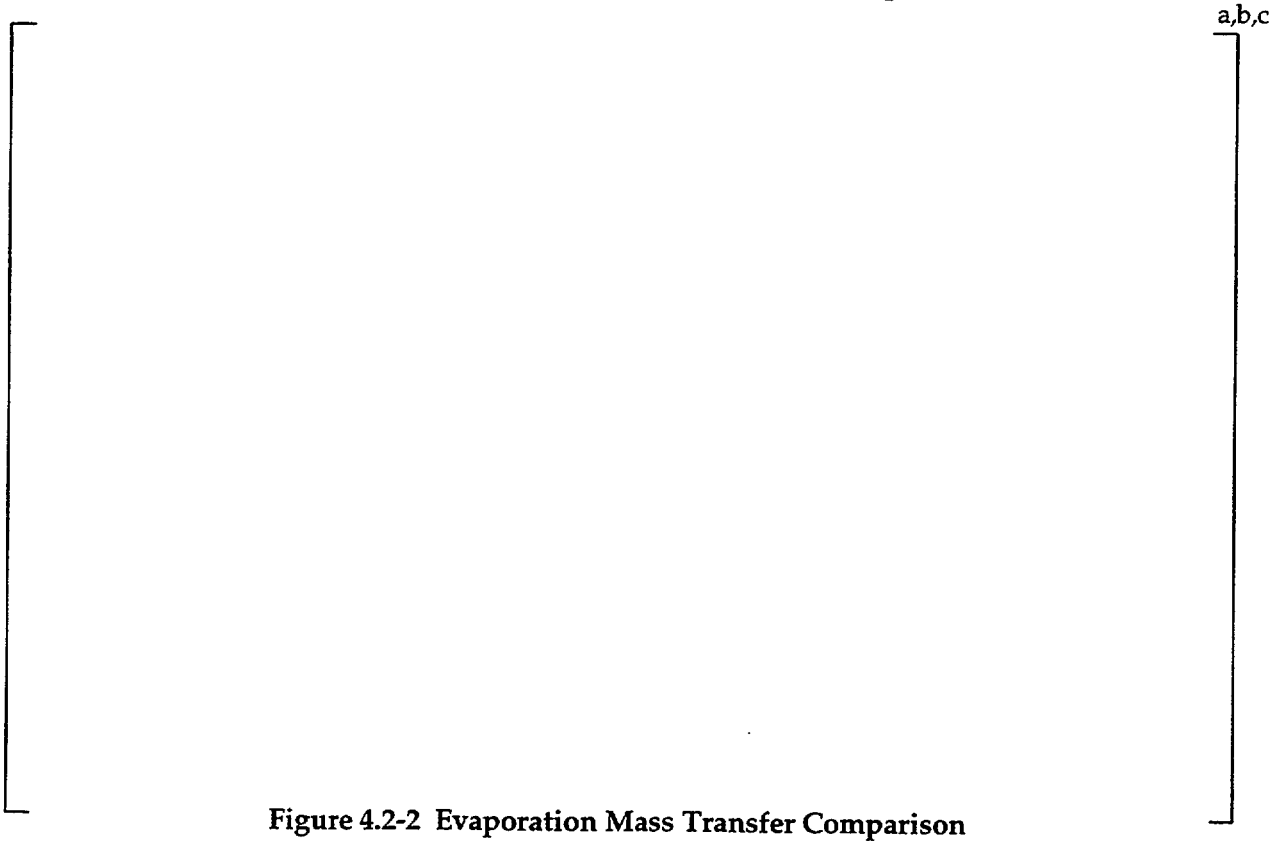

Figure 4.2-2 Evaporation Mass Transfer Comparison

a,b,c

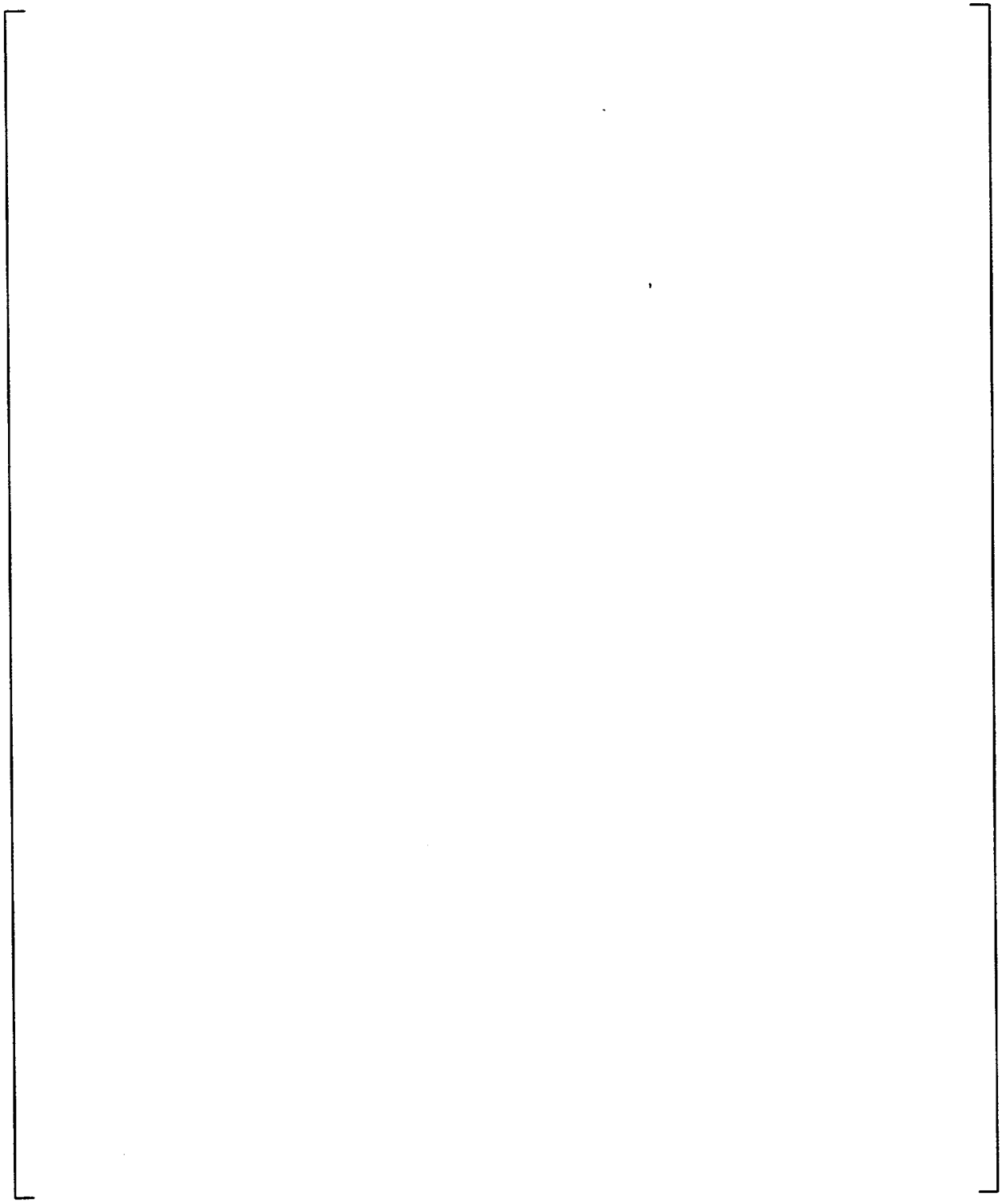

Figure 4.2-3 a) Coarse Mesh Applied for AP600 Calculation, b) Coarse Mesh Applied for AP1000 Calculation, c) Fine Mesh Applied for AP600 and AP1000 Calculation; Left Side – 0.8 m x 0.8 m Area Near the Corner is Presented, Right Side – 0.04 m x 0.04 m Area Near the Corner is Presented

a,b,c

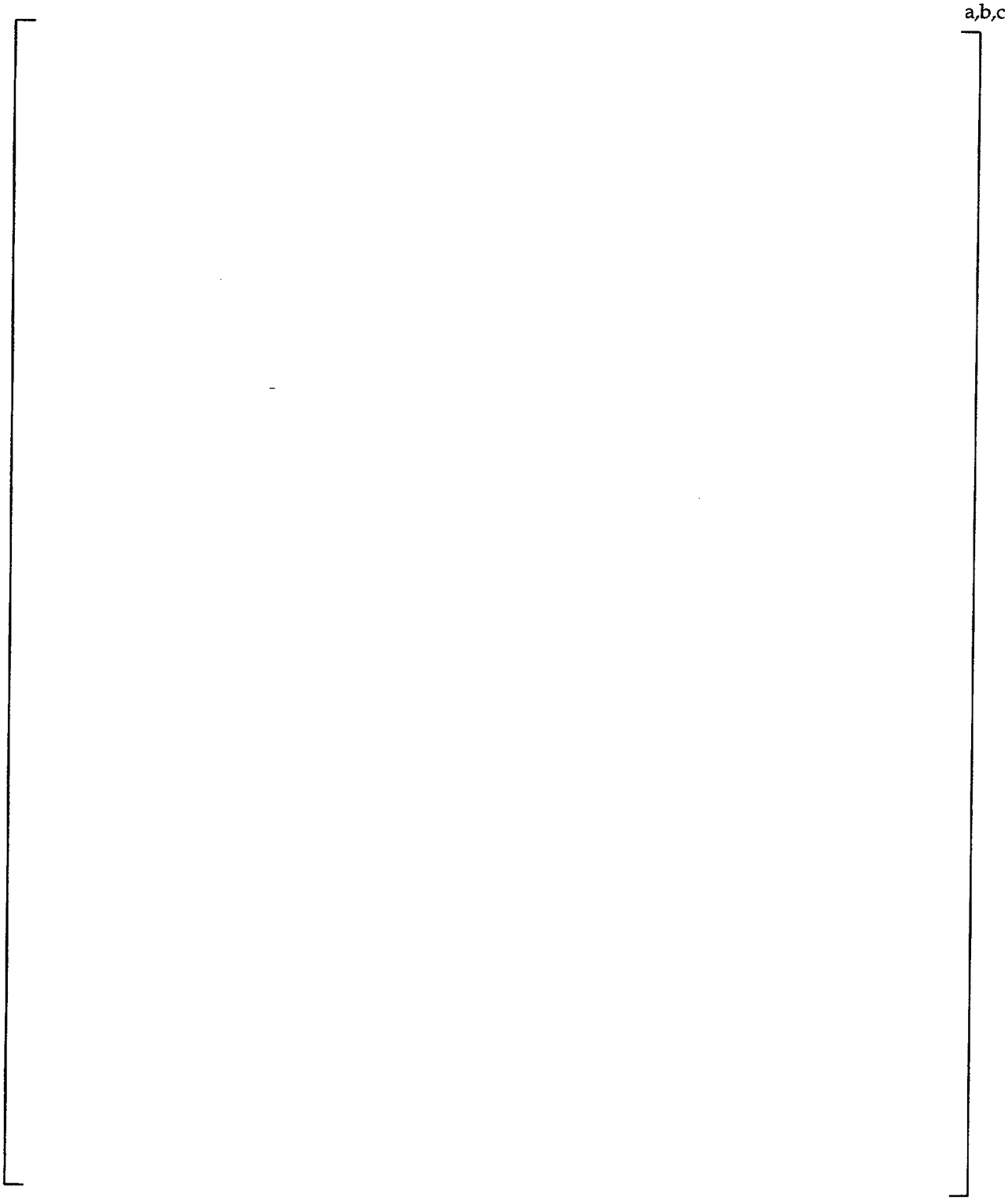

Figure 4.2-4 Convergence History for a) AP600 Calculation with Coarse Mesh, b) AP600 Calculation with Fine Mesh, c) AP1000 Calculation with Coarse Mesh, and d) AP1000 Calculation with Fine Mesh

a,b,c

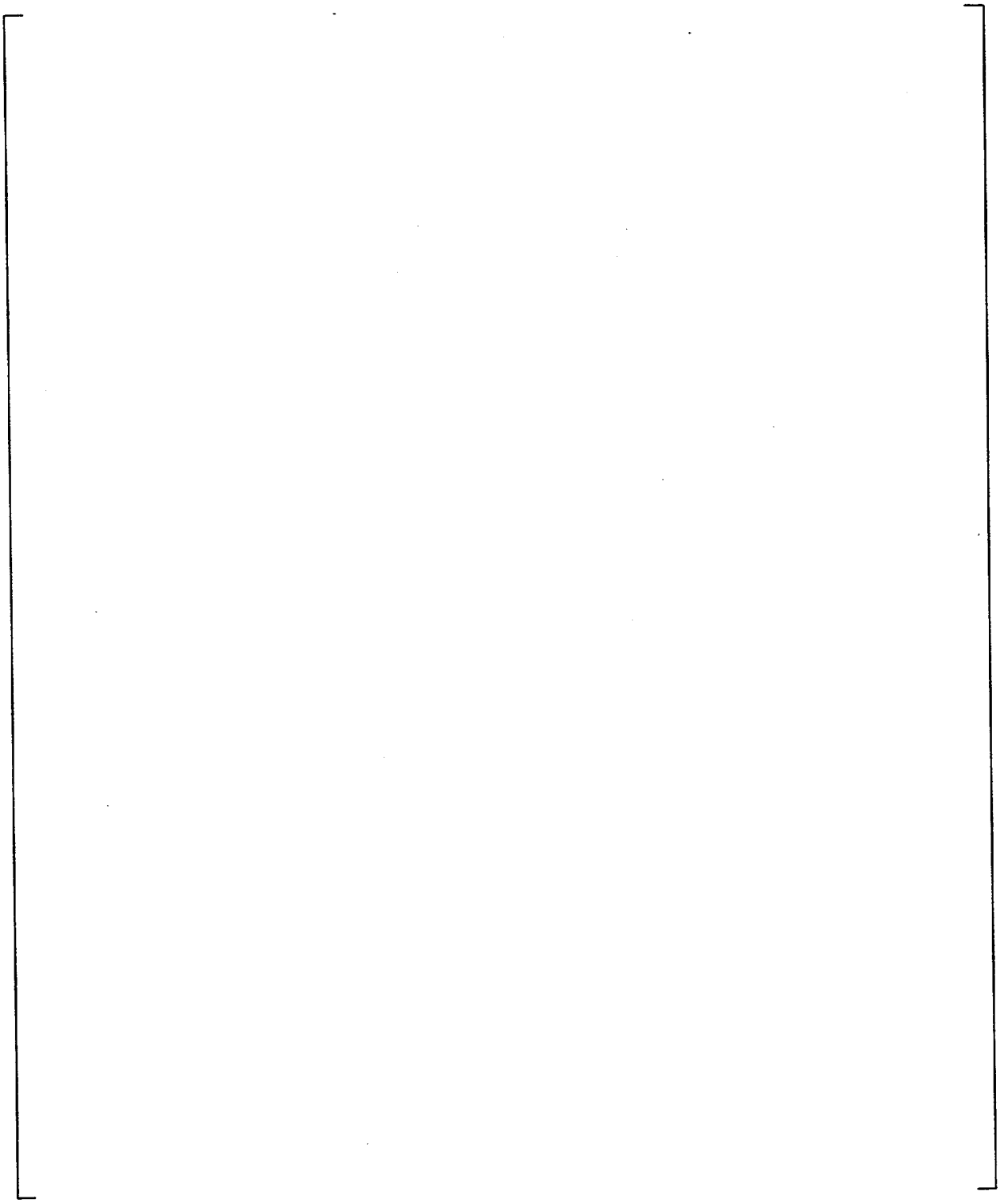

Figure 4.2-5 Temperature Distribution Inside AP600 Dome Region Obtained with a) Coarse Mesh After 1000 Iterations, b) Fine Mesh After 1214 Iterations

a,b,c

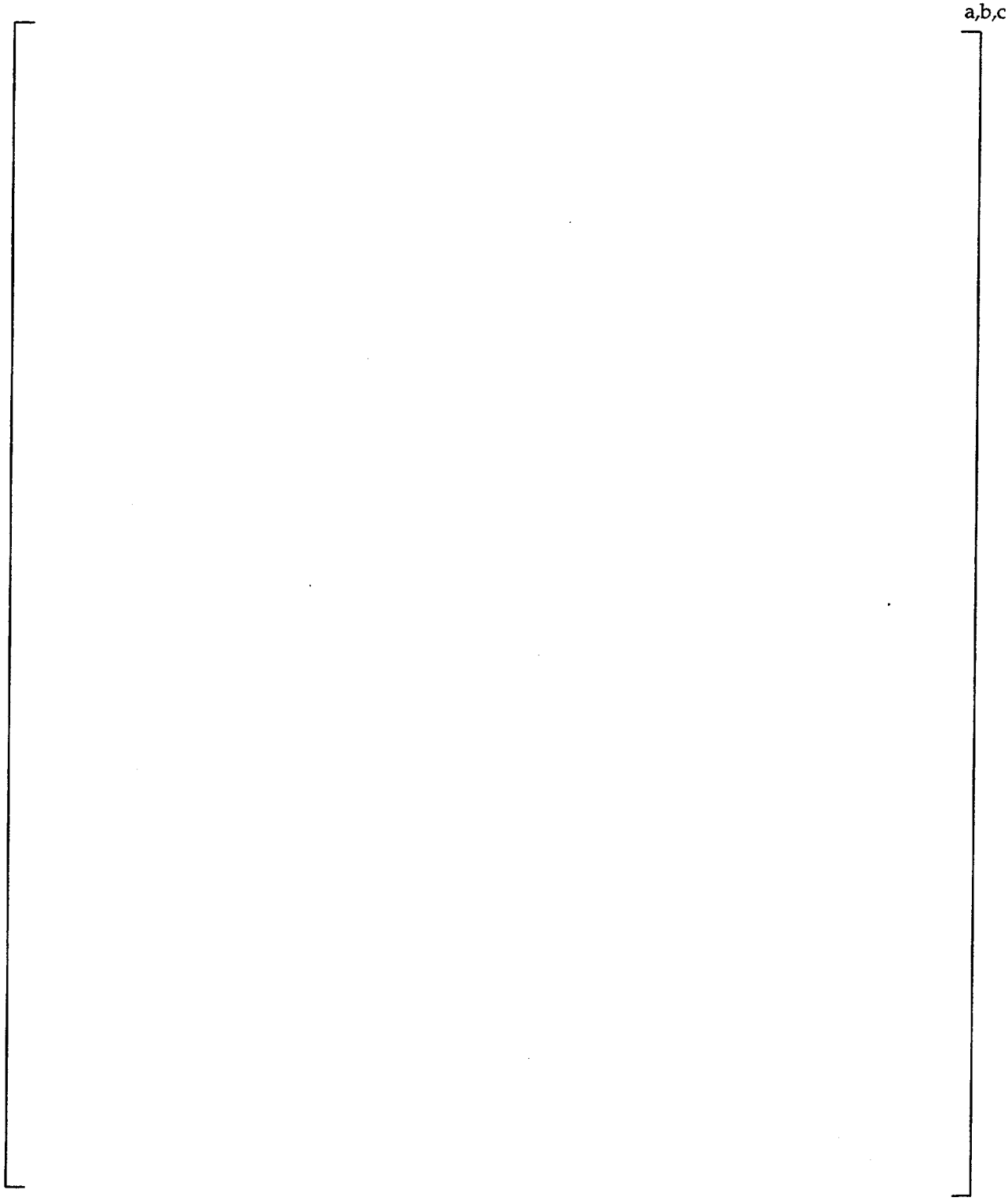

Figure 4.2-6 Velocity Distribution Inside AP600 Dome Region Obtained with a) Coarse Mesh After 1000 Iterations, b) Fine Mesh After 1214 Iterations

a,b,c

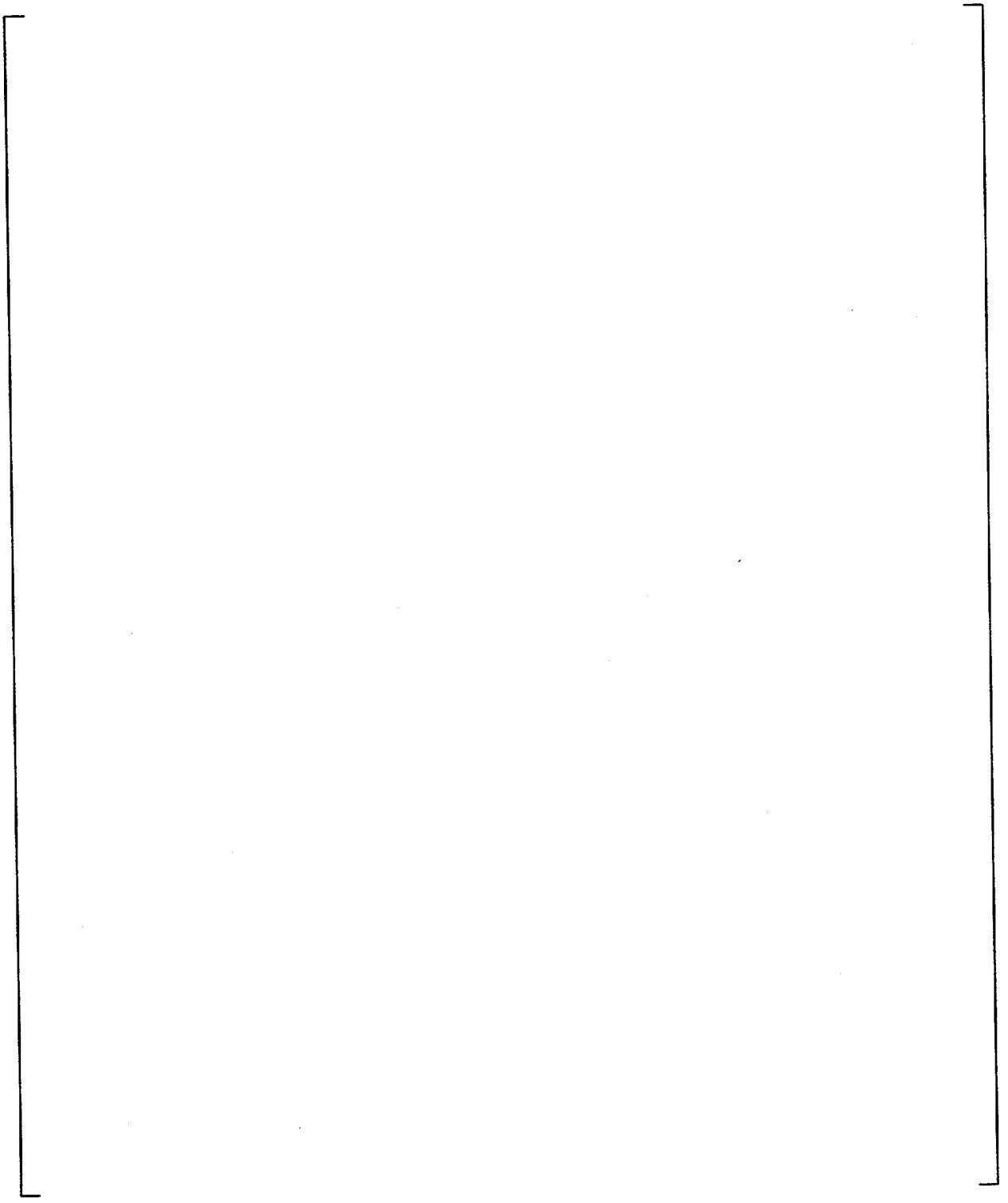

Figure 4.2-7 Temperature Distribution Inside AP1000 Dome Region Obtained with a) Coarse Mesh After 1612 Iterations, b) Fine Mesh After 1234 Iterations

a,b,c

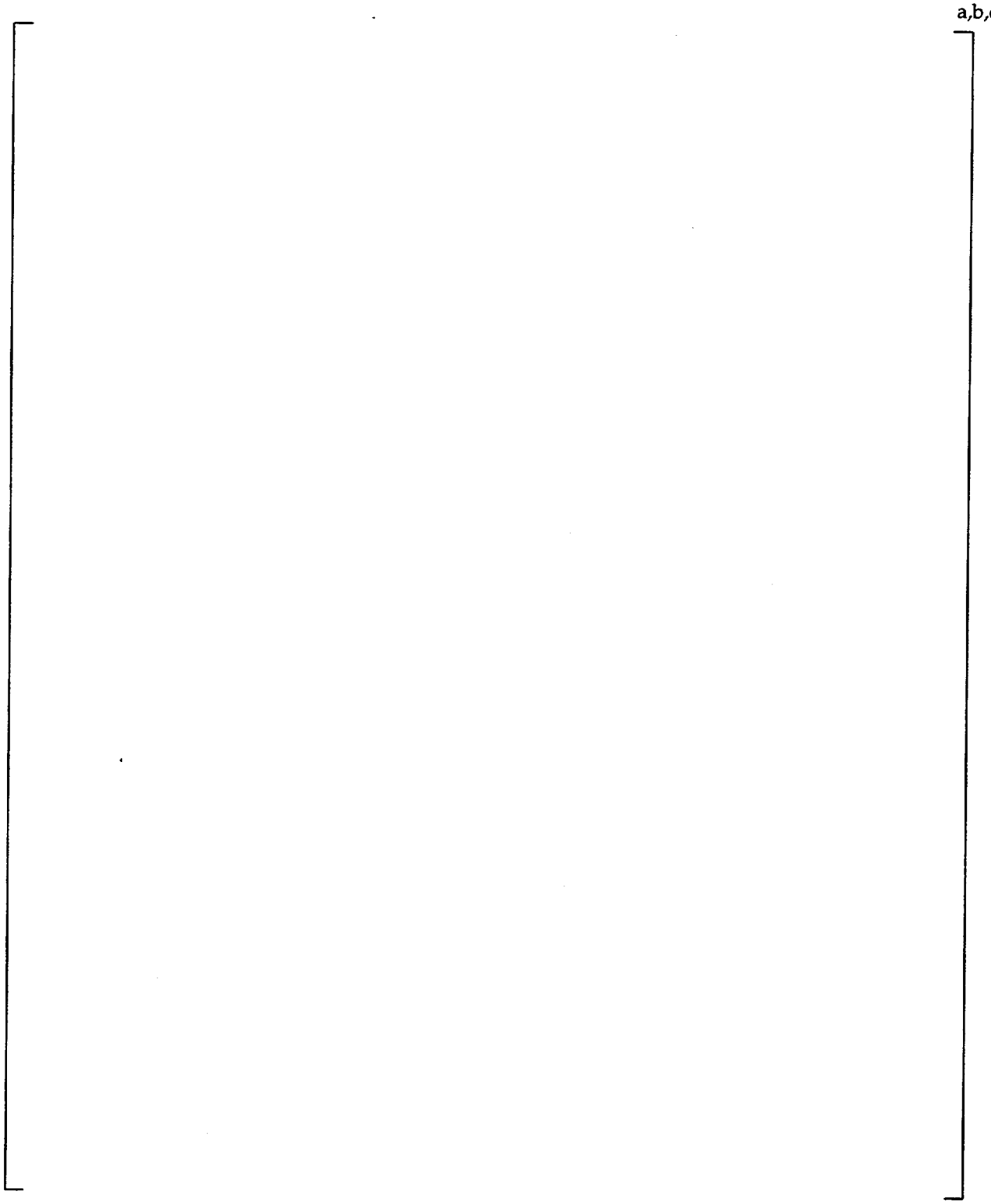

Figure 4.2-8 Velocity Distribution Inside AP1000 Dome Region Obtained with a) Coarse Mesh After 1612 Iterations, b) Fine Mesh After 1234 Iterations

a,b,c

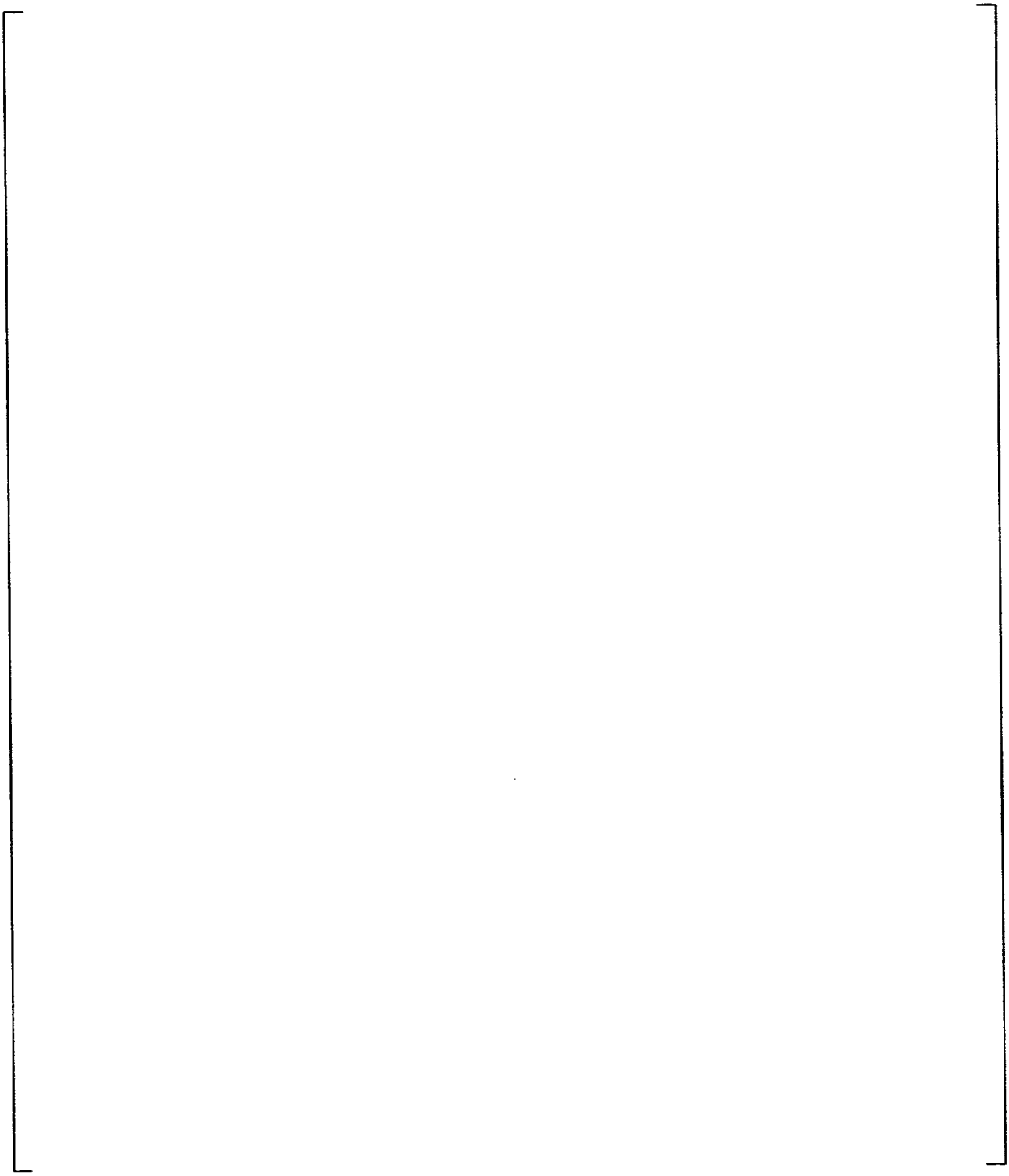

Figure 4.2-9 Temperature Distribution Obtained in AP1000 Dome After a) 610 Iterations, b) 825 Iterations, c) 1100 Iterations, d) 1234 Iterations

4.3 REFERENCES

1. WCAP-14270, "AP600 Low-Pressure Integral Systems Test at Oregon State University – Facility Scaling Report," J. N. Reyes, 1995.

2. NUREG/CR-5541, "System Scaling for the AP600 Pressurized Water Reactor and Related Facilities," W. Wulff and U. S. Rohatgi, 1998.

3. "Scaling Analysis for the OSU AP600 Test Facility (APEX)," J. N. Reyes and L. Hochreiter, Nuclear Engineering and Design, Vol. 186, 1998, pp. 53-109.

4. WCAP-14727, Rev. 2, "AP600 Scaling and PIRT Closure Report," W. L. Brown et al., February 1998.

5. "A Systems Approach to the Scaling Analysis of Integral Test Results," M. Oritiz, S. Banerjee, and T. Larson, Proceedings of the Fifth International Topical Meeting on Nuclear Thermal Hydraulics, Operation and Safety, 1997, Q1-Q7.

6. "Scaling Analysis of AP600 Long-Term Cooling Performance," M. Oritiz, C. Nielson, and L. Teerlink, 1997.

7. WCAP-14324, Rev. 1, "Final Data Report for ADS B1 Tests," September 1997.

8. WCAP-13963, "Scaling Logic for the Core Makeup Tank Test," L. E. Hochreiter et al., January 1995.

9. WCAP-12980, Rev. 3, "AP600 Passive Residual Heat Removal Heat Exchanger Test Final Report," April 1997.

10. WCAP-14305, Rev. 3, "AP600 Test Program ADS Phase B1 Test Analysis Report," April 1998.

11. WCAP-14254, "SPES-2 Test Analysis Report," May 1995.

12. WCAP-14292, "OSU Test Analysis Report," September 1995.

13. AP600 Document No. 796724, "Calculation for Data Overlap Between the ADS Separate Effects Test and Integral Effects Tests," December 1998.

14. WCAP-15612 "AP1000 Plant Description and Analysis Report," M. M. Corletti, et al., December 2000.

15. NUREG-1512, "Final Safety Evaluation Report Related to Certification of the AP600 Standard Design," September 1998.

16. NUREG/CR-5809, "An Integrated Structure and Scaling Methodology for Severe Accident Technical Issue Resolution, Appendix D: A Hierarchical Two-Tiered Scaling Analysis," N. Zuber, November 1991.

17. "Scaling Laws For Thermal-Hydraulic System Under Single-Phase and Two-Phase Natural Circulation," M. Ishii and I. Kotaoka, Nuclear Engineering and Design, Vol. 81, 1984, pp. 411-425.

18. "Scaling of Two-Phase Flow Transients Using Reduced Pressure System and Simulant Fluid," G. Kocamustafaogullari and M. Ishii, Nuclear Engineering and Design, Vol. 104, 1987, pp. 121-132.

19. Y. Taitel and A. E. Dukler, A Model for Predicting Flow Regime Transitions in Horizontal and Near Horizontal Gas-Liquid Flow, AIChE Journal, Vol. 22, No. 1, pp. 47-54, 1976.

20. W. Seeger, J. Reimann, and U. Muller, "Two-Phase Flow in a T-Junction with a Horizontal Inlet," Int. J. Multiphase Flow, Vol. 12, No. 4, pp. 575-585, 1986.

21. R. Mudde, J. Groen, H. Van Den Akker, "Two-Phase Flow Redistribution Phenomena in a Large T-Junction," Int. J. Multiphase Flow, Vol. 19, No. 4, pp. 563-573, 1993.

22. F. Moody, Introduction to Unsteady Thermofluid Mechanics, John Wiley & Sons, New York, 1990.

23. G. Yadigaroglou, Derivation of General Scaling Criteria for BWR Containment Tests, Intl. Confr. on Nuclear Eng., Vol. 2, ASME, 1996.

24. "An Analytical Model for Pressure Vessel Blowdown of Saturated Fluid Mixtures," J. N. Reyes, NURETH-9, October 1999.

25. R. K. Schwartzbeck and G. Kocamustafaogullari, Similarity Requirements for Two-Phase Flow Pattern Transitions, Nuclear Engineering and Design, 1989, pp. 135-147.

26. V. E. Schrock, S. T. Revankar, R. Mannheimer, 1986, Small Break Discharge – The Roles of Vapor and Liquid Entrainment in a Stratified Two-Phase Region Upstream of the Break, NUREG/CR-4761.

27. N. Zuber, "Problems in Modelling of Small Break LOCA," Heat Transfer in Nuclear Reactor Safety, Hemisphere Publishing, 1982.

28. "Transition from Depressurization to Long-Term Cooling in AP600 Scaled Integral Test Facilities," D. Bessette and M. di Marzo, Nuclear Engineering and Design, Vol. 188, 1999, pp. 331-344.

29. "Elements of Thermal Hydraulic Design," N. E. Todreas and M. S. Kazimi, Nuclear Systems II, Hemisphere Publishing, 1990.

30. "Natural Circulation Phenomena Relevant to Small Breaks and Transients," R. B. Duffey and J. P. Sursock, Nuclear Engineering and Design, Vol. 102, 1987, pp. 115-128.

31. J. N. Reyes, Jr., Scaling Single-State Variable Catastrophe Functions: An Application to Two-Phase Natural Circulation, Nuclear Engineering and Design, Vol. 151, 1994, pp. 41-48.

32. WCAP-14812, Rev. 1, "AP600 PIRT Closure Report," June 1997.

33. WCAP-14845, Rev. 3, "Scaling Analysis for AP600 Containment Pressure During Design Basis Accidents," D. R. Spencer et al., March 1998.

34. WCAP-14326, Rev. 3, "Experimental Basis for the AP600 Containment Vessel Heat and Mass Transfer Correlations," R. Ofstun, April 1998.

35. WCAP-14407, Rev. 1, "WGOTHIC Application to AP600," July 1997.